UNIVERSIDAD AUTÓNOMA DE MADRID

FACULTAD DE CIENCIAS

Departamento de Biología Molecular

MORPHOGENESIS OF THE ZEBRAFISH RETINAL PIGMENT EPITHELIUM AND ITS INVOLVEMENT IN OPTIC CUP FORMATION

Tania Moreno Mármol

Madrid, 2019

UNIVERSIDAD AUTÓNOMA DE MADRID

FACULTAD DE CIENCIAS

Departamento de Biología Molecular

Thesis dissertation submitted for the PhD degree in Molecular Biosciences:

MORPHOGENESIS OF THE ZEBRAFISH RETINAL PIGMENT EPITHELIUM AND ITS INVOLVEMENT IN OPTIC CUP FORMATION

Tania Moreno Mármol, Bachelor of Science in Biology

Thesis supervisors:

Prof. Paola Bovolenta Nicolao, PhD

Florencia Cavodeassi Madarro, PhD

The research presented in this thesis was carried out in the Department of Development and Regeneration in the Molecular Biology Research Center “Severo Ochoa” (CBMSO CSIC-UAM)

ACKNOWLEDGEMENTS

This thesis was supported by a fellowship from the CIBERER (Ayudas CIBERER al inicio de tesis doctorales en enfermedades raras 2014) as well as a fellowship from the Spanish Ministry of Education, Culture and Sports (FPU14/02867).

It also counted with the support of grants from the Spanish Ministry of Science, Innovation and Universities (BFU2016-75412-R and BFU2014-55918-P), from Fundación BBVA (IN[16]_ BBM_BAS_0078) and Fundación Ramón Areces. Institutional grants from the Fundación Ramón Areces and Banco de Santander to the CBMSO are also acknowledged.

We are thankful to Mario Ledesma from David Míguez's laboratory (CBMSO, Madrid) and to Lorena Buono from Juan Ramón Martínez-Morales' laboratory (CABD, Sevilla) for their collaboration in the work presented in this thesis.

ABSTRACT

Understanding the processes that govern the acquisition of organ shape during development is a main scientific goal, for which the eye has attracted notable attention. The eye primordium forms through the folding of a bi-layered structure, the optic vesicle, giving rise to the optic cup. This event occurs concomitantly with the differentiation of two main cell populations: the retinal pigmented epithelium (RPE) and the neural retina. While becoming specified, both cell types undergo extensive morphogenetic changes that have been proposed to act as driving forces for optic cup folding. This idea has been verified for the neural retina but not for the RPE. Using the zebrafish as a model, in this thesis we have studied in detail the changes that RPE cells undergo and asked if these are required for optic cup folding. To this end, we used a zebrafish line–based on an enhancer of the *bhlhe40* gene specifically expressed in the RPE–that allowed the early and specific visualization of RPE cells *in vivo*. Combining this tool with time-lapse analysis, we demonstrate that RPE specification occurs in a small group of cells located in the dorsal optic vesicle, which then extend to cover the whole surface of the eye. This expansion is largely linked to a dramatic cell shape conversion from a pseudostratified epithelium to a monolayer of flat and then squamous cells, on which cell proliferation has little influence. Indeed, RPE cells reduce their proliferation rate during this morphogenetic change, and this reduction is critical because forced maintenance of cell proliferation impairs morphogenesis. The notable surface increase of the RPE as a whole is instead concomitant with the reduction of the apico-basal axis of individual cells and the expansion of their surface area, so that cells undergo an apparent "stretching". Supporting this view, individual cell volume is conserved and there is only a minimal increase in the overall RPE volume. Both myosin II activity and microtubule dynamics are required for RPE cell flattening, and this event, in turn, actively contributes to optic cup folding. Our results suggest a model, based on analogies with other epithelia, in which myosin II could confer stiffness to RPE cells whereas changes in microtubule orientation could be instrumental for cell rotation, both making an elongated flat epithelium in a short time. Time-course RNAseq analysis of the gene regulatory network behind early RPE development indicates that RPE specification occurs very early, making the RPE rapidly diverging from the neural retina. Notably, among these genes there are transcription factors and cytoskeletal proteins that could increase RPE stiffness. The *bhlhe40* gene itself was found among the up-regulated genes. However, here we show that its function seems dispensable for eye morphogenesis.

All in all, this study shows that RPE cell flattening is a cell autonomous process promoted by cytoskeleton dynamics, which contributes to drive the folding of the zebrafish optic vesicle into a cup. It also provides initial cues of its genetic regulation.

Uno de los principales objetivos de la biología del desarrollo es entender los mecanismos por los cuales un órgano adquiere su forma final, y en este campo la formación del ojo en vertebrados ha atraído especial interés durante los últimos años. El primordio de ojo o copa óptica se forma a través de la invaginación de la vesícula óptica, una estructura formada por un neuroepitelio continuo y plegado en el que se diferencian dos capas. Al mismo tiempo que tiene lugar el proceso de invaginación, las células de la vesícula óptica se diferencian principalmente en dos tipos celulares: el epitelio pigmentario (EP) y la retina neural. Ambas poblaciones llevan a cabo extensas reorganizaciones a nivel celular que implican cambios de forma y que han sido propuestas como fuerzas que inducen la formación de la copa óptica. Esta idea ha sido probada para las células de la retina neural, sin embargo, la posible contribución del EP al desarrollo del ojo aún no ha sido analizada. Esta tesis se centra en estudiar los cambios de forma de las células del EP y aborda su papel durante la formación de la copa óptica usando el pez cebra como sistema modelo. Para ello hemos empleado una línea transgénica en pez cebra que permite la visualización *in vivo* del EP gracias a un elemento regulador del gen *bhlhe40*, el cual se expresa específicamente en este epitelio. Con esta herramienta hemos demostrado que la especificación del EP tiene lugar en un pequeño grupo de células en la región dorsal de la vesícula óptica que posteriormente se extienden para cubrir toda la superficie del ojo. En pez cebra esta extensión está directamente relacionada con los cambios de forma que sufren sus células. Inicialmente organizadas como un epitelio pseudoestratificado, las células del EP se aplanan hasta formar un monocapa de células escamosas. Durante este aplanamiento la superficie del EP aumenta tres veces, la longitud de su eje apico-basal se reduce a la mitad y únicamente se detecta un ligero aumento del volumen total del tejido, manteniéndose constante el volumen celular. Estos cambios de forma están directamente asociados con la actividad de componentes del citoesqueleto (miosina II y microtúbulos) y con una reducción en la tasa de proliferación celular, de forma que la interferencia con ambos procesos altera la morfogénesis del EP, y en último término la formación de la copa óptica. Mediante un análisis RNAseq de los genes que controlan el desarrollo temprano del EP hemos visto que la especificación de este tejido se produce de forma abrupta, divergiendo rápidamente de las células progenitoras de la vesícula óptica. Entre los genes sobreexpresados se encuentra el gen *bhlhe40*, sin embargo, hemos visto que su función en la formación del EP es prescindible.

Para concluir, esta tesis demuestra que la morfogénesis del EP es un proceso autónomo celular promovido por la actividad del citoesqueleto y que a su vez induce la invaginación de la copa óptica en pez cebra. Además, los datos obtenidos proporcionan indicios para comprender mejor qué genes controlan este proceso.

TABLE OF CONTENTS

ABBREVIATIONS

A: Anterior

A-B: Apico-basal

ABleb: Azidoblebbistatin

BrdU: 5-Bromo-2′-deoxyuridine

Cas9: CRISPR-associated protein-9 nuclease

cmz: Cilliary margin zone

CRISPR: Clustered Regularly Interspaced Short Palindromic Repeats

D: Dorsal

DEG: Differentially expressed genes

DMSO: Dimethyl sulfoxide

dpf: Days post fertilization

ECM: Extracellular matrix

FBS: Fetal bovine serum

GO: Gene ontology

hb: Hindbrain

hpf: Hours post-fertilization

il: Inner layer

ISH: *In situ* hybridization

L: Lateral

M: Medial

mb: Midbrain

MT: Microtubule

NR: Neural retina

nt: Neural tube

ol: Outer layer

OC: Optic cup

OV: Optic vesicle

P: Posterior

PBS: Phosphate buffer saline

pd: Pronephric duct

PFA: Paraformaldehyde

pMLC: phospho myosin light chain

pNR: Prospective neural retina

pRPE: Prospective retinal pigment epithelium

R: Rim

RPE: Retinal pigment epithelium

RT: Room temperature

ss: Somites

V: Ventral

vl: Virtual lumen

INTRODUCTION

1. Morphogenesis through developmental processes

Shape and function are closely related from a biological point of view. The acquisition by tissues and organs of a specific organization during development is essential for proper function in the adulthood. This process is known as morphogenesis and emerges from the complex integration of tightly regulated cell behaviors such as cell proliferation, cell death, cell shape changes, cell polarity changes and cell migration. Morphogenesis has been extensively studied during embryonic development for at least two reasons: the interest in knowing how the process of forming an organ occurs and for understanding how defects in morphogenesis, associated with numerous diseases, arise. Morphogenesis is tightly coordinated with fate specification. Indeed, the acquisition of a specific cell fate is linked to particular cell behaviors although often to discern cause-effect relationships is difficult.

Among vertebrates, the zebrafish (*Danio rerio*) stands out as an excellent model system for morphogenetic studies. This species is easily maintained in the laboratory and the access to its eggs is immediate after fecundation. Besides, embryo manipulation is simpler than in other research fishes as, for example, the medaka fish (*Oryzias latipes*). Zebrafish allows real time analyses because its embryonic development is fast (between 48 and 72 hours post fertilization (hpf) the embryos hatch and become larvae) and because embryos are transparent allowing for visual accessibility of all tissues. The understanding of the zebrafish genome has increased notably during the last years and, together with classic genetic techniques, has resulted in numerous transgenic lines labelling specific cell lineages with fluorescent proteins. Using zebrafish transgenic lines and thanks to the continuous advances in imaging, we can now follow any morphogenetic process *in vivo*. Genetic manipulation techniques are well established in the zebrafish. Among them the most commonly used are: morpholinos (Nasevicius and Ekker, 2000), the CRISPR-Cas9 technology (Hwang et al., 2013), chemical inhibitors and the yeast GAL4/UAS system (Asakawa and Kawakami, 2008). The first two allow interfering with gene activity, but do not provide any spatial or temporal specificity. Treatments with chemical compounds are very fast and can be performed at specific developmental stages but also lack spatial control. The GAL4/UAS system, in turn, allows targeting a tissue and/or a specific developmental stage. In addition to this, optogenetics has emerged as a promising approach to control molecular activity with spatial and temporal precision (Guglielmi et al., 2016). The combination of these techniques offers new perspectives of morphogenetic events. The work presented here has taken advantage of some of them to expand our understanding of retinal pigment epithelium (RPE) morphogenesis during development in zebrafish.

2. The retinal pigment epithelium: ensuring proper visual functions

Sight is an effective and fast way for animals to obtain information of their surroundings. This confers great advantages reflected in the fact that vision has been evolutionarily conserved despite being a highly energy demanding process. Eyes date back to the early Cambrian period, when, in what is considered an evolutionary short period of time, a wide variety of macroscopic organisms emerged and diversified. Many of them presented eyes and indeed vision is considered a potential motor of this episode known as the Cambrian explosion (Letelier et al., 2017, Land, 2012).

All current designs of functional eyes in the animal kingdom, but also the prototypic eye from which they have evolved, present two main components: photoreceptor and pigmented cells (Martinez-Morales and Locascio, 2016, Gehring and Ikeo, 1999). Photoreceptors are specialized cells able to detect light and transform the light input into nerve impulse while pigmented cells have primarily a shielding role, mainly protecting photoreception and generating directionality. With further additional roles, in vertebrates the RPE is the equivalent structure to the pigmented cell of the prototypic eye. The RPE consists of a monolayer of epithelial cells located at the back of the eye which are characterized by the production and accumulation of pigment. It is located between the neural retina (NR), which includes the photoreceptor layer, and the choroid (Figure 1A,B). Apart from photoreceptors (the closest neurons to the RPE) the NR contains five other cell types: retinal ganglion cells (the farthest from the RPE), amacrine cells, horizontal cells, bipolar cells and Müller cells (Avanesov and Malicki, 2010). Two main types of photoreceptors are found in zebrafish, as well as in mammals–cones and rods. Zebrafish retinas have one type of rods which are specialized for vision at low light levels and four types of cones for vision at high light levels, high spatial acuity and color vision (Nawrocki et al., 1985, Branchek and Bremiller, 1984).

The choroid, that is located at the back of the RPE, is a highly vascularized structure in which the circulating blood becomes highly oxygenated. It serves as a connection between the sclera, the most external layer, and the NR. The cornea, the lens, the iris and the ciliary body compose the so called anterior segment of the eye whereas the optic nerve is found at the posterior pole of the eye (Figure 1A).

The RPE has a protective role by counteracting the effect of photooxidative processes. Scattered light and high levels of oxygen induce the death of photoreceptors if accumulated in the NR. The RPE generates and accumulates pigments in specific organelles called melanosomes for absorbing the excess of light scattered from the photoreceptors. Melanin is the main pigment molecule present in the vertebrate RPE. RPE cells also produce several antioxidant molecules that scavenge the oxygen from choroid blood and the reactive oxygen species generated by RPE

physiological activity (Letelier et al., 2017, Strauss, 2005). The RPE constitutes a physical barrier between the NR and the vasculature in the choroid (blood-retinal barrier) so that transport of all molecules relies in this epithelium. Tight and adherent junctions keep RPE cells tightly bound one another apically serving as a mean to isolate the apical from the baso-lateral domain (Bonilha, 2014). RPE cells transport water and ions from the subretinal space to the blood, so that ion concentration in the subretinal space is maintained, despite of the variations that occur during dark/light periods. All this process is essential for photoreceptors excitability. Besides, RPE cells transports nutrients from the blood to the NR.

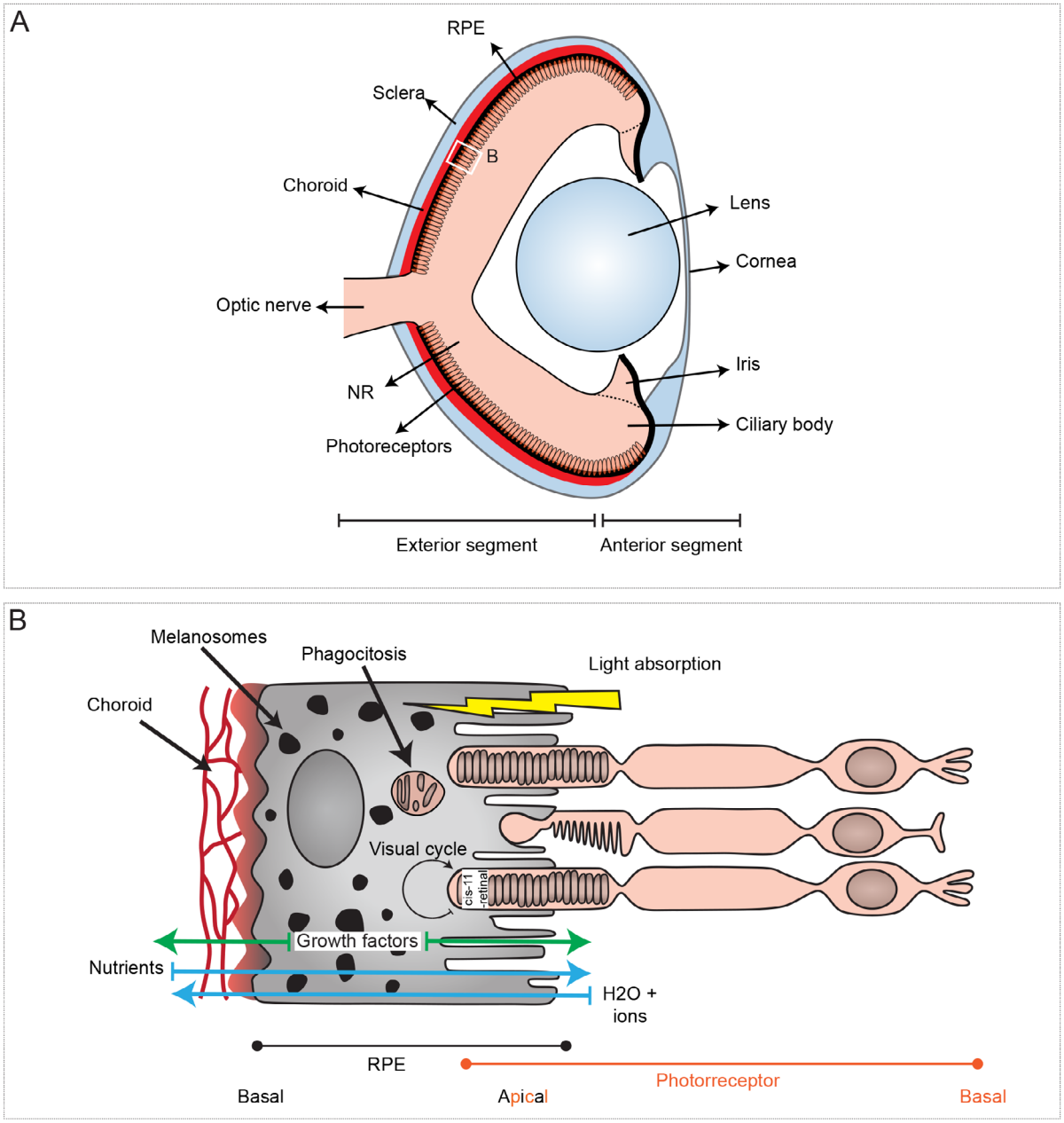

Figure 1: Structure of the adult zebrafish eye.

(A) Schematic diagram of an adult zebrafish eye. The different layers are indicated. The white square delineates the region represented in **B**. **(B)** Detailed diagram of the adult RPE environment. The main RPE functions are summarized. Photoreceptors are shown in orange and RPE in grey. Modified from Letelier et al. (2017).

RPE-photoreceptor association goes further. In synchrony with dark/light cycles, RPE cells phagocyte the outer segments of photoreceptors, which contain molecules that need to be recycled every day. As a key component of the visual cycle, RPE cells also revert the isomerization of 11-cis-retinal after photon absorption. Finally, they help maintaining NR and choroid homeostasis and integrity through the secretion of growth factors (Letelier et al., 2017, Sparrow et al., 2010, Strauss, 2005; Figure 1B).

All these functions reflect the physiological dependence between RPE and photoreceptors, so that these two main visual components are even considered a single functional unit. This is also highlighted by the physical connection through the apical regions of both cell types. RPE cells have a highly elaborated and expanded apical membrane with extensions that surround the photoreceptor outer segments (microvilli) (Bonilha, 2014, Strauss, 2005). Recently RPE-photoreceptor dependence has been shown in zebrafish through genetic ablation of the larvae RPE. The loss of RPE causes photoreceptor degeneration and their regeneration is limited to those regions in which the RPE has been previously recovered (Hanovice et al., 2019). These zebrafish experiments are representative of what happens in an extended group of eye degenerative diseases called retinal dystrophies, in which RPE alterations lead to photoreceptor cell death and vice-versa (Wright et al., 2010, Gregory-Evans and Bhattacharya, 1998). Understanding the mechanistic bases of retinal dystrophies will rely on a thorough understanding of RPE development and homeostasis.

3. Cytoskeleton in the RPE

The structure of the cytoskeleton underlies RPE development and functions (García and Koke, 1996) as well as cell shape and polarization, as generally occurs for other epithelia. Studies of cytoskeleton organization in RPE cells have focused on postembryonic stages (Bonilha, 2014), but how this organization is acquired during embryonic development remains unexplored. The cytoskeleton of eukaryotic cells is composed by three different types of structures: microfilaments, intermediate filaments and microtubules (MT). These elements have a specific subcellular distribution within the cell so that three compartments can be differentiated along the apico-basal (A-B) axis (Figure 2).

MTs and microfilaments are located in the apical compartment at the core of microvilli, the membrane prolongations that wrap the photoreceptors external segments. RPE microvilli are involved in vesicular processes driving phagosomes and melanosomes transport (Bonilha, 2014, Doctor, 2006). Phagosomes containing photoreceptors external segments are transported to the cell body where they fused with lysosomes, whilst melanosomes undergo the so called retinomotor movements. Pigment granules accumulate in the cell body in dark periods and

distribute along microvilli during light exposure (Doctor, 2006, Menger et al., 2005, García and Koke, 1996). RPE cells have also a primary cilium which is located in the apical domain and has a MT core. This structure is necessary for maturation of the RPE and its defects (ciliopathies) lead to photoreceptor degeneration (May-Simera et al., 2018). Underneath the apical compartment, actin filaments are organized as a belt and interact with adherens junctions (or zonula adherens) together with other cytoskeletal proteins such as myosins. At the apico-basolateral border, there are also tight junctions essential for sealing the intercellular space, making of the RPE an essential component of the blood-retinal barrier (Bonilha 2014). Along the basolateral, domain MTs are polarized with their minus end oriented towards the most apical region and the plus end toward the basal one. This organization is necessary to maintain RPE polarity and function. Besides, short MT fragments are found next to the cell cortex, under the plasma membrane. In the baso-lateral compartment, actin filaments are also polarized but they are limited to the cell cortex in contrast to MTs that are localized all over the cytoplasm (Bonilha, 2014, Doctor,

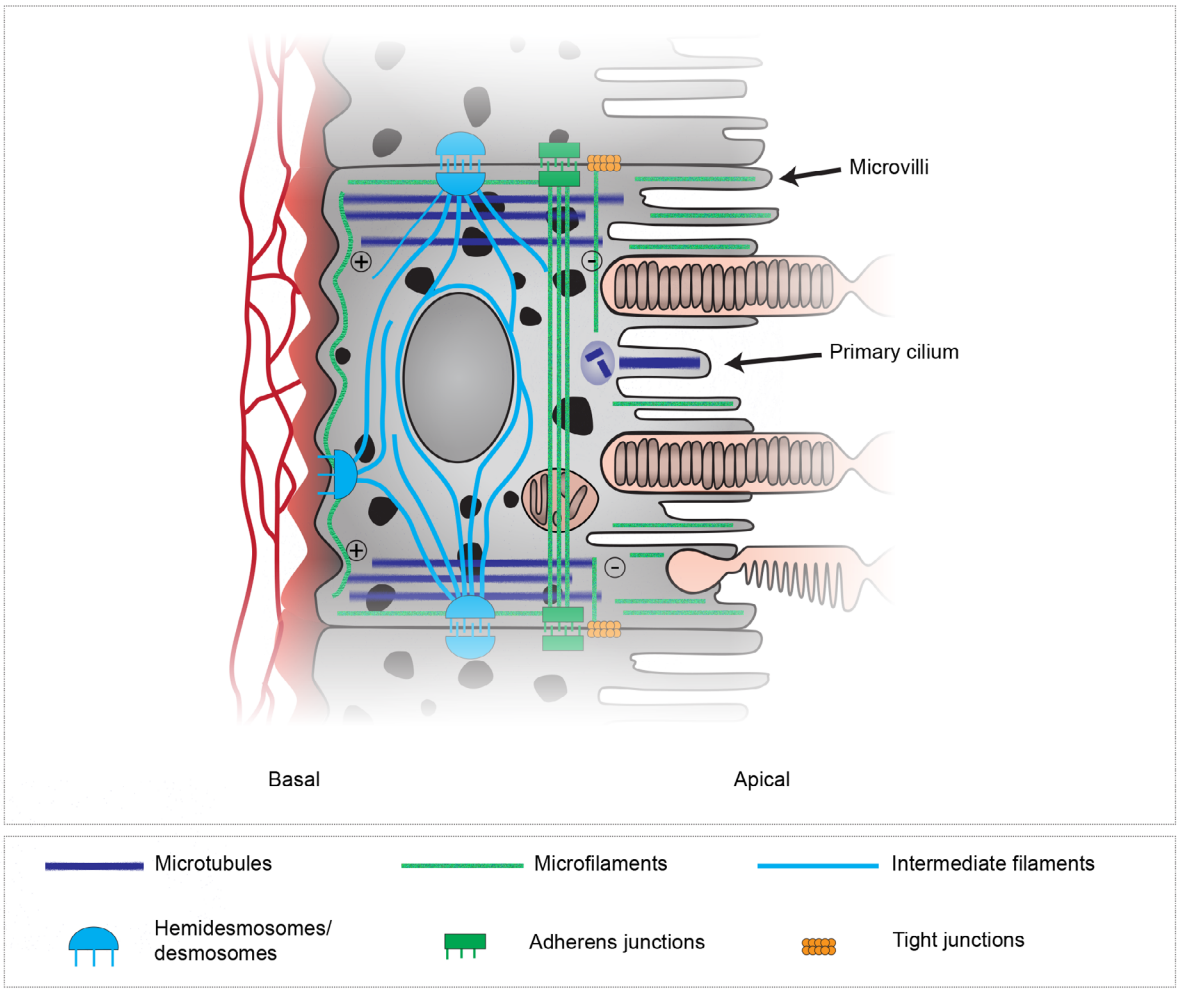

Figure 2: Cytoskeleton composition and organization in RPE cells.

Schematic diagram of RPE cells highlighting cytoskeleton and junction's components. Modified from Bonilha (2014).

2006, Turksen et al., 1989). Intermediate filaments are also found bound to desmosomes and hemi-desmosomes to reinforce adhesion among cells and with the extracellular matrix (ECM), respectively. In the RPE as in other epithelial cells, the intermediate filaments are mainly formed by keratins. Apart from intermediate filament, the most basal region of RPE cells contains also actin microfilaments (Bonilha, 2014, Doctor, 2006).

This thesis has focused on the role of the cytoskeleton during RPE development given that this has not been analyzed thus far.

4. Overview of eye morphogenesis in zebrafish

The morphogenetic events that precede the acquisition of the RPE and NR cells' structure and mature functions are of special interest in this thesis. The embryonic retina has a neuro-ectodermal origin. The specification of zebrafish retinal progenitor cells takes place in the center of the anterior neural plate at tailbud stage. In the zebrafish, retinal progenitors form a very cohesive group of cells, known as the retinal or eye field, which does not intermingle with progenitors of the abutting neural domains (Cavodeassi, 2014, Cavodeassi et al., 2013). In amniotes, retinal progenitors are specified in two separate and symmetric domains positioned laterally to the axial midline of the embryos (Inoue et al., 2000). Telencephalon progenitors are located anterior to the retinal field, diencephalon progenitors in the posterior region and the hypothalamic ones in a ventral/posterior position (Figure 3A). These four domains make up the forebrain and during morphogenesis they all undergo extensive reorganizations, although retinal progenitors are those that undertake the most extensive rearrangements (Cavodeassi, 2018, Martinez-Morales et al., 2017).

In zebrafish, neural plate cells initially show a mesenchymal appearance and subsequently arrange as a pseudostratified epithelium. Retinal field cells are the earliest in the forebrain changing from a mesenchymal to a neuroepithelial organization. They elongate and polarize apico-basally whilst dividing into two lateral groups and organizing into two optic vesicles (OV) (Ivanovitch et al., 2013, Rembold et al., 2006). The zebrafish OV is a flat out-pocket of neuroepithelial tissue, which is folded in two layers: the outer or medial layer and the inner or lateral layer. These two layers are connected distally by a region that is known as the rim or hinge (Figure 3B). The cells in each layer face each other by their apical side, and are separated by a virtual lumen. In amniotes, the OV structure is slightly different. It has a balloon-like shape formed by a cuboidal neuroepithelium with a proper lumen (Figure 3B).

As eye morphogenesis takes place, the OV folds over itself and gives rise to the optic cup (OC) that constitutes the final shape of the organ (Figure 3C). The transition from OV to OC is concomitant to the specification of retinal progenitors into three different populations: the RPE,

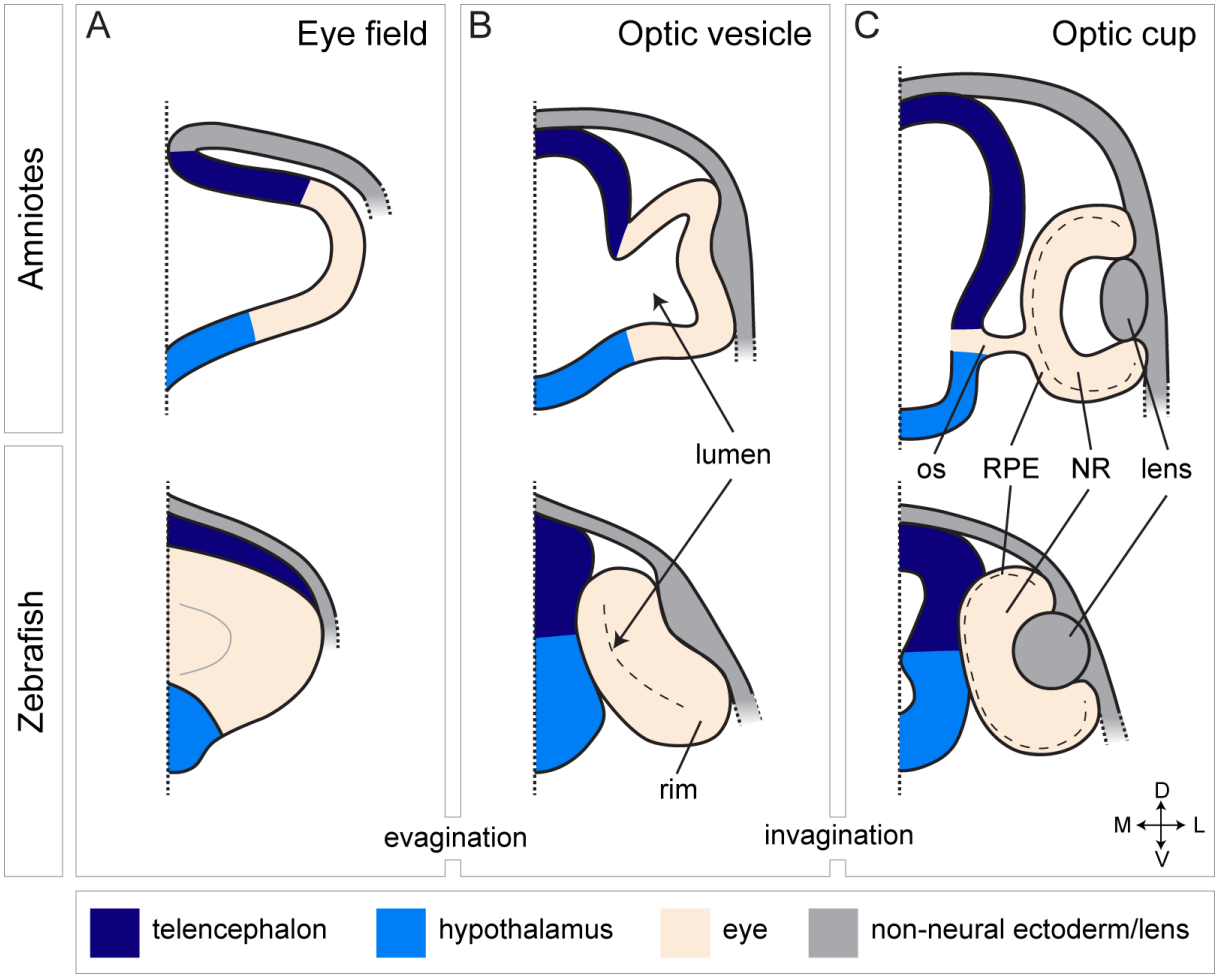

Figure 3: Comparison of eye morphogenesis in amniotes and zebrafish.

Schematic illustration of the forebrain structures during **(A)** eye field, **(B)** optic vesicle and **(C)** optic cup stages. The upper row corresponds to amniotes (i.e. mouse) and the bottom row to zebrafish.

the NR and the optic stalk. According to zebrafish fate map studies the RPE derives from the OV cells located in outer/dorsal layer, the NR from the outer/ventral and inner layers (Figure 4A) and the optic stalk from the most anterior/ventral group of cells (Kwan et al., 2012, Li et al., 2000a). The acquisition of different cell morphologies accompanies the specification of each one of these three domains. In particular, RPE cells become a thin monolayer of cells that cover the whole eye. The NR differentiates into several neuronal types that are collectively involved in reception and transmission of visual information. The optic stalk is initially the region that keeps connected the OV and the forebrain and then wraps the projecting axons of the retinal ganglion cells to finally form the optic nerve. The optic stalk is specified in the anterior region of the OV but it ends in a ventral position due to the rotation of the entire OC as part of its morphogenesis.

OC folding is asymmetric, such that it leaves a ventral opening called the choroid or optic fissure. The optic fissure will close at later stages of OC maturation in a process that involves

basal membrane degradation (James et al., 2016) and the formation of tight links among the cells located at the lips of the choroid fissure. The lip cells are next to the RPE and after the closure they become incorporated into both the NR or the RPE (Gestri et al., 2018). The improper fusion of the optic fissure leads to a congenital disease known as coloboma in which there is a gap in the ventral region of the eye. Apart from optic fissure organization, RPE differentiation has been involved in other late events in eye development such as NR neurogenesis, layer organization or axonal projection (Bharti et al., 2006).

By the end of eye morphogenesis, the lens has also formed through a process intimately coordinated with OC folding. The lens derives from the lens placode, a thickening of the non-neural ectoderm overlying the OV (Figure 3C). The lens placode becomes visible at 12 somites (ss) stage (Kwan et al., 2012) as an invagination of ectodermal tissue that eventually buds off the ectoderm to form the lens vesicle. Subsequent differentiation of the lens vesicle leads to the most anterior cells giving rise to the lens epithelium and the most posterior elongating and becoming transparent fibers (Cvekl and Ashery-Padan, 2014).

5. Morphogenetic mechanisms in eye development

Sculpting an organ such as the eye requires the integration of several mechanisms taking place at different scales. It involves the reorganization of intracellular components, the coordination of cell behavior and/or the response to external inputs. In recent years, many efforts have been made to understand the mechanisms driving OC folding. Most studies have been performed in zebrafish embryos due to the visual accessibility of their morphogenesis, which is instead not easily accessible in species that develop *in utero*. Chicken embryos and organoids derived from mouse/human-embryonic stem cells (Nakano et al., 2012, Eiraku et al., 2011) have also shed light on this complex event. Below we describe some of the most frequent events related with tissue/organ shape changes, with special focus on the formation of the zebrafish OC.

5.1 Programmed cell death

Programmed cell death is an essential mechanism during development. Eliminating cells produced in excess induces the reorganization of the surrounding ones, generates force or releases tension among others and allows for the acquisition of specific shapes. A classic example of programmed cell death needed for the latter purpose is the formation of digits during limb development in vertebrates, in which the interdigital cells need to disappear to separate the different digits (Monier and Suzanne, 2015, Suzanne and Steller, 2013). Another example is the dorsal closure of the *Drosophila* embryo in which amnioserosa cells die inducing shape changes in their neighbors and creating pulling forces (Monier and Suzanne, 2015, Suzanne and Steller,

2013). In contrast to what happens in chicken or mouse (Trousse et al., 2001), previous studies have shown that cell death has no notable contribution to zebrafish eye morphogenesis (Li et al., 2000b, Cole and Ross, 2001). From 12 to 30 hpf only few apoptotic cells are detected in the eye with no specific pattern. Cole and Ross (2001) suggested that this apoptotic cells would serve as a way to generate space needed for reorganization in a very cohesive tissue such as the OV. Later, around 36 hpf the apoptotic rate increases coinciding with the development of the projection of retinal ganglion cell axons. In this case, cell death seems to generate space needed for the axons to cross the NR and form the optic stalk (Cole and Ross, 2001).

Cell death and cell prolifeartion are frequently coregulated, and together they establish the final number of cells in a tissue. In some cases apoptotic cells are able to produce signals to induce proliferation and compensate the loss of cells (Suzanne and Steller, 2013).

5.2 Cell proliferation

Orientation of cell division is a commonly used mechanism for controlling tissue shape change. Elongation of the body axis in several species (Keller, 2006) or the formation of the zebrafish neural tube are examples of such mechanisms. In the second scenario, the cells rotate 90º their mitotic spindle so that one daughter cell is able to cross the midline contributing to the proper formation of the tube lumen (Castanon and González-Gaitán, 2011). Proliferation can also shape a tissue when there is a differential rate at specific locations. This is the case for example of the dorsal portion of the chicken OC, which is larger than the ventral part due to a differential proliferation rate along the dorso-ventral axis of the OC (Trousse et al., 2001).

The role of proliferation in zebrafish eye morphogenesis has been analyzed by several groups, mainly focusing on the NR. During OC folding retinal cells increase the duration of their cell cycle and therefore reduce their proliferation rate (Li et al., 2000b). At 24 hpf eye morphogenesis is completed and the OC is considered fully formed (Li et al., 2000a). From 27 hpf the proliferation rate of retinal cells increases coinciding with the beginning of NR neurogenesis (Li et al., 2000b). Consistent with this data, little change in the volume of the eye is detected *in vivo* between 14 ss and 24 hpf and mitotic figures do not display specific patterns (Kwan et al., 2012). Based on these observations, proliferation is unlikely to have a major impact on eye morphogenesis. Indeed, studies in which proliferation is inhibited by chemical treatments support this idea. When mitosis is impaired zebrafish embryos have smaller but properly shaped and patterned eyes (Cechmanek and McFarlane, 2017, Sidhaye and Norden, 2017, Heermann et al., 2015, Kwan et al., 2012).

Cell cycle kinetics has not been analyzed to the same extent in the RPE. However, RPE and NR have very different behaviors and thus they may present differences in proliferation rates. In

this thesis, we have experimentally addressed this issue and we have studied RPE proliferation to assess its contribution to RPE morphogenesis.

5.3 Cell movements

Individual or collective cell movements are known to be essential for tissue morphogenesis in response to external signals (Aman and Piotrowski, 2010, Locascio and Nieto, 2001). In fish embryos, dynamic movements of eye cells are well-characterized thanks to *in vivo* imaging experiments and fate maps. Rembold et al. (2006) proposed individual cell migration as the motor of OV evagination in medaka fish. Later on, extensive cell-cell intercalation was found responsible for this process in zebrafish (Ivanovitch et al., 2013). Two cell populations can be differentiated in the zebrafish retinal field. First, the more external and basal cells elongate and polarize apico-basally. Subsequently, the remaining cells in the core of the retinal field intercalate among the elongated ones, whilst also polarizing and driving the evagination process. Once this process is completed, and the OVs are formed, additional movements of cells from the brain to the eye extensively contribute to increase volume and cell number in OVs (Cavodeassi et al., 2013, Kwan et al., 2012). Concomitant to the lateral evagination of retinal cells, telencephalic cells converge dorso-medially in response to midline signals, a process mediated by cell adhesion molecules such as Nlcam (Brown et al., 2010). The evagination process is essential for proper eye development since defects in this cell movement, in which retinal cells remain in a medial position, cause the emergence of congenital defects such as cyclopia (England et al., 2006).

The transition from OV to OC involves extensive changes in cell organization and cell shape. Presumptive NR cells are localized in both the inner and the ventral/outer layer of the OV but in the OC all NR cells are restricted to the inner layer (Figure 4A). This is the result of an active process called rim involution or epithelial flow (Sidhaye and Norden, 2017, Heermann et al., 2015, Kwan et al., 2012, Picker et al., 2009, Li et al., 2000a). The prospective NR cells in the ventral region of the outer layer generate basal lamellipodia to attach to the ECM and migrate into the inner layer through the rim (Sidhaye and Norden, 2017; Figure 4B). This is accompanied by a reduction in volume and cell number of the outer layer and by the corresponding increase in the inner layer (Kwan et al., 2012, Li et al., 2000b). If rim movements are impaired, NR cells accumulate in the outer layer and the eye acquires an aberrant shape particularly in the ventral region. It has been proposed that rim involution may occur in other vertebrates and even organoids since a rim is always formed during OC folding (Heermann et al., 2015). However, so far, cell movements similar to rim involution have not been described in other species. Furthermore, in mouse/human organoids rim cells' behavior seems different. These cells undergo both apical and lateral constriction, mediated by actomyosin and calcium,

which reinforce OC folding (Okuda et al., 2018, Eiraku et al., 2011; Figure 4E).

5.4 Cell shape changes

The shape of a cell depends on the combination of intrinsic and extrinsic forces. Intracellular components exert forces on the plasma membrane and among them the cytoskeleton is a major player. Adhesion to neighboring cells and the ECM also generate forces that together with the cytoskeleton determine cell shape (Paluch and Heisenberg, 2009). In the zebrafish eye, both RPE and NR cells undergo shape changes in which cytoskeleton and adhesion complexes play a central role.

NR shape changes

During zebrafish OC invagination NR cells change their columnar-like morphology into a cone-like shape (Figure 4C) as a consequence of a basal constriction (see below). The apical area of NR cells is enlarged while the basal area is reduced (Sidhaye and Norden, 2017). When the total perimeter of the NR is analyzed, the apical perimeter significantly increases whilst the basal perimeter remains constant (Nicolas-Perez et al., 2016). Total NR basal area, however, suffers a 4.7 fold increase, mainly due to rim movements and cell proliferation (Heermann et al., 2015). The thickness or the A-B length of the NR layer is maintained over time (Nicolas-Perez et al., 2016), something that does not happen in other vertebrates. In chicken, the neuroepithelium has also a pseudostratified organization but NR cells elongate during OC folding (Hilfer, 1983).

RPE shape changes

The remaining cells of the outer layer will form the RPE and undergo complex shape changes. At OV stages, RPE cells are organized as a pseudostratified epithelium as the rest of the retinal progenitors, but soon they reorganize as a monolayer, in which all nuclei are aligned and the length of their A-B axis is reduced to become cuboidal. RPE cells continue to reduce their A-B length until they become flat, squamous cells (Li et al., 2000a; Figure 4D). Cell flattening is coupled with a general tissue spreading for finally cover the whole apical surface of the NR (Cechmanek and McFarlane, 2017; Figure 4D). Thus, in zebrafish the A-B axis of the RPE is reduced while maintained constant for the NR. Cuboidal cells represent an intermediate shape in the zebrafish RPE but the final RPE shape in amniotes (Bok, 1993). In chicken and mouse, RPE cells form a monolayer of cuboidal cells reducing the initial A-B length of the pseudostratified epithelium of the OV (Hilfer, 1983).

Mechanical properties coupled with shape changes in eye cells

Shape changes in NR cells occur as a consequence of basal constriction. This constriction is actomyosin mediated (Nicolas-Perez et al., 2016) and also depends on the formation of focal adhesions with the ECM (Bryan et al., 2016, Martinez-Morales et al., 2009). In medaka fish there is polarization of integrins location, a key component of focal adhesions. Integrins are accumulated in the basal membrane of NR cells where the transmembrane protein Opo (Ojoplano) blocks their endocytosis through the inhibition of Numb and Numb-like receptors (Bogdanović et al., 2012b). In zebrafish the ECM protein Laminin1 was also shown to contribute to the formation of NR focal adhesions and to the basal constriction process (Bryan et al., 2016, Nicolas-Perez et al., 2016). Apart from shaping NR cells, the basal constriction of the inner layer is a direct force inducing OC folding (Figure 4C). Its impairment through myosin II, integrin or laminin inhibition results in eyes unable to fold properly (Bryan et al., 2016, Nicolas-Perez et al., 2016, Martinez-Morales et al., 2009). In mouse/human organoids, the NR was also shown as an active motor of OC folding. However, in this model NR cells undergo a reduction of actomyosin in the apical side that generate an apical relaxation and induce the invagination (Okuda et al., 2018; Figure 4E).

RPE shape changes in zebrafish have not been properly studied so far. However, evidence from other organisms suggests that the RPE would contribute to OC folding. In organoids a loss of phospho-myosin light chain levels is detected in the NR, which correlates with a lower stiffness when comparing with the RPE (Okuda et al., 2018, Nakano et al., 2012, Eiraku et al., 2011; Figure 4E). Increased levels of phospho-myosin II in the RPE were also detected in mouse embryos during OC stages, which seems to be induced by Wnt signaling (Carpenter et al., 2015). The observation that the RPE is stiff and the NR flexible led Eiraku et al. (2011) to propose differential mechanical properties between the two layers as a motor for OC folding. It is easy to think that this would also happen in the zebrafish since the squamous morphology could be easily associated with the acquisition of specific mechanical properties. In addition, the absence of the RPE in mouse causes severe defects in OC folding. Mouse *Otx* mutants (*Otx1*$^{-/-}$; *Otx2*$^{+/-}$) have eyes formed by two opposed NRs that result in aberrantly folded OCs (Martinez-Morales et al., 2001).

Based on this data, we decided to explore whether RPE morphogenesis has an active role in zebrafish OC folding. We also considered the alternative possibility in which flattening of the RPE would occur as a consequence of the forces exerted by the surrounding tissues remaining as a passive tissue. Indeed, *in vitro* experiments show that confluent cell monolayers stretch when a force is applied to it in a specific region (Aragona et al., 2013). Besides, the eye neuroepithelium was shown to have a plastic behavior when an external force is applied and maintained through

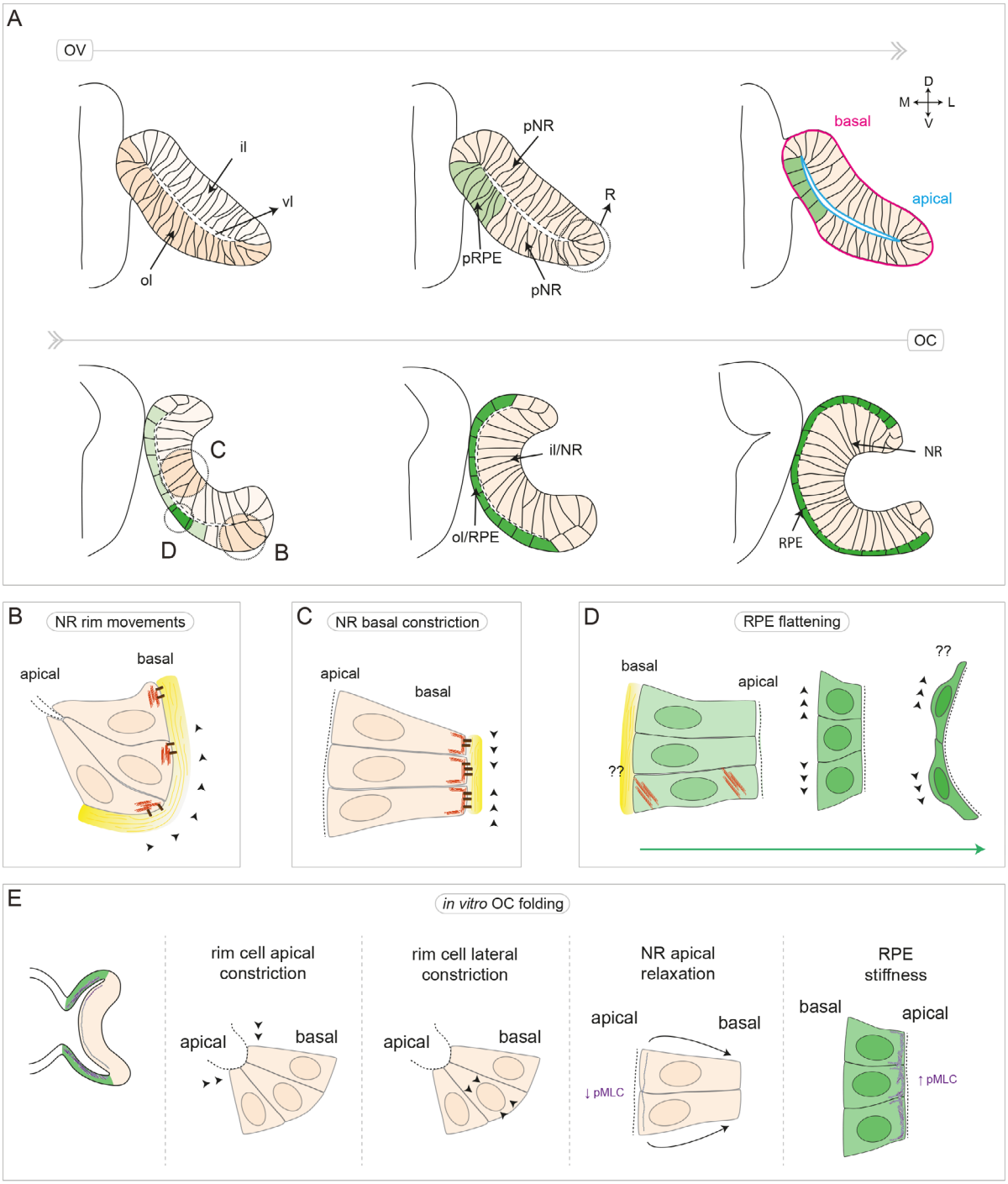

Figure 4: Morphogenetic mechanisms controlling OC invagination.

(A) Schematic diagram of the zebrafish eye at several stages during formation of the OC. Cell polarity and morphology are indicated. **(B)** Detailed diagram of NR cells undergoing rim involution. **(C)** Detailed diagram of basal constriction in NR cells. **(D)** Detailed diagram of RPE shape changes proposed as a force for OC folding. **(E)** Schematic representation of the main processes described for *in vitro* OC formation. Eye populations are color coded: RPE cells are shown in different grades of green and NR cells in light orange tones. Forces are represented with black arrowheads, ECM in yellow, actin in red, myosin II in purple and integrins in brown. Schemes in **A** adapted from Moreno-Marmol et al. (2018).

Abbreviations: il, inner layer; NR, neural retina; OC, optic cup; ol, outer layer; OV, optic vesicle; pMLC, phospho myosin light chain; pNR, presumptive neural retina; pRPE, presumptive retinal pigment epithelium; R, rim; RPE, retinal pigment epithelium; vl, virtual lumen.

time (Okuda et al., 2018). In this thesis, we tried to understand how RPE shape changes happen in zebrafish and to elucidate if they are an active or passive process, mainly using cytoskeletal manipulations.

5.5 Tissue coordination

Acquiring a final shape in complex systems such as a developing embryo is the result of tissue interactions and emerging properties. The events described in the previous section take place simultaneously, while the OC is being formed. The OC is a continuous epithelium formed by different cell types (RPE and NR cells) undergoing very different cell shape changes. It is thus plausible that the three morphogenetic processes described above–cell flattening, rim involution and basal constriction–depend on each other. In addition, the coordinated morphogenesis of the lens, NR and extraocular cell populations may also determine OC shaping. Below, we summarize our current understanding of how these different cell populations interact with one another.

NR basal constriction and rim movements are largely independent mechanisms. In the absence of rim involution no major effect is detected on basal constriction except from a small decrease in actomyosin accumulation. Knockdown of Ezrin, a protein that binds actin to the plasma membrane, impairs the formation of lamellipodia in NR cells; instead, they form blebs and rim involution is perturbed. This leads to the accumulation of NR cells in the outer side of the rim, but RPE and lens formation are normal (Sidhaye and Norden, 2017). Similarly, inhibition of basal constriction does not affect rim involution. Accumulation of NR cells in the outer layer was not found when NR basal constriction did not happen properly (Heermann et al., 2015, Bogdanović et al., 2012b). RPE morphogenesis has been proposed to collaborate with rim involution while flattening and extending (Heermann et al. 2015). However, this possibility still remains unexplored. In contrast to zebrafish, in organoids Okuda et al. (2018) found that rim and inner layer cell behaviors influence one another. NR invagination induces lateral constriction of rim cells, which, in turn, increases global OC folding.

Lens morphogenesis occurs concomitantly to the above described events. Due to its close proximity to the NR, the lens was initially proposed to actively contribute to NR invagination. Supporting this hypothesis, a species-specific physical connection between the two tissues through the formation of fillopodia has been shown (Porazinski et al., 2015, Chauhan et al., 2009). Later, several studies demonstrated that the physical presence of the lens is not necessary for the morphogenesis of the OC (Oltean et al., 2016, Eiraku et al., 2011).

Neural crest cells have been recently involved in OC folding. Nidogen is a component of the ECM of the eye produced by the surface ectoderm and neural crest cells. If neural crest cells

are absent, OC folding is defective, RPE cells are aberrantly positioned and rim involution is delayed (Bryan et al., 2018). These findings suggest that ECM is also important for RPE morphogenesis, although cell shape was not specifically analyzed. As mentioned before, other ECM components such as Laminins have been analyzed during OC morphogenesis. In the absence of Laminins, the RPE undergoes normal morphogenesis (Sidhaye and Norden, 2017, Bryan et al., 2016); however more detailed analysis of the shape of RPE cells is needed.

Intrinsic and extrinsic forces during zebrafish RPE morphogenesis remain mostly unknown. Further analyses regarding the role of cytoskeleton components, ECM or the influence of surrounding tissues including the NR are needed and the hypothesis that RPE morphogenesis is a potential motor for OC folding has not been formally explored.

6. Gene regulatory network controlling RPE specification

The different cellular components involved in the acquisition of a specific cell shape such as cytoskeleton, ECM or adhesion proteins are under the control of transcription factors that confer identity to a cell type. However, this regulation is very complex and we are just beginning to understand it. For instance, in the last years different examples have pointed out that shape changes can also determine gene expression with a feedback mechanism (Gilmour et al., 2017). Understanding the genetic control of RPE shape changes is a long-term goal since the gene regulatory network controlling the specification of this epithelium is still poorly defined. Known RPE determinants are conserved as frequently occurs for developmental processes and, even further, genes associated with eye pigmented cells appear both in vertebrates and invertebrates (Letelier et al., 2017).

The formation of a mature OC is the consequence of a number of inductive events dependent on signaling molecules from surrounding tissues (reviewed in Martinez-Morales, 2016, Fuhrmann, 2010, Martinez-Morales et al., 2004). The three eye-derived populations are characterized by the expression of specific transcription factors, which cross-interact to define the tissues limits. An example is represented by Otx/Mitf in the RPE, Vsx2 in the NR and Vax1/2 in the optic stalk (Figure 5). The current data regarding the inductive signals that establish this pattern is mostly derived from mouse and chicken studies with a surprising absence of information on what happens in the zebrafish. Therefore, here we summarize the process of RPE specification taking into account different species.

The combined expression of Six3, Pax6 and Rx genes in the anterior neural plate (Otx2 positive) leads to eye field specification (Sinn and Wittbrodt, 2013). These transcription factors are maintained until OV to OC transition, when specific RPE, NR and optic stalk genes start

to be detected. The main sources of signaling molecules controlling this patterning process are the extraocular mesenchyme, the surface ectoderm and the central nervous system midline (Martinez-Morales, 2016).

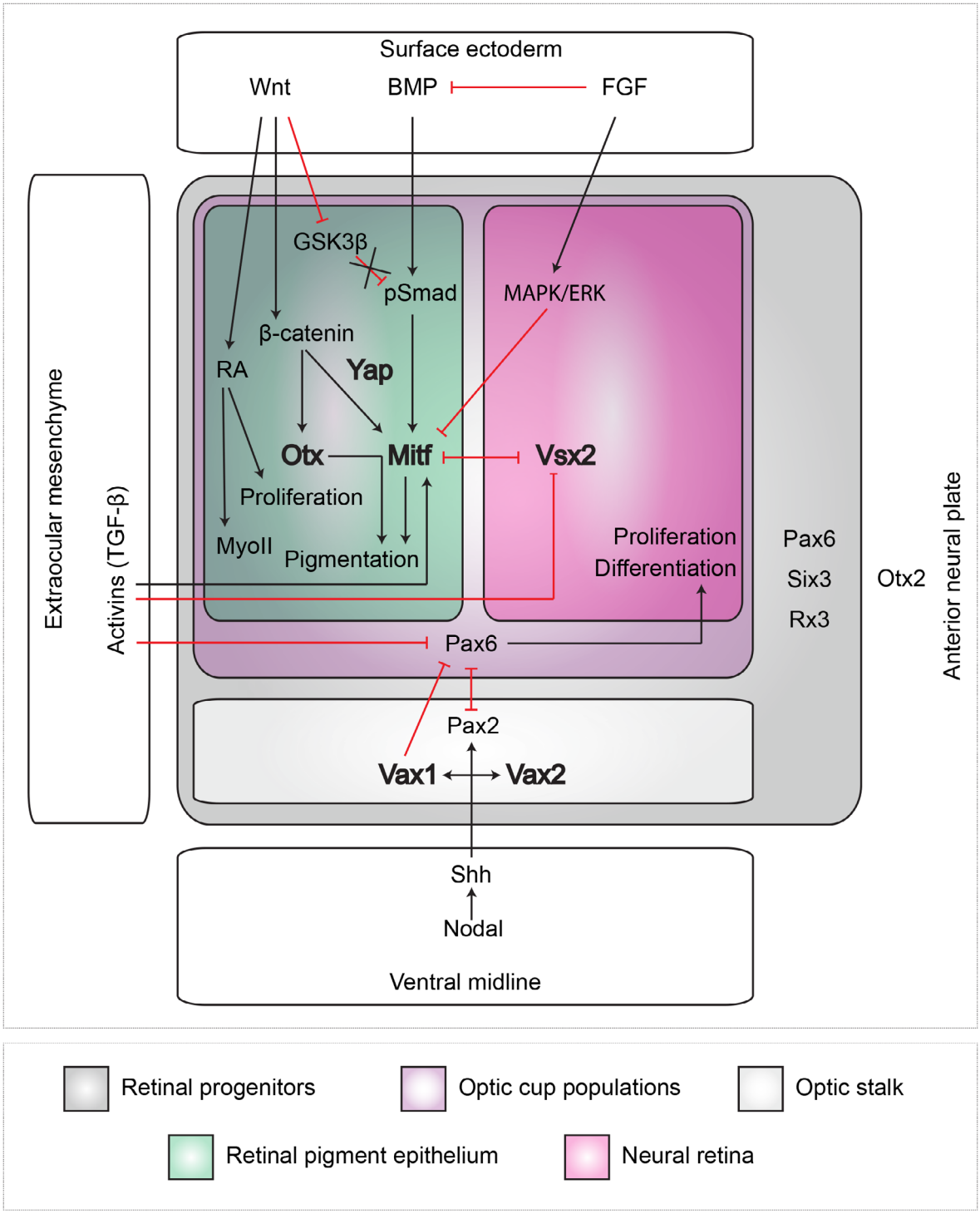

Figure 5: Gene regulatory network controlling the specification of the different eye domains.
The main tissues and signaling pathways involved in eye patterning are represented in color coded boxes.

The optic stalk becomes specified in the most medial position due to midline signaling. Shh is released from midline cells and induces the expression of Pax2 and Vax1/2 that impose optic stalk identity (Take-uchi et al., 2003). Pax2 in the optic stalk and Pax6 in both RPE and NR inhibit each other expression and establish a boundary between the optic stalk and the two populations of the OC (Schwarz et al., 2000, Macdonald et al., 1995). Pax2 or Shh inactivation results in a medial expansion of the NR. Besides, Nodal signaling acts at the midline upstream of Shh (Take-uchi et al., 2003, Rebagliati et al., 1998).

The surface ectoderm from which the lens will form has been proved essential for NR specification. The lens releases FGF molecules that favor NR over RPE identity through the activation of the *Vsx2* gene and suppression of *Mitf* (Hyer et al., 1998, Pittack et al., 1997, Horsford et al., 2005, Nguyen and Arnheiter, 2000). Both in chicken and zebrafish FGF sources act as trigger for the beginning of retinal neurogenesis (Martinez-Morales et al., 2005). FGF activity seems to activate MAPK/ERK pathway in the NR (Galy et al., 2002) and at later stages the NR itself produces FGF for the maintenance of *Vsx2* expression (Müller et al., 2007). Pax6 controls different processes including NR neurogenesis (Philips et al., 2005, Schwarz et al., 2000).

Studies in chicken indicate that the surface ectoderm is also a source of BMP and Wnt molecules that are essential for RPE specification. Wnt signaling stabilizes the BMP mediator Smad through the inhibition of GSK3β so that both signals together induce RPE fate. Indeed, when expressed in the NR, they change its fate to RPE (Steinfeld et al., 2013, Steinfeld et al., 2017). In mouse, Wnt has been involved in RPE specification through β-catenin by directly promoting both *Otx* and *Mitf* expression (Fujimura et al., 2009). Wnt signaling from the surface ectoderm also induces the production of Retinoic Acid in the RPE, promoting proliferation and production of myosin, which contributes to OC folding (Carpenter et al., 2015). The cooperation of Pax6, β-catenin and Mitf regulates the expression of pigmentation genes (Fujimura et al., 2015). Activins (members of the TGF-β family) generated by the extraocular mesenchyme (Fuhrmann, 2010) are also involved in the induction and repression of *Mitf* and *Vsx2* expression in the RPE, respectively. Wnt inactivation is instead necessary for RPE maturation, so that β-catenin does not enter the nucleus and accumulates in the tight junctions. At these late stages, the primary cilium collaborates to suppress Wnt signaling, thus leading to cell cycle exit, and contributes to RPE maturation (May-Simera et al., 2018). In addition, BMP produced in the RPE or in the extraocular mesenchyme helps to maintain *Mitf* expression (Müller et al., 2007) and *Pax6* is down-regulated.

As a consequence of all these inductive events, *Otx* and *Mitf* become expressed in the RPE. These two genes are considered as the core genes in RPE specification since the corresponding

mouse mutants do not develop a proper RPE, showing instead eyes with two confronted NR (Martinez-Morales et al., 2001, Nguyen and Arnheiter, 2000).

Mitf is basic helix-loop-helix transcription factor that regulates the expression of pigmentation genes as well as microRNAs important for RPE differentiation (Adijanto et al., 2012, Lister et al., 2001, Nguyen and Arnheiter, 2000). Two *mitf* orthologs are found in the zebrafish, *mitfa* and *mitfb*. The combined expression of *mitfa/b* matches the distribution found for the several isoforms that exist in mammals (Bharti et al., 2008, Lister et al., 2001). In medaka there are also two *mitf* genes and one of them also generates several isoforms (Li et al., 2014). Zebrafish *mitf* genes are both expressed in the RPE but, *mitfa* is also expressed in neural crests cells and *mitfb* in the pineal gland. *mitfa* product has higher similarities with the mammalian M isoform (characteristic of pigmented cells) while *mitfb* product is more similar to the A isoform (RPE enriched), specifically in the N-terminus region (Lane and Lister, 2012). Although *mitf* expression pattern is maintained across species, the relevance of Mitf functions in RPE specification in the zebrafish is unclear, since this epithelium develops properly in absence of *mitfa* and *b* (Lane and Lister, 2012).

MITF interacts with OTX2 at the protein level in mouse RPE cells. OTX2, as MITF, is also able to activate the transcription of melanogenic genes (Martinez-Morales et al., 2003). In zebrafish there are three *otx* genes *otx1*, *otx2a* and *otx2b*. As already mentioned, mouse $Otx1^{-/-}$; $Otx2^{+/-}$ mutants show an absence of the RPE which acquires instead NR fate, originating an ectopic NR (Martinez-Morales et al., 2001). However, similarly to what happens with *mitfa/b*, *otx* knockdown in zebrafish causes a less severe phenotype. Of the three *otx* genes, *otx2a* and *otx2b* seem to be the most relevant to RPE formation. *Otx* morphant embryos lack the ventral RPE with a consequent failure of optic fissure closure (Lane and Lister, 2012). Moreover, while in mouse *Otx* and *Mitf* gene expression is interdependent (Martinez-Morales et al., 2001, Nguyen and Arnheiter, 2000), in zebrafish *mitfa* and *b* double mutants the expression of *otx* genes is normal (Lane and Lister, 2012). This observation suggests that the role of these genes is not fully conserved in zebrafish, in which Otx would have a more prominent role in RPE specification.

More recently, *yap* and *taz* have also been found to be critical for RPE specification (Kim et al., 2016, Miesfeld et al., 2015). Yap and Taz are transcriptional regulators whose activity is modulated by mechanical inputs and controls diverse cellular processes, including mechanical cell properties (Totaro et al., 2018). In *Yap* conditional mouse mutants, the prospective RPE layer develops as an ectopic NR and the expression of *Otx2* is not detected (Kim et al., 2016). In zebrafish *yap* and its paralog *taz* have been proposed to control RPE specification (Miesfeld et al., 2015). Loss of Yap/Taz leads to a partial loss of the RPE. This is a cell-autonomous function,

given that embryonic transplanted cells null for *yap* and *taz* cannot contribute to RPE formation. Complementarily, ectopic expression of *yap* in the NR produces pigmented cells (Miesfeld et al., 2015).

The development of an ectopic NR in mutants lacking either MITF, OTX or YAP activity is observed in mouse and chicken (Kim et al., 2016, Martinez-Morales et al., 2001, Nguyen and Arnheiter, 2000), and highlights the early potential of the OV progenitor cells to give rise to the RPE, NR or optic stalk. In vertebrates this plasticity is lost in the adult, although in amphibians mature eyes, differentiated cells are able to switch their fate during healing processes (Del Rio-Tsonis and Tsonis, 2003). Contrary to what is found in mouse and chicken, loss of function of these RPE determinants in zebrafish does not result in an ectopic NR suggesting an early divergence between populations in this species.

Further studies are needed to complete the gene network involved in RPE specification. Moreover, how these RPE specification genes ultimately control the activity of cytoskeleton and adhesion dynamics modulators during morphogenesis is largely unknown.

OBJECTIVES

The main goal of this thesis work was to expand our understanding of RPE morphogenesis. Based on the current knowledge on eye morphogenesis we hypothesize that RPE shape changes actively contribute to the acquisition of the eye final shape. We intended to assess the validity of this hypothesis, as well as to identify new members of the gene regulatory network behind RPE specification. For this purpose, we first needed to develop a number of genetic tools. Therefore our specific objectives were:

1. Generate genetic tools to address RPE development.
2. Define the changes in cell shape accompanying RPE morphogenesis and determine how they may influence OC folding.
3. Identify and characterize new members of the gene regulatory network controlling RPE specification.

MATERIALS AND METHODS

1. Maintenance of zebrafish lines

Adult zebrafish (*Danio rerio*) were maintained under standard conditions as previously described (Westerfield, 1993) at 28ºC on 14 h-light/10 h-dark cycles. AB/Tübingen lines were used both as wild type fishes and as background to generate the different transgenic and mutant lines. Zebrafish embryos and larvae were kept in E3 medium (5 mM NaCl, 0.17 mM KCl, 0.33 mM $CaCl_2$, 0.33 mM $MgSO_4$) supplemented with Methylene Blue (Sigma) also at 28ºC. They were staged according to somite number and morphology (Kimmel et al., 1995; Figure 6). The transgenic and mutant lines used in this work are summarized in Table 1.

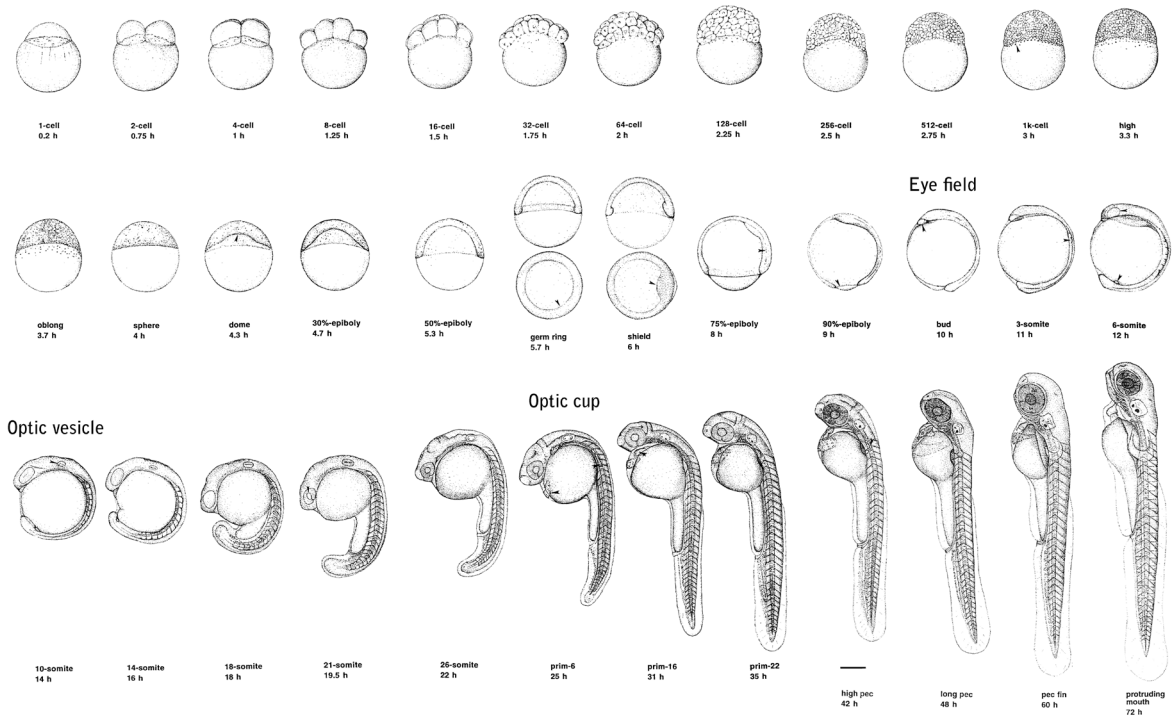

Figure 6: Stages of embryonic zebrafish development.

Diagram representing zebrafish at different stages comprised between the one cell and 72 hours stage. Key events in eye morphogenesis are highlighted: eye field, optic vesicle and optic cup. The image is adapted from Kimmel et al. (1995).

2. Microinjection of zebrafish embryos

Embryos at one cell stage were manually injected using a microinjector (Narishige) and glass needles prepared by horizontally pulling standard capillaries (filament, 1.0 mm, World Precision Instruments) with a P-97 Flaming/Brown Micropipette Puller (Sutter Instrument Company). A total of 30 pg were injected for vectors, between 50 and 100 pg for mRNA and 300 pg for protein, all in a 1 nl volume. The volume injected was calculated using a graticule (S1 Stage Micrometer, 10 mm/0.1 mm, Pyser Optics). RNAs were injected in the yolk and DNAs and proteins in the cell.

Name	Expression pattern	Generation
Tg(enh1-*bhlhe40*:GFP)	RPE	ZED vector (Bessa et al., 2009)
Tg(*rx3*:GAL4-VP16^{vu271}; UAS:RFP)	Eyes and hypothalamus	(Weiss et al., 2012)
Tg(enh1-*bhlhe40*:GAL4-VP16)	RPE	Tol2kit (Kwan et al., 2007)
Tg(*vsx2.2*:GFP-caax)	Eye progenitors and NR	(Gago-Rodrigues et al., 2015)
Tg(β*actin*:*myl12.1*-GFP)	Whole organism	(Maître et al., 2012)
-/- *bhlhe40* E2	---	CRISPR Cas9
-/- *bhlhe40* E5	---	CRISPR Cas9

Table 1: Transgenic and mutant zebrafish lines used for the experiments presented in this thesis.

3. Generation of the transgenic line enh1-bhlhe40:GFP

The transgenic zebrafish line was generated by Sergio Salgüero, a former member of the laboratory. For this purpose, a genomic map from José Luis Gómez-Skármeta laboratory that shows predictive enhancer and promoter epigenetic marks (Bogdanovic et al., 2012a) was used. The map allowed the identification of different potential regulatory elements of the *bhlhe40* gene, including the promoter and four upstream regulatory sequences (Figure 7A). All the selected regulatory regions are inactive at 80% epiboly but active at 24 hpf indicating that they are potentially involved in the activation of *bhlhe40* expression in the RPE. Each regulatory region was amplified by PCR with specific primers (Table 2) and cloned using the pCR™8/ GW/TOPO® TA Cloning® Kit (Invitrogen). In all cases, the plasmids were check for enhancer insertion in the 3' → 5' direction and then used for Gateway recombination with the ZED vector (Bessa et al., 2009). The Gateway™ LR Clonase™ Enzyme Mix was used for the recombination (Invitrogen). The resulting vectors (Figure 7B) were injected together with the Tol2 mRNA to generate the corresponding transgenic line. As the vector contains a marker for determining transgenesis efficiency (cardiac actin promoter:RFP), larvae with RFP expression in the somites were selected and grew up into adulthood (F0). The adults were individually outcrossed with wild type partners to identify founders. A general analysis of the generated lines was performed using confocal microscopy and the line corresponding to enhancer 1 was selected as the most accurate RPE reporter. From this point, the subsequent generations of the transgenic line were maintained by in-crossing of siblings.

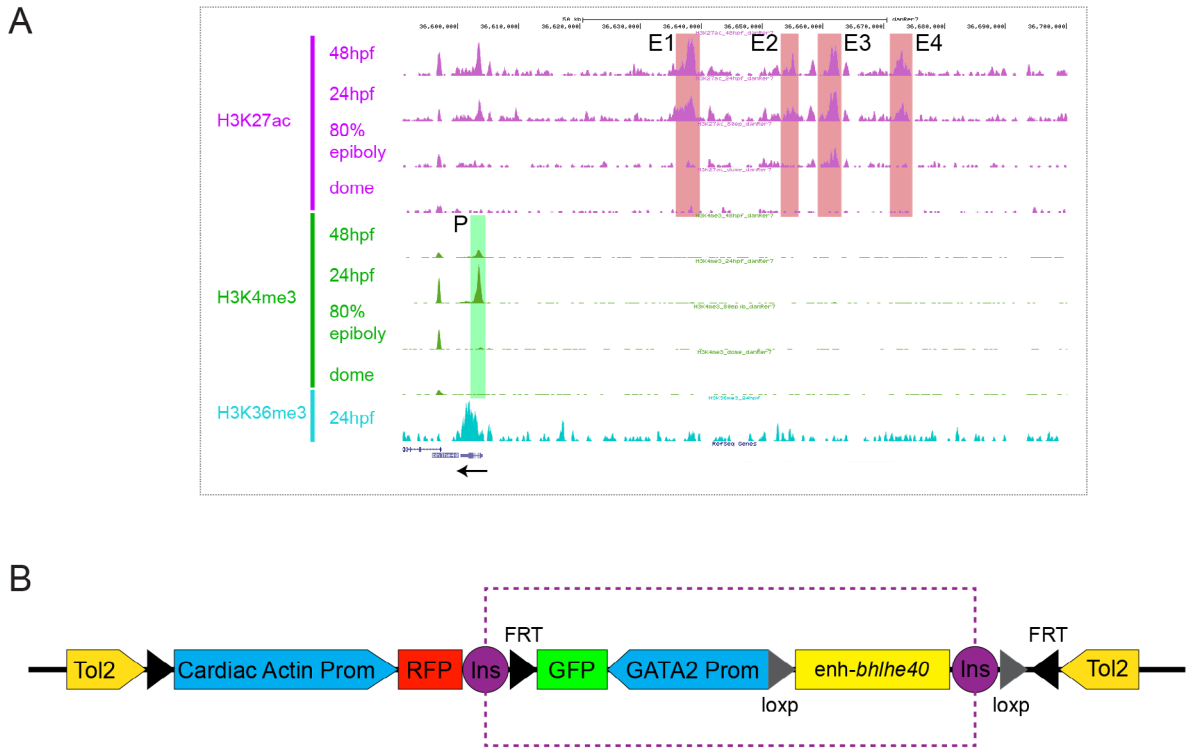

Figure 7: Tools used for the generation of the transgenic line enh1-*bhlhe40*:GFP.

(A) Upstream genomic locus of *bhlhe40* gene (50kb). The black arrow indicates the position and direction of the gene. The first four rows (H3K27ac, purple) show genomic regions that could be potential active enhancers; the next four rows (H3K4me3, green) represent regions that could be active promoters and the last row (light blue, H3K36me3) corresponds to regions transcriptionally active. The promoter (P) and the four selected enhancers (E1 to E4) are highlighted with a box of their corresponding color. **(B)** Diagram of the ZED vector containing *bhlhe40* enhancers. The region boxed with purple dashed line is flanked by two insulators that avoid position effects. Modified from Bessa et al. (2009).

P	Fw- G AATAGGCTGTCCATGTGGTC	Rv- CAAGCCTCAGAAGTAGGACG
E1	Fw- GTGTAAGGGATGGTCAACAGTG	Rv- CAGTTGGGTCAGTTTGAGTTCG
E2	Fw- GCTTGATGTGTGGACGTTAC	Rv- TGTCGCATCACCAGGCTATC
E3	Fw- GTCCTTGCATGTCAGTGTTTAG	Rv- GTAAATCAGCGTTCATCCCAC
E4	Fw- ACACTGTACGCTTATGGGAG	Rv- CCAGAACACCAGGGATAGAC

Table 2: Primers used for the PCR amplification of the regulatory regions tested for the generation of a RPE reporter zebrafish line.

4. Generation of the transgenic line enh1-bhlhe40:GAL4

Using the enhancer 1, we generated the line enh1-*bhlhe40*:GAL4 in which the transcription factor GAL4 is expressed specifically in the RPE. For this purpose we used the Tol2kit (Kwan et al., 2007). We amplified by PCR the enhancer together with the minimal promoter GATA2 from the previously generated ZED vector (Figure 7B) using the following primers: Fw- GTGTAAGGGATGGTCAACAGTG, Rv- AGTGTCCGCGCTTAGAAAATGC. Amplification

was performed with the Expand™ High Fidelity PCR System. The PCR product was inserted in the pSC-A vector from the StrataClone™ PCR cloning kit (Agilent) then digested with BamHI (Takara) and Asp718I (Roche) and subcloned in the p5E-MCS vector (Tol2kit) using the T4 DNA ligase (Roche) and following the manufacturer's protocol. The resulting vector was recombined using the Gateway™ LR Clonase™ II Enzyme Mix with the vectors pME-Gal4VP16, p3-polyA and pDestTol2CG2 (Tol2kit). In this way, we obtained a vector with the construct enh1-*bhlhe40*; GAL4-VP16;polyA flanked by Tol2 sites (Figure 8). Finally, we injected the vector (30 pg) together with Tol2 mRNA (50 pg) in wild type embryos to generate the transgenic line. As the vector has a marker to determine effective transgenesis (*cmlc2*:EGFP), we selected the embryos with GFP expression in the heart to grow them up into adulthood (F0). The adults were individually outcrossed with wild type partners to identify founders among which we selected a founder female. Its progeny was grown up (F1) and from this point, the line was maintained by in-crossing of siblings from the same generation and selection of GFP heart expression.

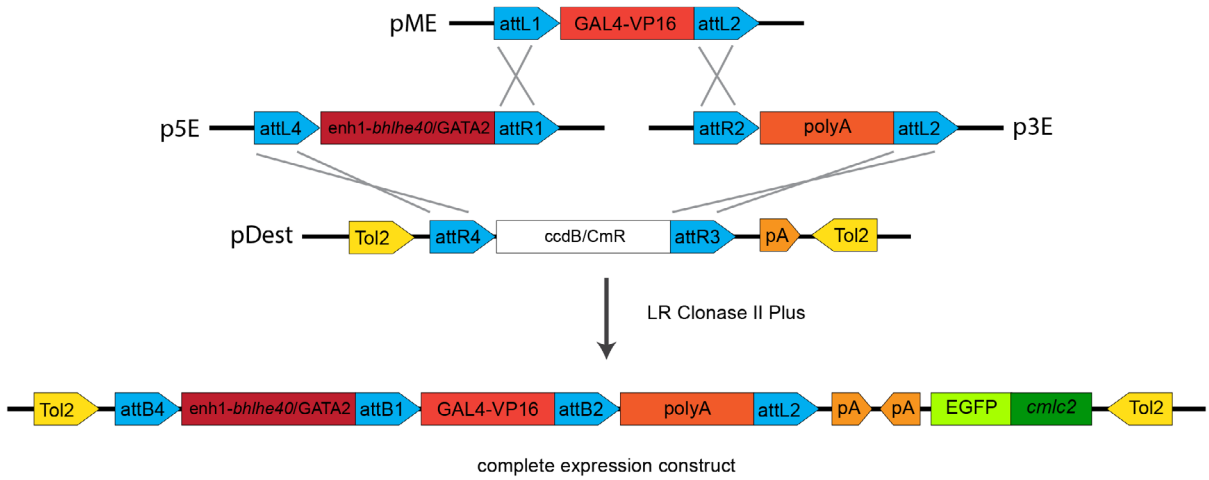

Figure 8: Tol2kit reaction used for the generation of the transgenic line enh1-*bhlhe40*:GAL4.

Diagram of the three different entry Tol2kit vectors (p5E, pME and p3E) and the destination vector (pDest) used for the LR recombination (above) and the resulting construct (below). Tol2 transposase target sites are represented in yellow, recombination sites in light blue (att), the construct in different red tones and the marker for effective transgenesis in green. Modified from Kwan et al. (2007).

5. In vitro transcription

pCS2 vectors containing the corresponding constructs were linearized and transcribed using the mMessage mMachine™ SP6 transcription kit (Invitrogen), following the manufacturer's protocol. The vectors used to obtain mRNA are summarized in Table 3. After transcription mRNAs were purified using the NucleoSpin® RNA Clean-up kit (Machery Nagel) following the manufacturer's protocol.

Plasmid	Generation
pCS2:Kaede	(Ivanovitch et al., 2013)
pCS2:EB3-GFP	Gift from Clare Buckley (Buckley et al., 2013, Stepanova et al., 2003)
pCS2:H2b-RFP	(Cavodeassi et al., 2013)
pCS2:*bhlhe40*	Generated for this work (see below)

Table 3: pCS2 vectors used for mRNA generation.

6. Cryosectioning

Zebrafish embryos at the corresponding stage for each experiment or after *in situ* hydridization (ISH) were fixed with 4% (w/vol) paraformaldehyde (PFA, Merck) in 0.1 M phosphate buffer overnight at 4ºC or 20 min at room temperature (RT), respectively. Then embryos were washed several times in phosphate buffer saline (PBS) 1X, dechorionated if needed, incubated in 15% sucrose-PBS overnight at 4ºC, embedded in 7.5% gelatin (Sigma) 15% sucrose (Merck), frozen in isopentane (PanReac) between -30 and -40ºC and kept at -80ºC. Cryosectioning was performed with a cryostate (Leica CM 1950) at 20 µm thickness and dried overnight at RT. Sections were processed for immunofluorescence or mounted in Mowiol (Calbiochem).

7. Immunofluorescence

Zebrafish embryos at the appropriate stage were fixed in 4% PFA overnight at 4ºC. Embryos were washed several times in PBS-Triton (PBST, 0.6% Triton X-100 Sigma), dechorionated if needed and washed again. Embryos were blocked in PBST with Fetal Bovine Serum (FBS) 10% for at least 1 h and incubated overnight at 4ºC in primary antibodies (Table 4) diluted in PBST containing 2% FBS. The next day, embryos were washed several times in PBST and incubated overnight at 4ºC in the secondary antibodies and Hoechst (Table 4) diluted in PBST/2% FBS. When immunofluorescence was performed on sections, the incubation with secondary antibodies was performed for 2 h at RT. Then sections were washed several times, nuclei were counterstained for 1 min at RT with Hoechst (Invitrogen) and then washed and mounted in Mowiol (Calbiochem).

8. RNA extraction and cDNA synthesis

Total RNA was isolated using the trizol method. A total of 20 embryos were used to obtain RNA at stage 24 hpf whereas only 5 larvae heads were used to obtain RNA of the 5 days post fertilization (dpf) stage. 500 µl of trizol (Sigma) were added to the embryos or larvae heads

Primary antibodies				
Antigen	Species	Reference	Whole mount dilution	Slice dilution
GFP	Chicken	Abcam (ab13970)	1:1000	1:2000
β-catenin	Mouse	BD Transduction Laboratories (610154)	1:400	1:400
Arrestin3 (zpr1)	Mouse	Abcam (ab174435)	---	1:1000
BrdU	Mouse	Becton Dickinson (347580-B44)	---	1:200
Laminin	Rabbit	Sigma Aldrich (L-9393)	1:200	---
ZO-1	Mouse	Invitrogen (339100)	1:400	---
Secondary antibodies				
Antibody	Species	Reference	Whole mount dilution	Slice dilution
Alexa Fluor 488 anti-chicken	Goat	Thermo Fisher (A-11039)	1:500	1:1000
Alexa Fluor 647 anti-mouse	Donkey	Thermo Fisher (A-31571)	1:500	1:1000
Alexa Fluor 594 anti-mouse	Donkey	Thermo Fisher (A-21203)	1:500	1:1000
TRITC -Phalloidin		Sigma (P-1951) - Stock 0.5µg/µl	1:400	---
Hoechst 33342		Invitrogen (H1399)	1:400	1:1000

Table 4: Antibodies used in the present work.

followed by 10 min incubation at RT. 100 µl of Chloroform (Merck) were added to the samples that were shacked vigorously and again incubated 10 min at RT. Samples were centrifuged at 4ºC and 12000 g for 15 min. The transparent top phase was isolated and 250 µl of isopropanol (Merck) were added, delicately mixed and incubated for 10 min at RT and then centrifuged again at 4ºC and 12000 g for 20 min. The supernatants containing the isopropanol were discarded and the pellets washed with 1 ml of cold 75% ethanol (Merck) and centrifuged at 4ºC and 12000 g for 5 min. The supernatants were discarded and the pellets eluted in 50 µl of RNAse-free water. RNA samples were retrotranscribed to cDNA with the First-Strand cDNA Synthesis Kit (GE Healthcare) following the manufacturer's protocol.

9. Riboprobe synthesis and in situ hybridization (ISH)

otx1 (previously known as *otx1b*) and *mitfa* probes were gifts of Prof. Steve Wilson laboratory (UCL, London UK). *bhlhe40* and *bhlhe41* probes were generated by PCR from 24 hpf cDNA with the primers described in Table 5 using the Expand™ High Fidelity PCR System. Reverse primers included the T3 promoter sequence (grey) to *in vitro* transcribe the PCR product. For *in vitro* transcription, we used T3 RNA polymerase and DIG RNA labelling Mix (Roche) following the manufacturer's protocol. The transcription products were precipitated with LiCl (20 µl transcription reaction, 80 µl H_2O, 10 µl LiCl 5 M and 300 µl ethanol 100%) overnight at -20ºC. The samples were centrifuged at 4ºC and 12000 g for 30 min. The pellets were washed with ethanol 70% and centrifuged at 4ºC and 1200 g for 15 min, dried out and eluted in 15 µl of RNAse free water and 15 µl Ultra-Pure Formamide (Panreac). ISH was performed as previously described (Xu et al., 1994).

Probe	Primers
bhlhe40	Fw- TGCTACGTAAAAGAAAGCGGG Rv- TCCATTAACCCTCACTAAAGGGAATTCGGGAGCTTATTCAGCAGG
bhlhe41	Fw- CCAAAGAAGTCCTGCAGTATC 3' Rv- TCCATTAACCCTCACTAAAGGGAATTCTTTGGGGCTGATGACTTG

Table 5: Primers used for *bhlhe40* and *bhlhe41* probe amplification. T3 promoter sequence is highlighted in orange.

10. Drug treatments

Embryos at the desired developmental stage were manually dechorionated and placed in a 24 Well Cell Culture Plate. The bottom of each well was covered with 100 µl of 1% agarose (Conda) in E3 medium. Each well hosted 15 embryos that were treated with appropriate concentration (Table 6) of the drug diluted in E3 medium (900 µl) to reach the final volume of 1 ml.

Compound	Reference	Concentration of use	Duration of treatment
Blebbistatin	Calbiochem CAS 674289-55-5	100µM	3 hours
Nocodazole	Sigma M1404	10ng/µl	3 hours
Azidobblebistatin	Optopharma	5µM	15 minutes (previous to mount and photoactivate)

Table 6: Chemical compounds used in this work for the inhibition of cytoskeleton components.

11. Confocal imaging

For confocal imaging acquisition, embryos were mounted in 1.5% low melting point agarose (Conda) diluted in E3 medium (for *in vivo* recording) or PBS (for fixed samples). Embryos were viewed mostly dorsally or frontally and occasionally laterally. Images were acquired either with a Nikon A1R+ High Definition Resonant Scanning Confocal Microscope connected to an Inverted Eclipse Ti-E Microscope (20X/0.75 Plan-Apochromat, 40X/1.3 oil Plan-Fluor and 60X/1.4 oil Plan-Apocromat objectives) or with a Zeiss LSM710 Confocal Laser Scanning Microscope connected to a Vertical AxioImager M2 Microscope (40X/1.3 oil Plan-Apochromat, W N-Achroplan 20x/0.5, W Plan-Apochromat 40x/1.0 DIC VIS-IR).

12. Kaede photoconversion

Wild type embryos were injected with Kaede mRNA. Embryos (12 ss) with homogeneous green fluorescence were selected, mounted and visualized under the Nikon AR1+ Confocal Microscope using the 20X objective. A specific z position of the OV dorsal region of each eye/embryo was selected and a round ROI was drawn in the outer layer, corresponding to the position of the RPE progenitors. This ROI was irradiated with the 405 nm laser at 21% of power for 10 loops to switch Kaede emission from green to red fluorescence. Because of confocality, photoconvertion occasionally extended further than the selected plane, so that the tissues present above or below (i.e. skin) also underwent photoconversion. After photoconversion embryos were let develop to OC stage and then fixed (around 30 hpf stage) and analyzed by confocal microscopy.

13. Azidoblebbistatin photoactivation

Azidoblebbistatin (ABleb) was photoactivated with a Zeiss LSM 780 Upright multiphoton FLIM system with a W Plan-Apochromat 20x/1,0 DIC M27 75 mm WD 1.8 mm dipping objective. For each eye a specific ROI was drawn including RPE cells identified by GFP fluorescence. ABleb was activated in the ROIs using 860 nm wavelength and 20 mW laser power (this corresponds to 9-14 $\mu W/\mu m^2$ inside the ROI).

14. Measurement of cell parameters

Cell area

Cell area was measured in a medial position in a total of five cells for each class (progenitor, RPE and NR) corresponding to five different embryos. The contour of the cell was drawn using the segmented line tool in Fiji (Schindelin et al., 2012).

Length of the A-B axis in RPE cells

For each eye the length of the RPE A-B axis was measured in a cell located in the central region of the RPE. For the selected cells a line was manually traced from the basal membrane to the apical one using the straight line tool in Fiji (Schindelin et al., 2012). This was performed in the z position in which the nucleus had its larger surface (Figure 9). Zebrafish embryos develop with a little asynchrony (Kimmel et al., 1995) so that their developmental stage influences the A-B length of RPE cells. To normalize for this asynchrony, the value of A-B length of the irradiated eye was divided by that of the non-irradiated eye. Values above 1 indicate less flatten RPE cells in the experimental eyes. Normalization was performed only when eyes from the same embryo were differentially treated (in Figure 19 and 20); otherwise, the A-B length of only one eye per embryo was measured (in Figure 22). Statistical analyses were performed with IBM SPSS Statistics Version 20.0.

15. Measurement of eye invagination angle

The invagination angle was determined as previously described by Sidhaye and Norden (2017) using manual drawing with the angle tool of the Fiji software (Schindelin et al., 2012). The vertex of the angle was placed approximately in the center of the basal surface of the NR and the vectors were drawn up to the edges of the ciliary margin zone (Figure 9). The angles were measured in the z positions in which the RPE showed the larger effect and in equivalent positions in the controls. Again small variations in the developmental stage affect the invagination angle and therefore angle values were normalized with those of the contralateral non-irradiated eye. Values above 1 indicated folding defects. Normalization was performed when eyes from the same embryo were differentially treated (in Figure 19 and 20); otherwise, the angle of only one eye per embryo was determined (in Figure 22). Statistical analyses were performed with IBM SPSS Statistics Version 20.0.

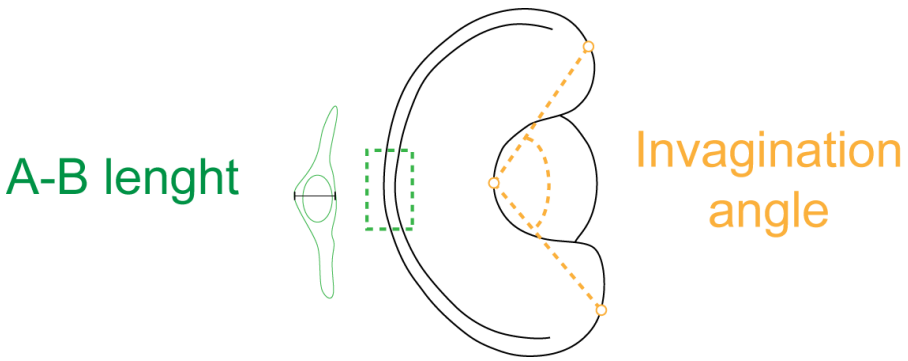

Figure 9: Eye measurements.

Diagram representing how eye invagination angle (yellow, right) and the length of the A-B axis of RPE cells (green, left) were measured.

16. 3D reconstructions

For 3D movies (Movie 2, 3 and 4) we integrated the information from full stacks using the 3D project option in Fiji (Schindelin et al., 2012). RPE surface renderings in Figure 10 were generated using Imaris (Bitplane). Stacks of the eye at different stages (18 ss, 20 ss, 24 hpf and 30 hpf) were directly used for surface rendering with a value of 6 in Surface Area Detail and 7 in Background Subtraction.

17. Quantification of RPE and full eye parameters

All quantifications were performed in collaboration with Mario Ledesma Terrón (David Míguez's laboratory, CBMSO). Unless otherwise specified, image processing and analysis were performed using Fiji (Schindelin et al., 2012).

17.1 RPE quantifications

The GFP reporter of the transgenic line used in this study (enh1-*bhlhe40*:GFP) is not completely specific for the RPE and some fluorescence appears in extraocular tissues. Therefore, we isolated the RPE (green) signal in the movies, using a script that allows to easily isolating 3D structures, which were then manually checked. The movies were processed to remove the noise and the background. For the 16 to 22 hpf Movie (corresponding to the first 60 time points of Movie 2) we used the following routine: first, we applied a median filter with a kernel radius equal to 10 to remove the noise (Arce, 2005); second, we established the background intensity values for each 2D image of the movie using a cutoff value obtained by subtracting the median intensity of the blurred image to the median intensity of the raw image. For the 24 to 37 hpf Movie (corresponding to the Movie 4) we used a slightly different approach: first we applied a median filter with a kernel radius equal to 10 to remove the noise (Arce, 2005); second, we equalized the intensity across the images based on the subtraction of the morphological opened images to the raw images (Hassanpour et al., 2015); and third we determined the background intensity values for each 2D image of the movie using a cutoff value defined as the average intensity plus the standard deviation intensity to extract the foreground values.

The processed images were used to quantify the following parameters, scaling all results with the known parameters in μm of voxel width, voxel height and voxel depth:

- Total RPE volume (μm^3): calculated as the scaled number of voxel with intensity higher than zero at each time point.
- RPE volume in specific regions (μm^3): regions were created using the XY coordinates extracted from the z projection of the first time point and divided equally in seven blocks. After the regions were defined, the volume was calculated as the scaled number

of voxels.

- Total RPE apical surface (μm^2): using the XYZ coordinate for each pixel higher than zero, we did a second order adjustment on the plane YZ to get the points corresponding to the RPE apical surface using the fit function of Matlab© (The Mathworks©, Natick, MA). Subsequently, the size was calculated as the number of scaled pixels of the estimated surface.
- RPE A-B length (μm): all planes were analyzed to select that with the largest area for each time point. In these planes, we extracted the XY coordinates in order to apply a fourth order adjustment using the fit function of Matlab© (The Mathworks©, Natick, MA). The trajectory of each time point was calculated as the total length of the estimated function by the fitting. Finally, the value of the A-B length was obtained by dividing the area with the trajectory and scaling the result.

17.2 Whole eye quantifications

We used the previously processed fluorescent images as a guide to determine and delete the extraocular signal, mainly the hypothalamus in the 16 to 22 hpf Movie and all extraocular nuclei in the 24 to 37 hpf Movie.

Image processing consisted in a median filter to remove the noise (Arce, 2005) and background removal for each 2D image using the median value intensity of each plane as cutoff value. For processing, we used a Gaussian blur filter to remove noise (Arce, 2005), a morphological opening (Serra and Vincent, 1992) and a background removal also using the median value intensity of each plane as cutoff value. Kernel radius value was 10 for both movies. Using the processed movies we quantified the following parameters:

- Eye volume in the 16 to 22 hpf Movie (μm^3): in this case the eye marker is the transgenic line *rx3*:GAL4;UAS:RFP. We calculated the scaled number of voxels with a value higher than zero in each time point.
- Eye volume in the 24 to 37 hpf Movie (μm^3): in this movie there is no specific eye marker but the mRNA of a nuclear marker H2b-RFP was injected before recording. To estimate the volume of the retina, we calculated the convex hull structure of the retina (Jayaram and Fleyeh, 2016), taking into consideration the empty space of the lens, and we calculated the scaled number of voxels with a value higher than zero at each time point.
- Invagination angle (º): we obtained Z projections for each time point and used them to manually calculate the invagination angle as it is explained in the previous section.

18. Proliferation analysis

BrdU (5-Bromo-2′-deoxyuridine, Roche) was resuspended in DMSO (Dimethyl sulfoxide, Sigma) to generate stocks of 50 mg/ml that were kept at -20ºC. Groups of 15 embryos of stages comprised between 16 ss and 48 hpf were dechorionated and placed in BrdU solution (5 mg/ml in E3 medium) for 30 min on ice. Afterwards, the BrdU solution was replaced with fresh E3 medium and embryos were let recover at 28ºC for 10 min before fixation in PFA 4% overnight at 4ºC.

Embryos were cryosectioned as previously described and sections were used for inmunolabelling and BrdU detection. Sections were hydrated with PBS 1X during 5 min and incubated in HCl during 40 min at 37ºC. After HCl treatment, each slide was individually rinsed with PBS 1X ten times, and then processed with the described immunofluorescence protocol using anti-GFP and anti-BrdU primary antibodies (Table 4). GFP and BrdU positive cells were manually counted for each section and statistical analyses were performed with IBM SPSS Statistics Version 20.0.

19. UAS vectors

The UAS:*STMN1* and UAS:*ccnd1* vectors were generated from the bidirectional UAS:GFP vector (Kajita et al., 2014, Distel et al., 2010). Both genes were amplified by PCR using specific primers (Table 7) flanked by StuI restriction sites and the Expand™ High Fidelity PCR System. *STMN1* human gene was amplified from the pQTEV-*STMN1* (Addgene #31326) and *ccnd1* zebrafish gene isolated from 24 hpf cDNA. Both PCR products were digested with StuI (Takara) and cloned into the pCS2 vector. They were thereafter isolated together with the polyA sequence of the pCS2 vector by digestion with HindIII and SacII (Takara) and subcloned into the UAS:GFP vector. These vectors (30 pg) were injected together with the Tol2 mRNA (50 pg) to increase efficiency.

Gene	Primers
STMN1	Fw- GGAAAGGCCTATGGCTTCTTCTGATATCCAGGTG
	Rv- GGAAAGGCCTTTAGTCAGCTTCAGTCTCGTC
ccnd1	Fw- GGAAAGGCCTGAGGCAGCAAAAAGCATCCAC
	Rv- GGAAAGGCCTCTCGGTCATCAAAGCCACAG

Table 7: Primers used for *ccnd1* and *STATHMIN* cloning. StuI restriction sites are highlighted in orange.

20. CRISPR

bhlhe40

CRISPR-Cas9 technology was used for the generation of the exon2 (E2) and exon5 (E5) *bhlhe40* mutants. The two mutants were not generated at the same time and therefore the strategies used to design and synthesize the guides were different (Table 8), according to the constant updates of this technique.

Exon	Software for design	Guide sequence	Modifications
2	CRISPR Design tool based on Hsu et al. (2013) algorithm http://www.genome-engineering.org/crispr/	GGGAGGAATGAAGCGCAGTGAGG	Addition of GG in 5'
5	CRISPRscan (Moreno-Mateos et al., 2015)	GGTCCACTTGTGCGCCAAGGAGG	Substitution of the second base pair T > G
Exon	Ordered oligos		
2	**Oligo 1-** TAGGGAGGAATGAAGCGCAGTG **Oligo 2-** AAACCACTGCGCTTCATTCCTC		
5	**Oligo A-** TAATACGACTCACTATAGGTCCACTTGTGCGCCAAGGGTTTTAGAGCTAGAA **Oligo B-** AAAAGCACCGACTCGGTGCCACTTTTTCAAGTTGATAACGGACTAGCCTTATTTTAACTTGCTAT TTCTAGCTCTAAAAC		

Table 8: Guides sequence and synthesis strategy followed for the different *bhlhe40* exons. PAM sequence is highlighted in yellow and guide modifications in green. For E2 oligos the protuberant ends are highlighted in dark red. For E5 oligos T7 promoter sequence is highlighted in light blue and the complementary region between oligo A and oligo B in dark blue.

For the synthesis of the E2 guide we first aligned oligo 1 and 2 (Table 8). We mixed 1.5 µl of each oligo at 100 µM with 23 µl of H_2O and 24 µl of annealing buffer (10 mM Tris pH 7.5-8.0, 50 mM NaCl, 1 mM EDTA). The resulting mix was heated at 95ºC for 5 min in a hot water bath and then cooled to RT. At the same time, the pDR274 vector (Addgene #42250) was linearized overnight at 37ºC using BsaI enzyme (NEB), the extent of linearization was determined in a 0.8% agarose gel and the band was purified using the NucleoSpin® Gel and PCR clean-up kit (Macherey-Nagel). Annealed oligos and linearized pDR274 were ligated overnight at 16ºC using T4 DNA ligase (Roche). The resulting vector was linearized with HindIII (Takara) and transcribed *in vitro* using the MAXIscript™ T7 Transcription Kit (Invitrogen) following the manufacturer's protocol. For the synthesis of the E5 guide we followed the protocol described by Varshney et al. (2015). Oligo A and B (Table 8) were annealed and extended to generate a template used for *in vitro* transcription. The transcription products were precipitated with

LiCl (20 µl transcription reaction, 2 µl EDTA 0.5 M, 30 µl LiCl 5 M and 200 µl ethanol 100%) overnight at -20ºC. The samples were centrifuged at 4ºC and 12000 g for 30 min. The pellets were washed with 70% ethanol centrifuged for 15 min at 4ºC and 12000 g and finally dried out and eluted in 20 µl of RNAse free water.

The guides were injected in wild type embryos (50 pg) with EnGen Cas9 NSL protein (NEB, 300 pg). A volume of 1 nl was injected in each embryo. Some F0 embryos were used to check guide efficiency using the CRISPR-STAT method (Carrington et al., 2015) whereas the rest were let develop. The CRISPR-STAT method allows detecting small insertions or deletions (indels) in short DNA sequences (up to 300 bp). First the gDNA is extracted, either from a pool of embryos or from fin clipping, and then the region where the mutation has been designed is amplified using three different primers (Table 9). The first is the M13 Fw primer tagged with the FAM fluorochrome, the second is a specific Fw primer complementary to the genome with the M13 Fw sequence at the 5' end and the third is a specific Rv primer complementary to the genome with a pig-tailed sequence at the 5' end, which is designed to avoid replication errors. Once the F0 reached sexual maturity they were individually outcrossed with wild type fishes to identify founders. Eggs resulting from the outcrosses were also analyzed by the CRISPR-STAT method. One fish for each mutant was used to raise the following generation (F1). F1 fishes were subjected to fin clipping and CRISPR-STAT analysis to identify heterozygous individuals. They were incrossed and the F2 generation was raised. Fin clipping and CRISPR-STAT analysis were also used to identify homozygous fishes, which were used to generate the embryos analyzed in this thesis.

Exon2	**FAM-** 6FAM-TGTAAAACGACGGCCAGT **Fw-** TGTAAAACGACGGCCAGTACGCGACGCAGTTCTCTTAT **Rv-** GTGTCTTGCAAATTGCGCACTTGTTTA
Exon5	**FAM-** 6FAM-TGTAAAACGACGGCCAGT **Fw-** TGTAAAACGACGGCCAGTTGCGCAACACAAAGAATGAT **Rv-** GTGTCTTGCCACTTTTTGAAGGTGCTC

Table 9: Primers used to amplify a fragment containing the sequence were the *bhlhe40* guides would cut for its analysis by CRISPR-STAT method. M13 Fw primer sequence is highlighted in dark blue and pig-tail sequence in dark green.

bhlhe41

CRISPR technology was also used to generate a *bhlhe41* knockout zebrafish line. Several guide RNAs against this gene were designed and analyzed for their efficiency using the CRISPR-STAT method (Table 10). Unfortunately, none of them was able to drive efficient Cas9 mediated breaks *in vivo*.

Guide	Exon	Software for design	Guide sequence	Modifications
1	1	CCTop (Stemmer et al., 2015)	GGTCTGGATCACGCGGATTTCTTGG	Addition of GG in 5′
2	1	CCTop (Stemmer et al., 2015)	GGCTGGATCACGCGGATTTCTTGGG	Addition of GG in 5′
3	2	CCTop (Stemmer et al., 2015)	GGTCTACATGTGCAAATCCAAAAGG	Addition of GG in 5′
4	2	CCTop (Stemmer et al., 2015)	GGTCTCTCTTCATCCCCCTTTTGG	Addition of G in 5′ Substitution of the first base pair C > G
Guide	Exon	Ordered oligosA		
1	1	TAATACGACTCACTATAGGTCTGGATCACGCGGATTTCTGTTTTAGAGCTAGAA		
2	1	TAATACGACTCACTATAGGCTGGATCACGCGGATTTCTTGTTTTAGAGCTAGAA		
3	2	TAATACGACTCACTATAGGTCTACATGTGCAAATCCAAAGTTTTAGAGCTAGAA		
4	2	TAATACGACTCACTATAGGTCTCTCTTCATCCCCCTTTGTTTTAGAGCTAGAA		
CRISPR STAT primers				
FAM- 6FAM-TGTAAAACGACGGCCAGT **Fw-** TGTAAAACGACGGCCAGTGAATATCGAGAATGCAGAACAG **Rv-** GTGTCTTTCACGTTTTCATCACGGGTC				

Table 10: At the top guides sequence and synthesis strategy followed for the different guides against *bhlhe41* gene. PAM sequence is highlighted in yellow, guide modifications in green, T7 promoter sequence in light blue and the complementary region between oligoA and oligoB in dark blue. At the bottom the primers used to amplify a fragment containing the sequence were the guides would cut for its analysis by CRISPR-STAT method are indicated. M13 Fw primer sequence is highlighted in dark blue and pig-tail sequence in dark green.

21. mitf MO

MO against *mitfa* and *mitfb* used for knockdown experiments in the *bhlhe40* mutants were gifts from Prof. James A. Lister laboratory (Virginia Commonwealth University, USA):

MO *mitfa*: CATGTCAACTATGTGTTAGCTTCA (translation blocking)

MO *mitfb*: CGGGATCTGCCACACACAGACCAAC (splice-blocking)

22. Overexpression of bhlhe40

cDNA from 24hpf embryos was used as substrate for PCR amplification of the *bhlhe40* gene with the following primers and the Expand™ High Fidelity PCR System: Fw-ATGGAGAGGATTACCAGTGCT, Rv- TTCGGGAGCTTATTCAGCAGG. The PCR product was cloned into the pSC-A vector from the StrataClone™ PCR cloning kit (Agilent) following

the manufacturer's protocol. The construct was digested with EcoRI and subcloned in the pCS2 vector using T4 DNA ligase (Roche). The resulting vector was linearized with SacII (Takara) and *in vitro* transcribed as previously described. *bhlhe40* mRNA (100 pg) was injected at one cell stage.

23. Photolesion

Wild type and *bhlhe40* E2 mutant embryos were collected and maintained in the darkness during five days. At 5 dpf 10 larvae were placed in a 50 ml beaker with 15 ml of E3. A cold light source was placed above the beaker (KL 1500 LCD, Leica) and the entire device was protected from light dissipation with aluminum foil. Light was shinned at the highest intensity for 30 min. Thereafter, the larvae were kept in the dark for two days and fixed with PFA 4% overnight at 4ºC. Larvae were cryosectioned as previously described and sections were used for immunofluorescence using zpr1 antibody (Table 4) and Hoechst for nuclei counterstaining.

24. Semi-quantitative PCR

To analyze *bhlhe41* expression levels in the *bhlhe40* mutants we used cDNA from 24 hpf embryos and 5 dpf larvae heads. We performed a semi-quantitative PCR using the primers for *bhlhe41* probe amplification (Table 5) and specific primers for *actb2* as a control: Fw-GTTGGTATGGGACAGAAAGAC, Rv- CCAGACAGAGTATTTACGCTC. PCR products were analyzed at 25 and 30 cycles.

25. RNAseq

The following experiment was performed in collaboration with Lorena Buono (Juan Ramón Martínez Morales' laboratory, CABD). Retinal progenitors (16 hpf) and RPE cell populations (18 hpf and 23 hpf) were isolated with FACS technology using as markers the GFP expression of the transgenic lines *vsx2.2*:GFP-caax and enh1-*bhlhe40*:GFP. Embryos were dechorionated and subjected to a cell dissociation protocol. Embryos were placed in deyolking tampon (NaCl 55 mM, 1.8 mM KCl, 1.25 mM $NaHCO_3$) and yolks were manually removed by pipetting up and down (800 µl of deyolking tampon per 100 embryos). The samples were centrifuged for 4 min at 4ºC and 300 g. The pellets were resuspended in 1 ml of Danieau's Solution 0.5X (29 mM NaCl, 350 µM KCl, 200 µM $MgSO_4*7H_2O$, 300 µM $Ca(NO_3)_2$, 2.5 mM HEPES buffer) and centrifuged at 4ºC and 300 g for 4 min. The pellets were resuspended in cold FACSMax Cell Dissociation Solution (AMS Biotechnology, 1 ml per 300 embryos). The samples were incubated on ice for 15 min with periodic manual agitation. Samples were then centrifuged for

4 min at 4ºC and 300 g. The pellets were again resuspended in cold FACSMax (500 µl per 300 embryos). 40 µm cell strainers (Falcon) were used to isolate single cells and the resulted solution was used for sorting.

A FACSAria™ Fusion flow cytometer was used with the help of the CBMSO Flow Cytometry facility. Total RNA was extracted with PicoPure RNA Isolation Kit (Thermo Fisher Scientific) according to manufacturer's protocol and then treated with TURBODNAse (Ambion). Libraries were prepared after RiboZero treatment and sequenced with Illumina 2.0 platform in SEx125bps reads. After initial quality check with FastQC software (Andrews, 2014), the obtained sequences were mapped against the zebrafish genome assembly version 10 (danRer10) from the Genome Reference Consortium and analyzed using the bioinformatic pipeline Tuxedo (Trapnell et al., 2012). Genes were considered as differentially expressed (DEGs) at p and q-values < 0.05. The list of differentially expressed transcription factors was extracted from general list of DEGs using the tool "Classification System" of PANTHER (Mi et al., 2013) filtering for the protein class PC00218 (transcription factors). Gene ontology (GO) enriched classes were identified and visualized using the GOrilla tool (Eden et al., 2009) and a single ranked list of DEGs (only up-regulated or only down-regulated) as input.

RESULTS

1. enh1-bhlhe40:GFP is an excellent tool to follow RPE morphogenesis in vivo

The fulfillment of this work needed the development of specific tools that were not available at the beginning. A specific and early zebrafish RPE reporter line was necessary to follow RPE morphogenesis *in vivo*. For this purpose a screening of RPE makers was performed in the laboratory using the ZFIN database (Howe et al., 2013). Among possible candidates, the *bhlhe40* gene became the main focus. *bhlhe40* (Basic Helix-Loop-Helix Family Member E40), also known as *dec1*, *stra13*, *sharp2* or *bhlhb2*, encodes a light and hypoxia-induced transcription factor involved in several processes such as differentiation, proliferation or circadian rhythms (Yamada and Miyamoto, 2005). Its expression is restricted to the RPE at early zebrafish stages (Yao et al., 2006) and a similar distribution is observed also in other organisms, such as the chicken or the mouse. This distribution makes of the *bhlhe40* gene a very suitable marker for the RPE, because there is no interference with the nearby NR and neural tube. Besides, in comparison with other known RPE markers such as *mitf*, *tfec, cx43* or *yap*, *bhlhe40* is among the earliest. Sergio Salgüero, a former member of the laboratory, analyzed *bhlhe40* regulatory regions and identified a specific enhancer that controls the expression of the gene in the RPE. We have called this region enhancer 1, which was used by Sergio to generate the enh1-*bhlhe40*:GFP transgenic line (for detailed information see Material and Methods section 3).

The suitability of the enh1-*bhlhe40*:GFP line was proved comparing GFP distribution with the expression pattern of the *bhlhe40* gene itself and of the *otx1* gene (previously known as *otx1b*), which codifies a transcription factor essential for RPE specification across species (Nishihara et al., 2012, Lane and Lister, 2012, Martinez-Morales et al., 2001). By ISH, both genes are firstly detected in a dorsal region of the OV but with a slight time variation: *otx1* is expressed at 10 ss (Figure 10A,A') whereas *bhlhe40* expression starts around 14 ss (Figure 10B,B'). During the transition between OV and OC the area of expression of both genes narrows laterally (Figure 10C,C') and expands ventrally (Figure 10D,D') to finally become a thin layer covering the NR and corresponding to the entire outer layer of the OC (Figure 10E,E'). The transgenic line enh1-*bhlhe40*:GFP was able to recapitulate the expression of the *bhlhe40* gene when analyzed by *in vivo* monitoring of the most anterior structures in the embryo. We used the previous line combined with an eye reporter line (*rx3*:GAL4;UAS:RFP). GFP expression starts in a discrete group of cells in the dorso-medial region of the OV at the 14-15 ss stage, as occurs with the first cells detected by the ISH for *bhlhe40* mRNA. At this stage, the GFP positive cells have already started to change shape, and during subsequent stages they continue narrowing while expanding both posteriorly and ventrally (Figure 10F, Movie 1, 2 and 3). Finally, GFP

positive cells appear to comprehend the entire outer layer, wrapping around the inner layer (Movie 4). 3D reconstructions of selected embryos show the ventral expansion of the GFP positive territory that eventually covers the whole eye surface (Figure 10G). GFP expression pattern is nicely restricted to the RPE with few exceptions. At OV stages the NR presents a very slight GFP background that quickly disappears. At later stages, once the OC is formed, GFP expression is also activated in the ciliary margin zone (located in the limit between the NR and the RPE), in the pineal gland and in neural crest cells (Movie 1 and 2), as previously reported (Yao et al., 2006).

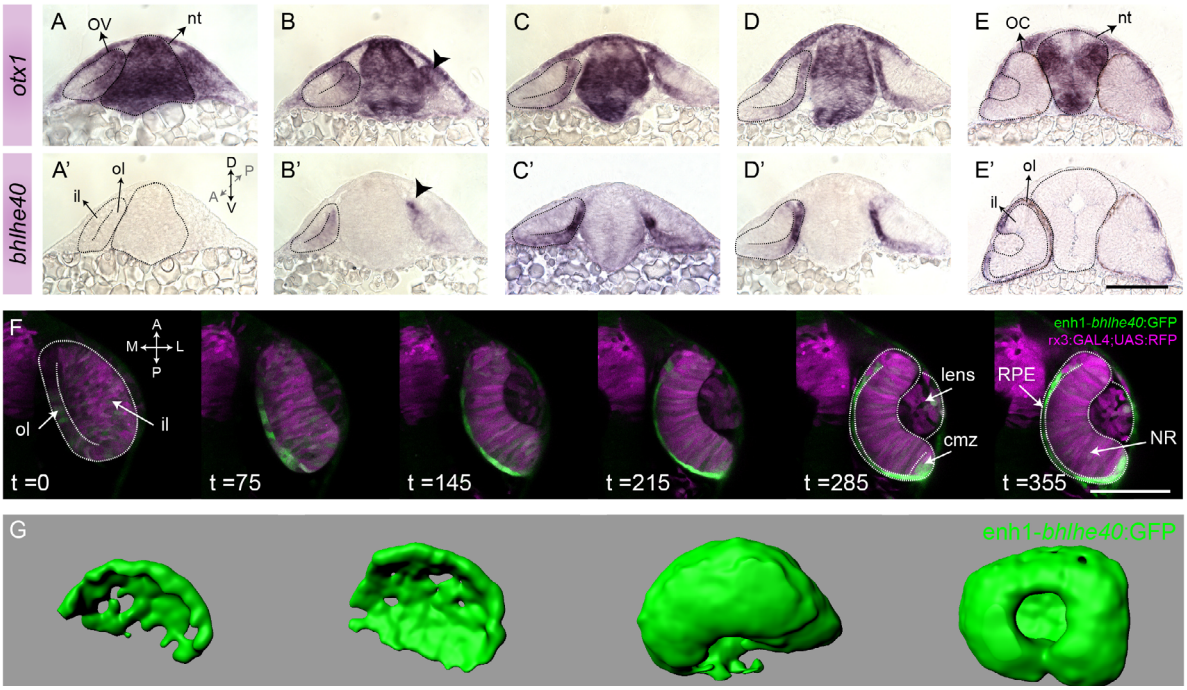

Figure 10: enh1-*bhlhe40*:GFP transgenic line reproduces the *bhlhe40* expression pattern.

(A-E) Frontal cryosections of wild type embryos hybridized *in toto* with *otx1* and **(A'-E')** *bhlhe40* specific probes from 10 ss (OV stage) to 24 hpf (OC stage). Both mRNAs are first detected in the more dorsal region of the outer layer (arrowheads in **B** and **B'**) and the signal expands ventrally while narrowing laterally. **(F)** Time points corresponding to the Movie 1 of a transgenic embryo resulting from the cross of the enh1-*bhlhe40*:GFP (green) and *rx3*:GAL4;UAS;RFP (magenta) lines between OV and OC stages. GFP signal is comparable to the pattern observed in the ISH. **(G)** RPE surface renderings from one eye of the enh1-*bhlhe40*:GFP line at 4 different stages. Black and white dashed lines delineate eye contour and virtual lumen in **A-F** and neural tube in **A, E**.

Abbreviations: cmz, ciliary margin zone; il, inner layer; NR, neural retina; nt, neural tube; OC, optic cup; ol, outer layer; OV, optic vesicle; RPE, retinal pigment epithelium. Scale bars: 100 µm in **A-F** and 50 µm in **G**.

A genetic tool to interfere specifically with RPE development was also desirable for the present work. Given that the enhancer 1 drove GFP expression basically only to the RPE, we used it to generate a transgenic line based on the GAL4/UAS system (enh1-*bhlhe40*:GAL4). This system is widely used in *Drosophila* and in zebrafish to modify gene expression in restricted and specific regions of the animal (Kawakami et al., 2016, Asakawa and Kawakami, 2008) and had been previously and successfully used in the laboratory (Hernandez-Bejarano et al., 2015). GAL4 is a transcription factor that binds the UAS sequence, promoting the transcription of any gene

Movie 1: OV to OC transition of an enh1-*bhlhe40*:GFP (green); *rx3*:GAL4;UAS:RFP (magenta) embryo (related to Figure 10, framerate 1/5min). Dorsal view of one eye from which an unique frame is show.

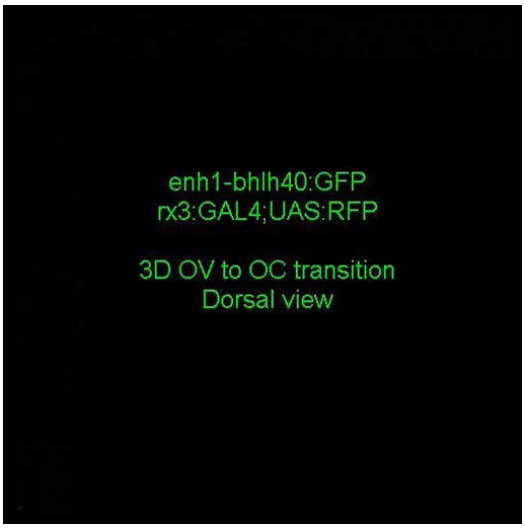

Movie 2: 3D reconstruction of the Movie 1 (framerate 1/5min). Dorsal view of one eye.

Movie 3: 3D reconstruction of the transition between OV and OC of an enh1-*bhlhe40*:GFP (green) in which H2b-RFP mRNA (magenta; nuclei) was injected (framerate 1/5min). Lateral view.

Movie 4: 3D reconstruction of the OC growth after morphogenesis is finished (24 hpf) of an enh1-*bhlhe40*:GFP (green) in which H2b-RFP mRNA (magenta; nuclei) was injected (framerate 1/5min). Lateral view.

located downstream to the sequence. The best efficiency is ideally obtained when two zebrafish lines, one containing a construct that allows GAL4 expression under the control of a tissue specific promoter/enhancer and the other containing the UAS regulatory sequence coupled to the sequence of the gene of interest, are crossed together. This solution is however time consuming. A faster analysis can be obtained by simply generating the GAL4 transgenic line and then using the corresponding embryos as receptors of a UAS vector. If the GAL4 protein is expressed in RPE cells we could express any construct located under a UAS regulatory sequence specifically in this epithelium. Therefore, this tool would offer a number of possibilities for interfering with

RPE development without affecting other eye cell populations. We generated the line using the Gateway system (Material and Methods section 4) and tested it by injecting a bidirectional UAS:GFP vector (Kajita et al., 2014, Distel et al., 2010). This vector drives the expression of GFP in one direction and the expression of a gene of interest in the other. To test the suitability of the generated transgenic line, we first injected a construct that only contained GFP (Figure 11A). Unfortunately, after the injection, we could detect GFP signal not only in the RPE but also in the NR (Figure 11B). This indicates that the enh1-*bhlhe40*:GAL4 line does not conserve the specificity of enh1-*bhlhe40*:GFP (Figure 11C). This could be due to a position effect associated to the region where the GAL4 transgene became inserted or perhaps associated to the lack of insulators at the side of the transgene that instead the enh1-*bhlhe40*:GFP line contains. In any case, the enh1-*bhlhe40*:GAL4 line we generated did not fulfill the initial purpose of being a tool for interfering with gene expression exclusively in the RPE. We therefore decided to use alternative approaches. For specific interference in the RPE we use photoactivable drugs, in addition to the *rx3*:GAL4 transgenic line (Weiss et al., 2012) as an approach to interfere with the retinal cells in general.

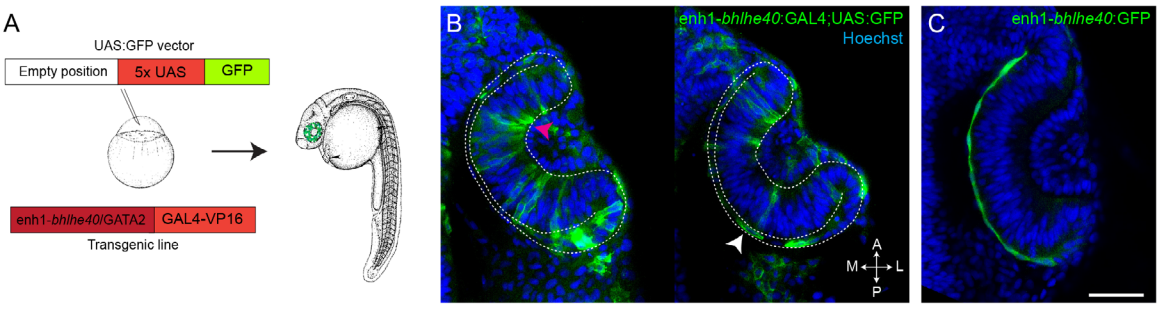

Figure 11: enh1-*bhlhe40*:GAL4 drives GAL4 expression outside the RPE.

(A) Schematic representation of the strategy followed to check the suitability of the enh1-*bhlhe40*:GAL4 line. **(B)** Dorsal view of enh1-*bhlhe40*:GAL4 embryos injected with the UAS:GFP vector. GFP expression is observed in both RPE (white arrowhead) and NR (pink arrowhead). **(C)** Dorsal view of a enh1-*bhlhe40*:GFP embryo. Embryos were fixed at 24 hpf stage and labeled with anti-GFP (green) and Hoechst (blue). White dashed lines delineate eye contour and virtual lumen in **B**. Scale bar: 50 µm.

In conclusion the transgenic line enh1-*bhlhe40*:GFP reproduced precisely *bhlhe40* expression and can be used as a tool to follow RPE *in vivo*. Indeed, we have used it to identify RPE cells in most of the following experiments. At the same time, we discard the enh1-*bhlhe40*:GAL4 line as a useful tool.

2. RPE morphogenesis occurs with no major cell volume changes and contribution of cell division

RPE morphogenesis involves complex changes of the cell shape, which have not been studied in detail before. The enh1-*bhlhe40*:GFP line gave us the opportunity to analyze these cell shape

changes from both a qualitative and quantitative point of view.

Initially, at OV stages all retinal progenitors have neuroepithelial morphology, organized as a pseudostratified epithelium (Figure 12A,A'). From the initial columnar shape, RPE cells start to shorten their A-B axis to form a monolayer of cuboidal cells that occupy the dorsal half of the outer layer of the OC (Figure 12B,B'). From this point on, cuboidal cells keep reducing their A-B axis, becoming more and more flat (Figure 12C,C') until they constitute a squamous monolayer of cells surrounding the whole increased apical surface of the NR. Notably, the cells closer to the rim are the last ones to become squamous. As already mentioned, GFP expression in our reporter line was first detected in the dorso-medial region of the OV, when RPE cells begin to shorten their A-B axis. Previous fate map studies had already indicated this region as the source of RPE progenitors (Kwan et al., 2012, Li et al., 2000a). Photoconversion experiments with the fluorescent protein Kaede (Ando et al., 2002) allowed us to corroborate that this is the origin of RPE cells. Kaede was photoconverted in a group of retinal cells located in the most dorso-medial region (Figure 12D) at the stage of 12 ss, when both layers are equal in thickness and no OV cells have begun to differentiate yet. Then embryos were allowed to develop until 24 hpf when the photoconverted cells were found in the thin outer layer that covers the back of the eye, corresponding to the RPE (Figure 12E).

Analysis of the medial surface of the embryonic eye reveals that both the apical and basal surface of the RPE undergoes a considerable expansion as compared to that of the NR (Figure 12F,G). In isolated eyes of 30 hpf embryos, NR cells present a rounded contour, whereas RPE cells have a polygonal, frequently hexagonal, morphology (Figure 12F',G'). Furthermore, the average area of RPE cells (22 μm^2) is approximately fourfold larger area than that of NR cells (5 μm^2) and retinal progenitors (7 μm^2). This considerable surface increase of each cell accounts for the global expansion of the RPE as a tissue, which can therefore cover the entire NR surface at OC stages. In fact, it has been proposed that RPE cells barely proliferate at this stage (Cechmanek and McFarlane, 2017) and therefore their morphological changes should be sufficient to explain tissue expansion. Detailed analyses of RPE proliferation however have not been performed and there are no quantifications of RPE shape changes. We therefore decided to analyze proliferation and cellular shape changes in the RPE to understand their relative contribution to RPE expansion. To this end, we performed BrdU incorporations and quantified several parameters during *in vivo* RPE development.

To analyze the proliferation rate of RPE cells, we performed BrdU incorporation studies in enh1-*bhlhe40*:GFP embryos from 16 ss to 48 hpf in which we manually counted the total number of RPE cells (GFP positive) and the number of proliferating RPE cells (GFP positive and BrdU positive). For each stage 5 eyes from 5 different embryos were used. The reliability of our data

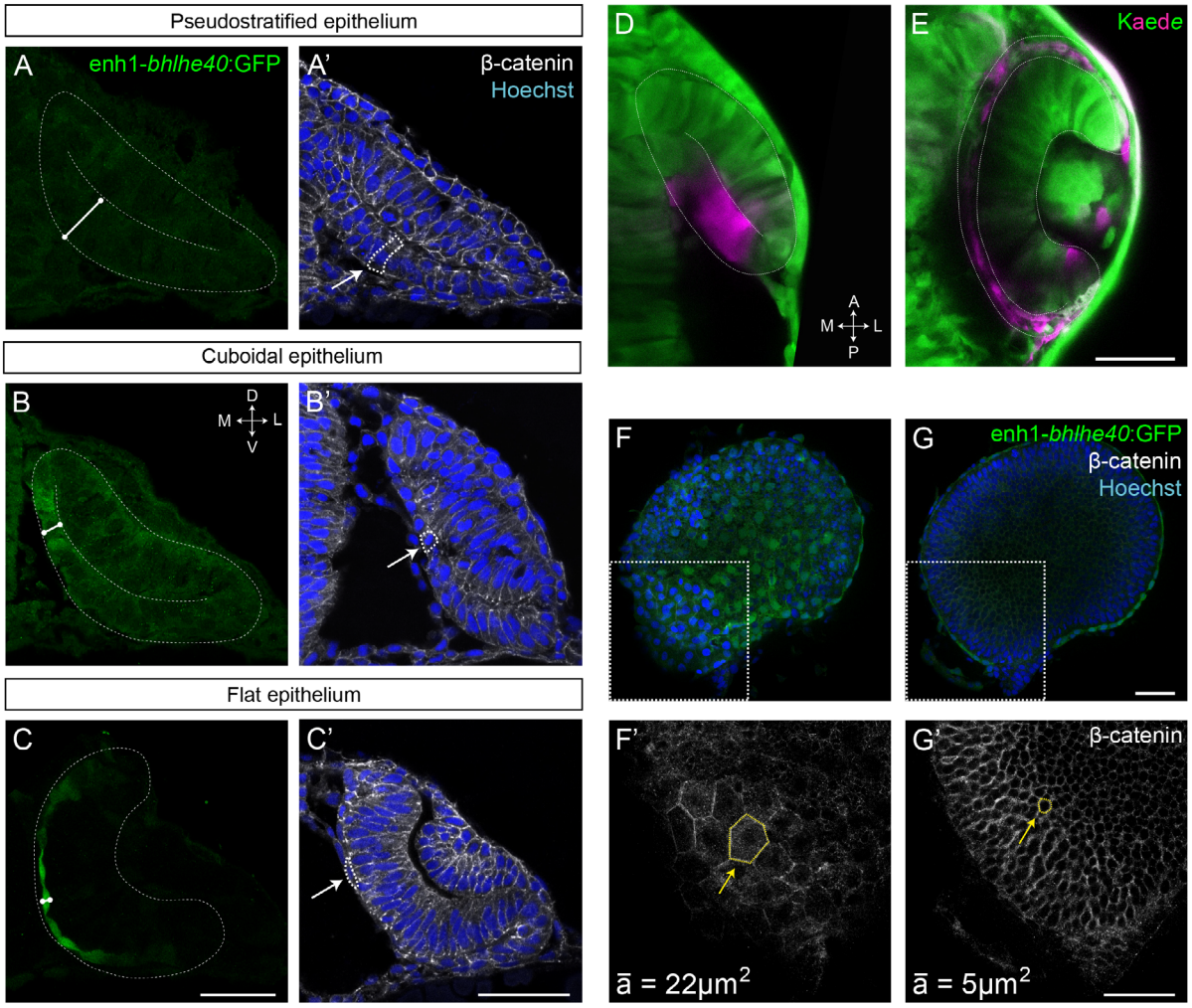

Figure 12: Descriptive analysis of RPE shape changes.

(A-C) Frontal cryosections of enh1-*bhlhe40*:GFP embryos labeled with anti-GFP (green) or **(A'-C')** anti-β-catenin (white) and Hoechst (blue). RPE cells reduce their A-B axis (white straight line in **A-C**) changing from columnar (arrow in **A'**) to flat cells (arrow in **C'**), passing through the intermediate cuboidal cell stage (arrow in **B'**). **(D)** Dorsal view of a wild type embryo injected with Kaede mRNA (green) at 12 ss. A group of cells in the dorsal region of the outer layer is photoconverted (magenta). **(E)** Dorsal view of the same embryo at 30 hpf. The photoconverted cells (magenta) originate the RPE confirming its dorso-medial origin within the OV. White dashed lines delineate eye contour and virtual lumen in **A-E**. **(F)** View of the RPE from an eye dissected from a enh1-*bhlhe40*:GFP embryo at 30 hpf labeled with anti-GFP (green), anti-β-catenin (white) and Hoechst (blue). **(G)** View of the NR from the same eye. **(F')** Magnification of the white box in **F**. RPE cells have a hexagonal morphology (yellow arrow) with an average area of 22 μm^2. **(G')** Magnification of the white box in **G**. NR cells have a rounded cross-section (yellow arrow) with an average area of 5 μm^2. Area here is considered as the pixels included in the cell contour. The average area is calculated using 5 cells from 5 different embryos. Scale bars: 50 μm.

is supported by the fact that the total number of RPE cells that we counted at the 24 hpf stage (Figure 13A) is close to the number previously obtained by other researches (Li et al., 2000b). RPE cells reduced their proliferation rate after their specification with no specific pattern or location of the BrdU positive cells. At the stage of 16 ss 49% of the RPE cells underwent proliferation. This fraction decreased to 34% at 18 ss and then stabilized around 20% from 20 ss to 48 hpf stage, when again decreased to 12 % (Figure 13B). We found a significant effect of the developmental stage over the percentage of proliferating cells that confirm the association

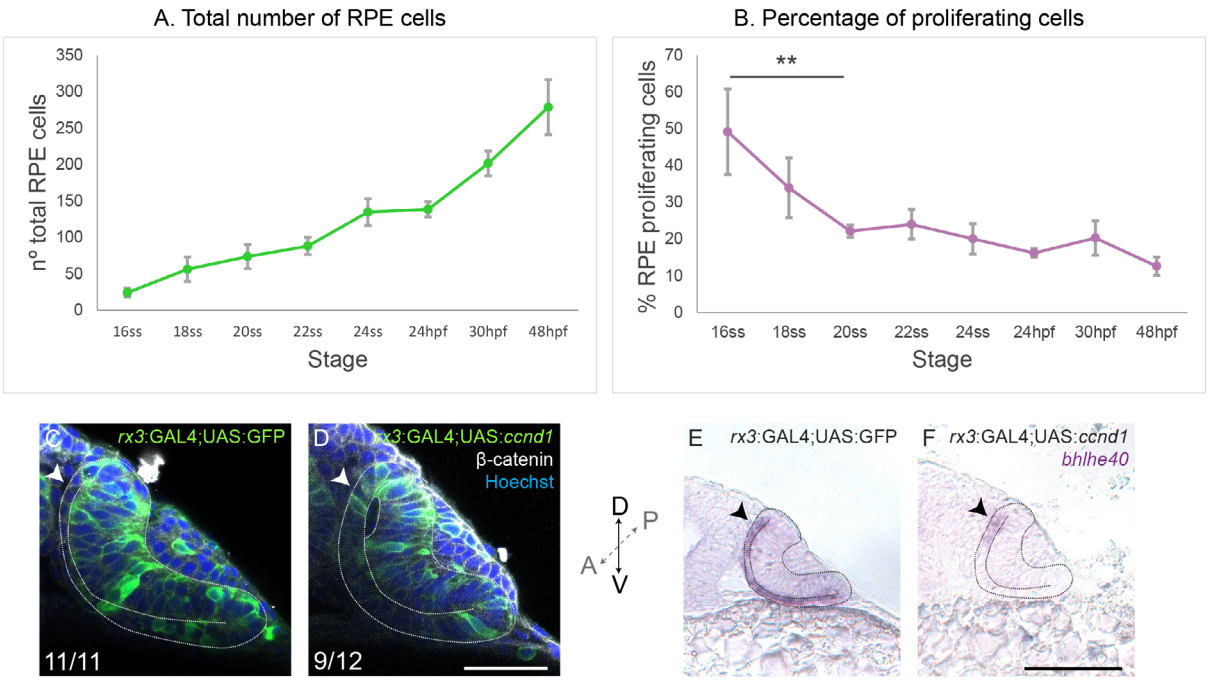

Figure 13: RPE proliferation rate decreases throughout its specification.

(A) The graph shows the total number of RPE cells in enh1-*bhlhe40*:GFP embryos between 16 ss and 48 hpf. Data represent mean ± SD; n=5 embryos per stage. GFP positive cells were considered as RPE cells. **(B)** The graph shows the percentage of RPE proliferating cells in enh1-*bhlhe40*:GFP embryos between 16 ss and 48 hpf. Proliferating RPE cells were counted as the number of BrdU positive cells over the total number of GFP positive. Data represent mean ± SD; n=5 embryos per stage. **(C)** *rx3*:GAL4 embryo injected with the UAS:GFP vector. **(D)** *rx3*:GAL4 embryo injected with the UAS:*ccnd1* vector. When *ccnd1* is overexpressed in the eye, RPE cells do not flatten and maintain a cuboidal-like shape (white arrowheads). Embryos were fixed at 24 hpf stage labeled with anti-GFP (green), anti-β-catenin (white) and Hoechst (blue). **(E)** *bhlhe40* ISH of a *rx3*:GAL4 embryo injected with the UAS:GFP vector. **(F)** *bhlhe40* ISH of a *rx3*:GAL4 embryo injected with the UAS:*ccnd1* vector. *bhlhe40* ISH reveals that when *ccnd1* is overexpressed in the eye, RPE cells are confined in most dorsal region of the outer layer (black arrowheads) likely due to the lack of flattening and alterations in RPE specification. All the images are frontal views of one eye. White and black dashed lines delineate eye contour and virtual lumen in **C-F**. Scale bars: 50 µm in **C-D** and 100 µm in **E-F**.

between the reduction in the proliferation rate and RPE morphogenesis (Kruskal-Wallis test: χ^2(df=7, n=40)=31,864; p<0.001). Specifically, there were statistically significant differences in the percentage of proliferating cells between the stages 16 and 20 ss, the interval when the reduction in the proliferation rate seems to occur (Mann-Whitney U test: z=-2.619, p<0.01, mean rank for 16 ss is 8 and for 20 ss is 3). Given that RPE specification begins more or less at the same time than GFP expression in the reporter line, these results indicate that the acquisition of RPE identity and final morphology occurs concomitantly to a reduction of the proliferation rate. To test if this reduction is a prerequisite for RPE flattening, we overexpressed *ccnd1*, a key regulator of the cell cycle, in retinal progenitors by injecting a UAS:*ccnd1* construct in the *rx3*:GAL4 transgenic line. Forced proliferation of the cells compromised RPE development. RPE cells failed to acquire a flat morphology and remained with cuboidal appearance (Figure 13C,D). Furthermore, ISH analysis showed that the expression of the *bhlhe40* gene was restricted to the more dorsal region of the outer layer whilst in controls it was properly expanded and covering

the whole eye (Figure 13E,F). The absence of flattening could explain why *bhlhe40* expression is not extended along the outer layer (Figure 13F). However, the maintenance of a proliferative state could in addition be interfering with the number of cells that acquire RPE identity. Thus, we conclude that proliferation does not greatly contribute to RPE expansion but its reduction is necessary for proper RPE morphogenesis.

Next we explored the role of cell shape changes in collaboration with Mario Ledesma (David Míguez's laboratory, CBMSO). For this purpose, we quantified different parameters of *in vivo* RPE development, taken the epithelium as a whole tissue. Specifically, two time periods were analyzed: from 17 hpf/16 ss to 22 hpf/26 ss (corresponding to the first 60 time points of Movie 2) and from 24 hpf to 37 hpf (corresponding to Movie 4).

During the first period, the RPE total volume showed two different dynamics. It initially increased very little likely associated to the activation of the GFP in new cells (Figure 14A

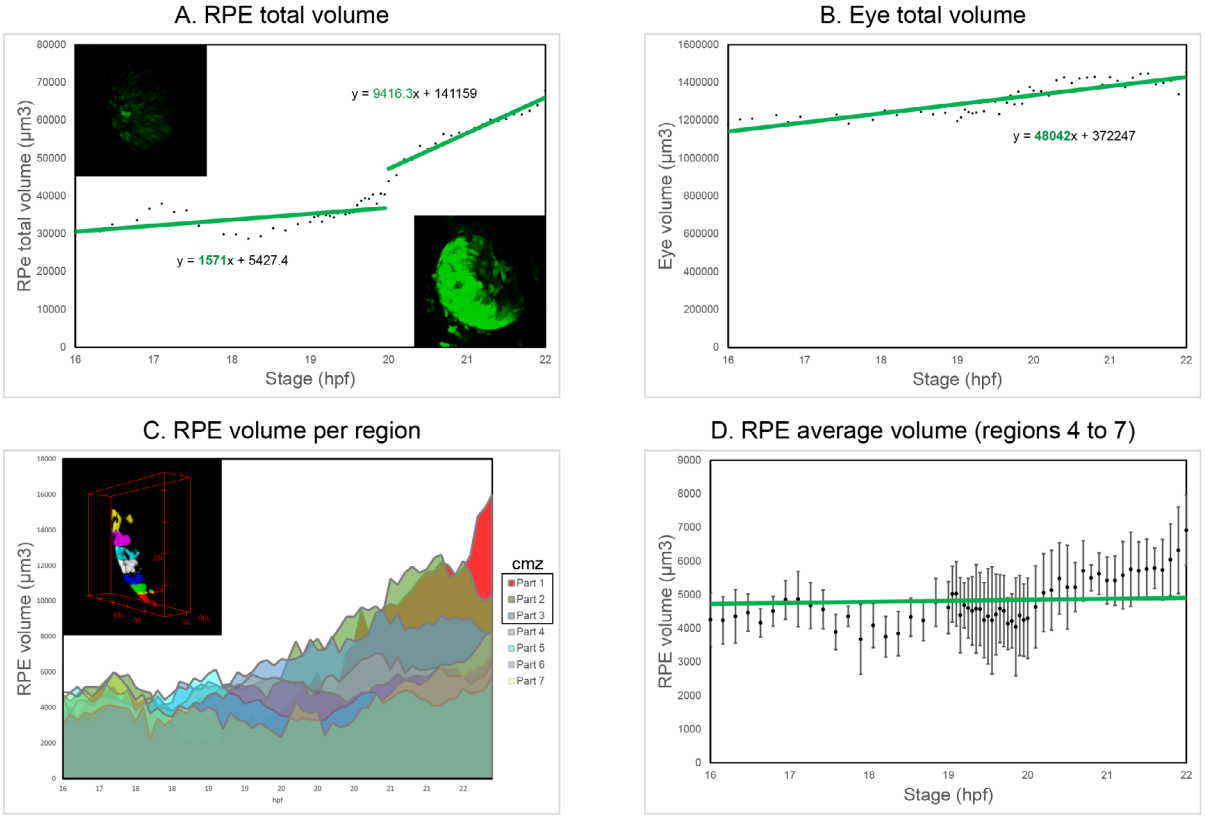

Figure 14: The total volume of the RPE does not change during morphogenesis.

(A) The graph shows the quantification of the total RPE volume. Two separate phases can be differentiated. Volume increase is initially slow but then it appears to rapidly increase from 20 hpf. This apparent second phase is linked to the activation of GFP in the ciliary margin zone and thus does not reflect a real increase in the RPE volume. **(B)** Quantification of the total eye volume, which increases at a faster rate than that of the RPE. The slope of the line indicates the velocity at which the tissue is increasing its volume: 1571 for the RPE and 48042 for the whole eye. **(C)** Quantification of RPE volume in specific regions along the medio-lateral axis of the OV. Regions 1 (red), 2 (green) and 3 (dark blue), close to the forming ciliary margin zone (cmz), have a noticeable volume increase from 20 hpf, as expected from the observations reported in **A**. Regions 4 (grey), 5 (light blue), 6 (purple) and 7 (yellow) instead maintain a constant volume. **(D)** Average volume of the regions 4 to 7 showing that RPE volume is constant during its morphogenesis. Data represent mean ± SD.

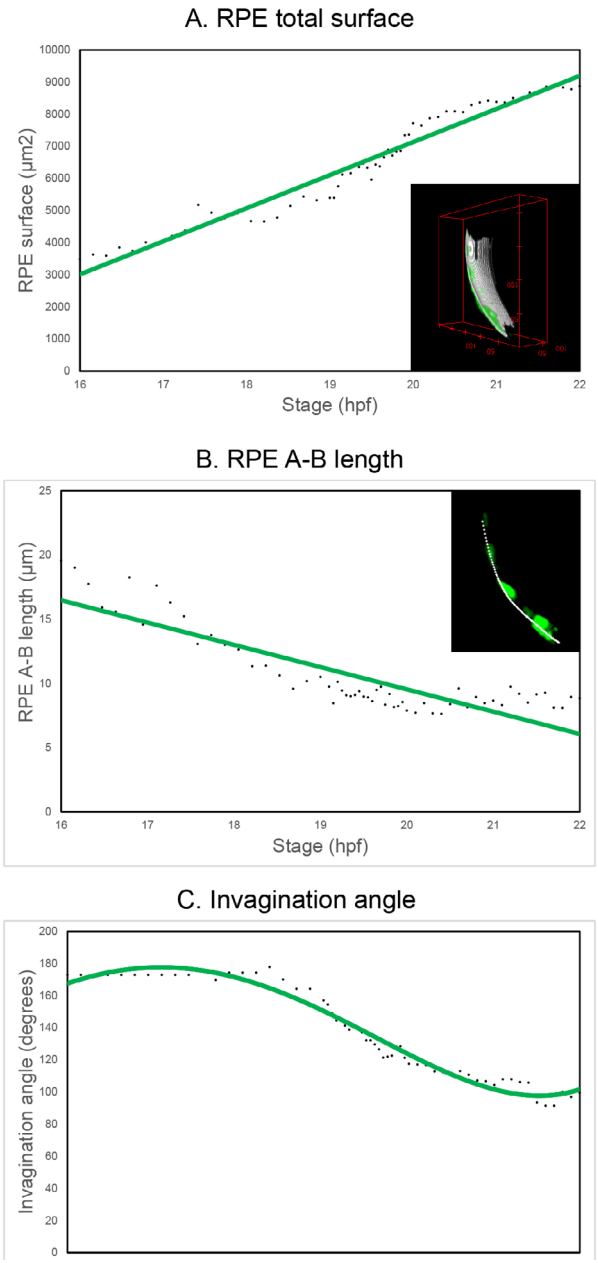

Figure 15: During RPE morphogenesis there is a three-fold surface increase and a half reduction in the length of the A-B axis.

(A) Quantification of the expansion of the RPE surface with time. There is a three-fold surface increase that corresponds to RPE ventral expansion. **(B)** Quantification of average length of the A-B axis along the whole tissue. RPE A-B length is reduced in half while the tissue extends, although this effect is more evident in the most central region. **(C)** Quantification of the invagination angle, which decreases from 18-19 hpf, right when basal constriction starts and first RPE flat cells are detected.

from 17 to 20 hpf). When compared with the growth of the whole eye (Figure 14B), this initial RPE volume increase was slow. Then, from 20 to 22 hpf there was a notably change in the global RPE volume (Figure 14A), although still slower than the general increase in eye volume. We hypothesize that this marked increase could reflect the activation of the GFP expression in the ciliary margin zone, especially evident in the posterior region (Movie 1). To check if this was the case, we quantified the RPE volume in representative regions across the entire tissue (Figure 14C). There was an evident and late volume increase in the most posterior regions (Figure 14C parts 1 to 3), those close to the GFP positive ciliary margin zone cells, whereas the volume slightly changed in the most central regions (Figure 14C parts 4 to 7). The fact that the average volume in the regions distant from the ciliary margin zone remained basically constant (Figure 14D) indicates that RPE cells, despite changing their morphology, maintain their overall volume. To complement these quantifications, we measured the total surface increase (Figure 15A), the decrease of the length of the A-B axis (Figure 15B) and the decrease in the invagination angle (Figure 15C). The RPE total surface underwent a three-fold increase during the first period analyzed from 3000 μm^2 to 9000 μm^2. This data correlates with the increase in area of RPE individual cells that also triplicated from 7 μm^2 in progenitors to 22 μm^2 in differentiated cells (Figure 12F'). During this same period

the whole tissue reduced by half the length of the A-B axis, on average from approximately 20 µm to 10 µm, but it should be considered that central cells reduce their A-B length more than peripheral cells. Finally, the invagination angle, as a representation of the folding process, remains basically invariant from 16 hpf to 19 hpf (around 170º). From this point, when evident basal constriction of the NR cells has been reported to start (Nicolas-Perez et al., 2016) and flat RPE cells are first detected (our observation), the invagination angle decreases to 100º by 22 hpf.

During the second period, after acquiring a cup shape, the increase in volume in the RPE continues to be evidently slow (Figure 16A) in comparison with the volume of the whole eye (Figure 16B). This indicates a further additional stretching of RPE cells at least until 37 hpf which might make them reach the really squamous morphology.

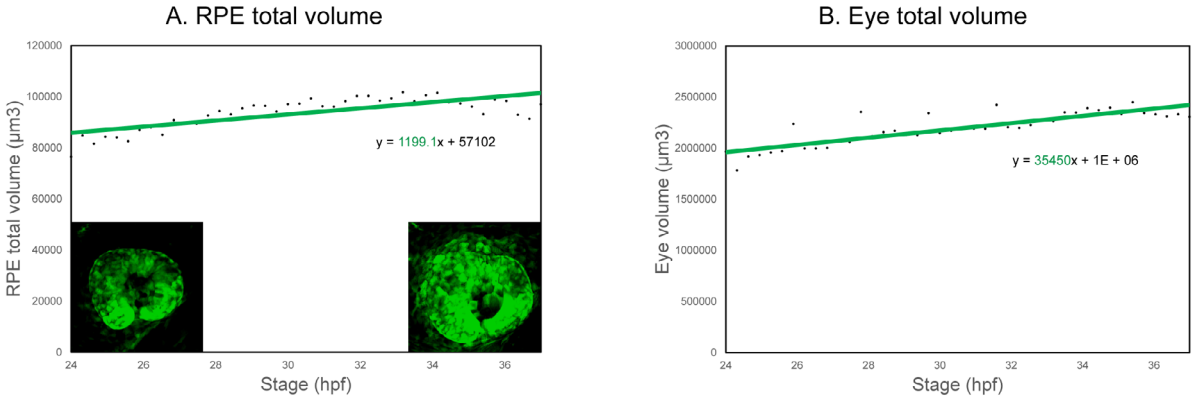

Figure 16: The RPE volume increases at a slower pace than the total eye volume after OC morphogenesis is completed.

(A) Quantification of the total RPE volume from 24 hpf to 37 hpf. **(B)** Quantification of total eye volume from 24 hpf to 37 hpf. The slope of the line indicates the pace at which both tissues increase their volume (1199.1 for the RPE and 35450 for the eye). This is higher for the eye than for the RPE.

In summary, the RPE volume remains nearly constant throughout the complex shape changes its cells undergo. Besides, cell proliferation does not account for this invariance, because actually the proliferation rate of RPE cells is significantly reduced during OC morphogenesis. Therefore, these results taken together prove that RPE cell flattening is the major driver of the RPE expansion.

3. Role of cytoskeletal components in RPE morphogenesis

Given the evident cell shape changes during RPE morphogenesis we asked which are the mechanisms that control them. Shape changes within a cell can be driven both by intracellular processes and/or external interactions, which directly determine the mechanical properties of the cell. Among the intracellular mechanisms, the reorganization of the cytoskeleton is crucial for

acquiring a new shape so that we analyzed the role of two of the main cytoskeletal components (myosin II and MTs) during RPE morphogenesis using different specific pharmacological inhibitors.

3.1 Myosin II activity is necessary for RPE flattening

Inhibition of myosin II activity has an important impact on zebrafish OC formation preventing its folding (Sidhaye and Norden, 2017, Nicolas-Perez et al., 2016). Previous studies are focused on the involvement of the NR in the folding process. These studies are limited because they neglected the potential contribution of the RPE. In this thesis, we analyzed the contribution of myosin II in OC folding separating the contribution of the NR from that of the RPE with tissue specific inhibition.

Analysis of RPE myosin distribution using the transgenic line β*actin*:*myl12.1*-GFP revealed an enrichment at the apical side (Figure 17A-C), similarly to actin filaments labeled by phalloidin staining (Figure 17D-E'). Specifically, the strongest signal intensity is found in dots corresponding to cell boundaries. However, since there is a virtual lumen between the apical surfaces of RPE and NR sometimes it was difficult to differentiate to which tissue the signal corresponds. When 24 hpf RPE cells were viewed from the apical side actin was seen as organized in a belt characteristic of epithelial cells (Figure 17F). No other specific accumulations of acto-myosin were detected beyond that would give clues about how these cytoskeletal components could affect cell shape.

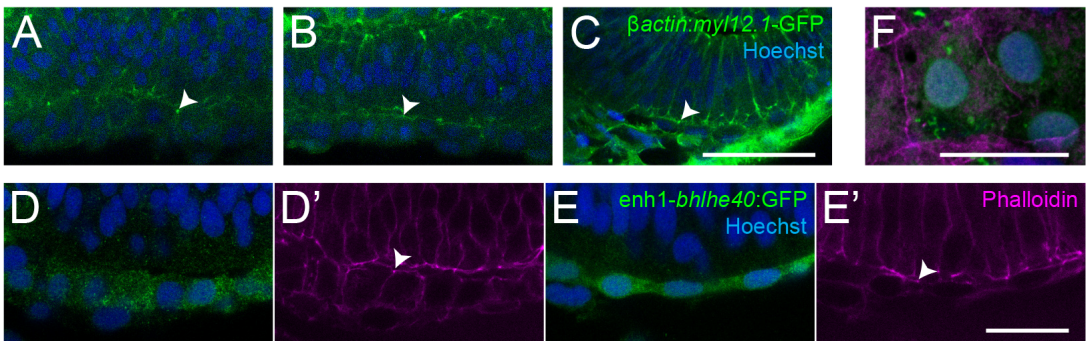

Figure 17: Myosin and F-actin distribution in the RPE.

(A) Pseudostratified, **(B)** cuboidal and **(C)** flat RPE of β*actin*:*myl12.1*-GFP embryos. White arrowheads point to myosin accumulation sites. β*actin*:*myl12.1*-GFP embryos were fixed at the corresponding stage and labeled with anti-GFP (green) and Hoechst (blue). **(D,D')** Cuboidal and **(E,E')** flat RPE of enh1-*bhlhe40*:GFP embryos. enh1-*bhlhe40*:GFP embryos were fixed at the corresponding stage and labeled with anti-GFP (green), TRITC-phalloidin (magenta) and Hoechst (blue). White arrowheads point to F-actin accumulation sites. All images are dorsal views of the RPE. **(F)** Basal view of an 24 hpf RPE cell from an enh1-*bhlhe40*:GFP embryo labeled with anti-GFP (green), TRITC-phalloidin (magenta) and Hoechst (blue). Scale bars: 50 µm in **A-C**, 20 µm in **D-E'** and 15 µm in **F**.

We then reproduced Blebbistatin treatments as previously done by Nicolas-Perez et al. (2016). To this end we used the transgenic line enh1-*bhlhe40*:GFP. Blebbistatin is a specific

inhibitor of most myosin II isoforms that binds to the myosin motor domain. This binding prevents the molecule to interact with actin, thereby impairing their participation in the ATP hydrolytic cycle (Rauscher et al., 2018). The entire embryo is usually incubated with these drugs so that in absence of spatial specificity the treatment tends to affect embryonic viability. Incubation cannot last more than 3 hours without causing embryonic death (in this experiment from 16 ss to 21 ss stage). When the embryos were placed in the drug, RPE specification had begun and cuboidal cells could be identified (Figure 18A). In controls, after incubation with DMSO, OC folding was not complete but flat cells surrounded the NR (Figure 18B). In contrast, after Blebbistatin treatment, OV invagination did not occur, as previously described (Nicolas-Perez et al., 2016). The NR remained open with no signs of basal constriction but, in addition, RPE cells were also altered showing more rounded and less spread morphology than in the control embryos (Figure 18C). Treatments with Para-nitroblebbistatin, a non-cytotoxic and photostable version of Blebbistatin, also impaired RPE flattening supporting the reliability of the phenotype (Figure 18D).

Figure 18: Myosin II inhibition impairs eye folding and RPE cell shape changes.

(A) Embryo at t = 0, before the drug was added to the medium. RPE cells still form a cuboidal monolayer of cells. **(B)** Control embryo incubated in DMSO. Eye development was not affected and RPE cells become flat especially in the most central region (white arrowhead). **(C)** Blebbistatin treated embryo. Eye folding is impaired (yellow arrowhead) and RPE cells do not flatten maintaining a cuboidal-like morphology (white arrowhead). **(D)** Para-nitroblebbistatin treated embryo. Effects are the same as with Blebbistatin. enh1-*bhlhe40*:GFP embryos were fixed at the corresponding stage (16 ss in **A** and 21 ss in **B**, **C** and **D**) and labeled with anti-GFP (green), anti-β-catenin (white) and Hoechst (blue). The frequency of embryos with the illustrated phenotype is indicated in the top right corner of each panel. All the images are dorsal views of one eye. Scale bar: 50 μm.

The results described above indicate that the lack of OC folding after myosin II inhibition could be due to the absence of either RPE flattening and/or NR basal constriction. To analyze to what extent each tissue contribute to eye morphogenesis, we used a photoactivable compound called Azidoblebbistatin (ABleb) that binds covalently to myosin II upon two-photon irradiation (Kepiro et al., 2012, Kepiro et al., 2015), thus allowing spatial specificity.

First, we inhibited myosin II activity specifically in the RPE. RPE cells, identified with the transgenic line enh1-*bhlhe40*:GFP, were irradiated around 16 ss stage. No detectable alterations

were found in irradiated eyes of embryos incubated in DMSO and in non-irradiated eyes of embryos incubated in ABleb (Figure 19A,B). However, RPE cells in those embryos in which irradiation led to ABleb activation acquired a round morphology (Figure 19C), similarly to those

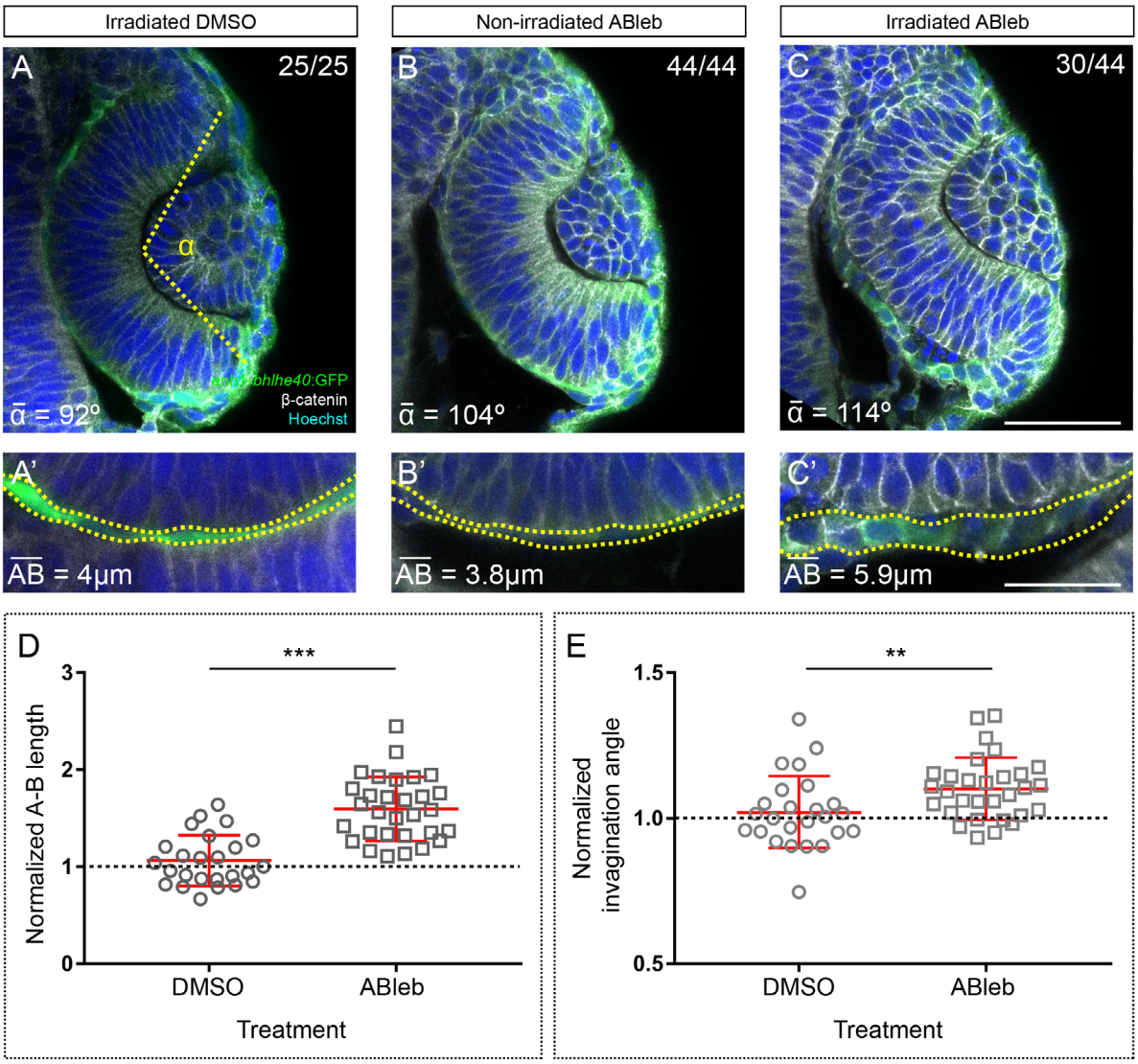

Figure 19: RPE cell shape change is a cell autonomous process dependent on Myosin II that contributes to eye invagination.

(A) Irradiated eye from an embryo incubated in DMSO. DMSO and RPE irradiation per se did not cause developmental eye alterations. **(A')** Magnification of RPE flat cells in **A**. **(B)** Non-irradiated eye from an ABleb treated embryo. ABleb treatment without irradiation does not affect eye development. **(B')** Magnification of flat RPE cells in **B**. **(C)** Irradiated eye from an ABleb treated embryo. Irradiation to activate ABleb in the RPE prevented cell flattening; cells are round as observed after Blebbistatin treatments. In the NR basal constriction occurs normally. **(C')** Magnification of rounded RPE cells in **C**. **(D)** The graph shows the normalized A-B length of the RPE in DMSO and ABleb treated embryos. Data represent mean ± SD. Differences in A-B length between the two groups are statistically significant ($p<0.001$). Inhibition of myosin II in the RPE alters its morphogenesis. **(E)** Normalized invagination angle in DMSO and ABleb treated embryos. Data represent mean ± SD. Differences in invagination angle between the two groups are statistically significant ($p<0.01$). Inhibition of myosin II in the RPE causes impairment of OC folding. enh1-*bhlhe40*:GFP embryos were fixed at the corresponding stage after irradiation and labeled with anti-GFP (green), anti-β-catenin (white) and Hoechst (blue). All the images are dorsal views of one eye. The frequency of embryos with the illustrated phenotype is indicated in the top right corner of each panel, whereas the average invagination angle in the bottom left corner (α). The yellow dashed line in **A** represents how the invagination angle was defined. The average length of the A-B axis in RPE cells (AB) is shown in **A'-C'**. Scale bars: 50 µm in **A-C** and 25 µm in **A'-C'**.

treated with Blebbistatin. The length of the A-B axis in these cells was on average 2 μm longer than in controls (Figure 19A'-C') with statistically significant differences in the normalized length of the A-B axis of RPE cells between DMSO and ABleb treated embryos (Figure 19D; Mann-Whitney U test: $z=-5.088$, $p<0.001$, mean rank for DMSO is 15.96 and for ABleb is 38.03). Improper RPE flattening in presence of a normal NR seemed to be associated with a reduction of OC folding (Figure 19A-C). This would imply an active participation of the RPE in the formation of the OC. This possibility was proved by measuring the invagination angle. Differences in the normalized invagination angles between DMSO and ABleb treated embryos were statistically significant (Figure 19E; Mann-Whitney U test: $z=-2.704$, $p<0.01$, mean rank for DMSO is 21.60 and for ABleb is 33.33). Non-irradiated eyes in the ABleb treated embryos were per se slightly less folded than the eyes in the DMSO treated embryos. This is probably due to a slight basal activation of the compound caused even in the condition of ambience dim light used during the experimental procedure. In conclusion, myosin II is required for cell shape changes of RPE cells and these changes are, in turn, required for OC folding.

Second, we test myosin II inhibition specifically in the NR using the same approach. The NR was identified also using the transgenic line enh1-*bhlhe40*:GFP as a reference. Areas equivalent to those used for the RPE were irradiated to activate ABleb in the basal region of the NR, where the acto-myosin contractility promotes tissue constriction. Control OCs had no noticeable alterations (Figure 20A,B), whereas in the irradiated eyes of ABleb treated embryos the NR was visibly more elongated (Figure 20C). This clearly affected the general folding of the OC and statistically significant differences were found in the normalized invagination angles between DMSO and ABleb treated embryos (Figure 20E; Mann-Whitney U test: $z=-3.035$, $p<0.01$, mean rank for DMSO is 10.29 and for ABleb is 20.06). RPE cells in the experimental eyes appeared to be properly flattened with an A-B length similar to that of controls (Figure 20A'-C'). Indeed, RPE flattening is independent of NR morphogenesis since we did not found statistically significant differences in the normalized length of the A-B axis between the two groups (Figure 20D; Mann-Whitney U test: $z=0.582$, $p>0.05$, mean rank for DMSO is 14.50 and for ABleb is 16.38).

Altogether these results support the notion that myosin II activity is necessary for RPE correct morphogenesis, which occurs cell autonomously, independently from NR basal constriction. These data also show that RPE flattening is needed to promote OC folding together with NR basal constriction. These findings therefore propose a model different from that proposed in previous studies (Sidhaye and Norden, 2017, Nicolas-Perez at al., 2016) demostrating that OC folding depends on the cell shape changes in both RPE and NR.

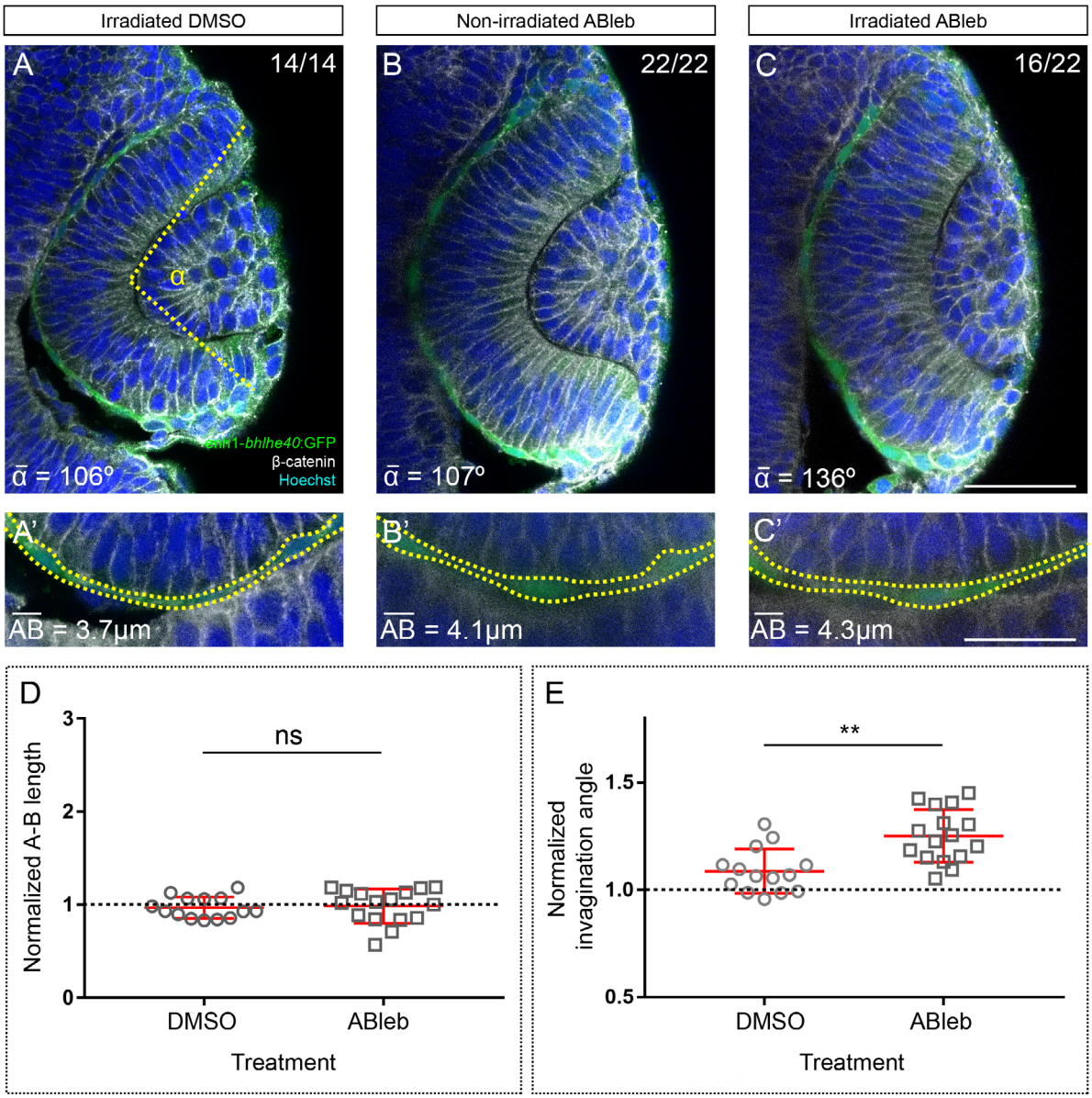

Figure 20: RPE morphogenesis is independent from NR basal constriction.

(A) Irradiated eye from an embryo incubated in DMSO. DMSO and NR irradiation per se do not affect the basal constriction or eye development in general. **(A')** Magnification of flat RPE cells in **A**. **(B)** Non-irradiated eye from an ABleb treated embryo. ABleb treatment per se does not affect eye development. **(B')** Magnification of flat RPE cells in **B**. **(C)** Irradiated eye from an ABleb treated embryo. Specific activation of ABleb in the basal NR region affects the basal constriction and eye invagination, as observed after Blebbistatin treatments, but RPE cells are not affected. The regions irradiated in the NR are equivalent in area to those used for the RPE. **(C')** Magnification of flat RPE cells in **C**. **(D)** The graph shows the normalized A-B length in DMSO and ABleb treated embryos. Data represent mean ± SD. There is no difference in RPE A-B length between the two groups ($p>0.05$). Impairment of NR basal constriction does not affect RPE flattening. **(E)** Normalized invagination angle in DMSO and ABleb treated embryos. Data represent mean ± SD. Differences in invagination angle between the two groups are statistically significant ($p<0.01$). Inhibition of myosin II in the NR basal region impairs OC folding. enh1-*bhlhe40*:GFP embryos were fixed at the corresponding stage after irradiation and labeled with anti-GFP (green), anti-β-catenin (white) and Hoechst (blue). All the images are dorsal views of one eye. The frequency of embryos with the illustrated phenotype is indicated in the top right corner of each panel, whereas the average invagination angle in the bottom left corner (α). The yellow dashed line in **A** represents how the invagination angle was defined. The average length of the A-B axis in RPE cells (AB) is shown in **A'-C'**. Scale bars: 50 µm in **A-C** and 25 µm in **A'-C'**.

3.2 MTs are essential for progression and maintenance of RPE shape changes

MTs are basic components of the cytoskeleton and their reorganization underlies cell shape changes. Specifically, they have been related with cell flattening processes in the amnnioserosa of *Drosophila* which initial columnar cells become flat through the rotation of their MT cytoskeleton (Pope and Harris, 2008). Given that RPE cells also change from a columnar to a flat morphology, we analyzed the role of MTs during OC morphogenesis.

Short movies using the fusion protein EB3-GFP in the eye allowed us following *in vivo* the positive end of the MTs (Buckley et al., 2013, Stepanova et al., 2003). At OV stages when all cells are organized in a pseudostratified epithelium, EB3-GFP dots moved along the A-B axis, mostly from the apical to basal side of the cells (Movie 5). This same directed movement was

Movie 5: EB3-GFP dynamics in an OV stage in which RPE cells still have neuroepithelial organization (continuous acquisition, n = 9).

Movie 6: EB3-GFP dynamics in an OV stage in which RPE cells are cuboidal (continuous acquisition, n = 10).

Movie 7: EB3-GFP dynamics in an OC stage when RPE cells are squamous (continuous acquisition, n = 15).

observed when RPE cells were in a cuboidal configuration (Movie 6). In contrast, when RPE cells presented a flattened morphology, the positive end of MT grew along the medio-lateral axis (Movie 7), indicating a reorganization of the MT cytoskeleton during RPE morphogenesis. These observations open the possibility that MT reorganization could induce RPE flattening, although it also could be the consequence of an internal reorganization of the cellular organelles promoted by an additional and undefined mechanism.

To further analyze MT dynamics during RPE flattening we used a depolymerizing agent called Nocodazole and the transgenic line enh1-*bhlhe40*:GFP. Nocodazole treatments affect the whole embryo with no tissue specificity so that in addition to the RPE most of the structures showed alterations. Incubating the embryos in the drug during the same temporal window used for Blebbistatin (treatments from 16 ss to 21 ss) resulted in RPE cells showing morphology in between columnar and cuboidal. This is surprising since when the compound was added to the embryos RPE cells were already cuboidal (Figure 21A) and suggests that RPE cells went back to a more undifferentiated state with an increase in the length of the A-B axis (Figure 21B,C). The cells seemed to be plastic, which is consistent with the idea that loss of MTs leads to cells with no capability of acquiring tension or stiffness. By changing the temporal window of the treatment, we observed that in all cases RPE cells returned to a more undifferentiated morphology. Adding the drug when the RPE was still a pseudostratified epithelium, at the 14ss stage (Figure 21D), led to the maintenance of a progenitor morphology (Figure 21F), while flattening progressed normally in the controls (Figure 21E). Interestingly, if Nocodazole was added at 23 ss, when RPE cells were already flat and covered the apical surface of the NR (Figure 21G), the tissue shortened and the cells went back to a more rounded stage (Figure 21H,I). At the same time NR cells that have underwent rim involution at the time the drug was added, were instead found in the outer layer. These cells could have been forced to go back to the outer layer by RPE shrinkage or perhaps have stopped their involution. These results suggest that MTs dynamics are essential for both flattening of RPE cells and maintenance of their differentiated morphological properties.

These Nocodazole experiments however have the limitation of affecting the entire embryos. We therefore decided to take advantage of a construct expressing the human gene *STMN1*. *STMN1* encodes a protein called Stathmin or Oncoprotein 18 that binds to tubulin dimers avoiding their incorporation to MTs, thereby decreasing the available tubulin levels and slowing MT growth (Belmont and Mitchison, 1996). Unfortunately, and as already mentioned, the enh1-*bhlhe40*:GAL4 line does not confer the expected specificity to the RPE. We then decided to use the *rx3*:GAL4 line, which, at least, allows limiting the manipulations to retinal cells. UAS:*STMN1* overexpression in the eye resulted in a phenotype similar to that observed

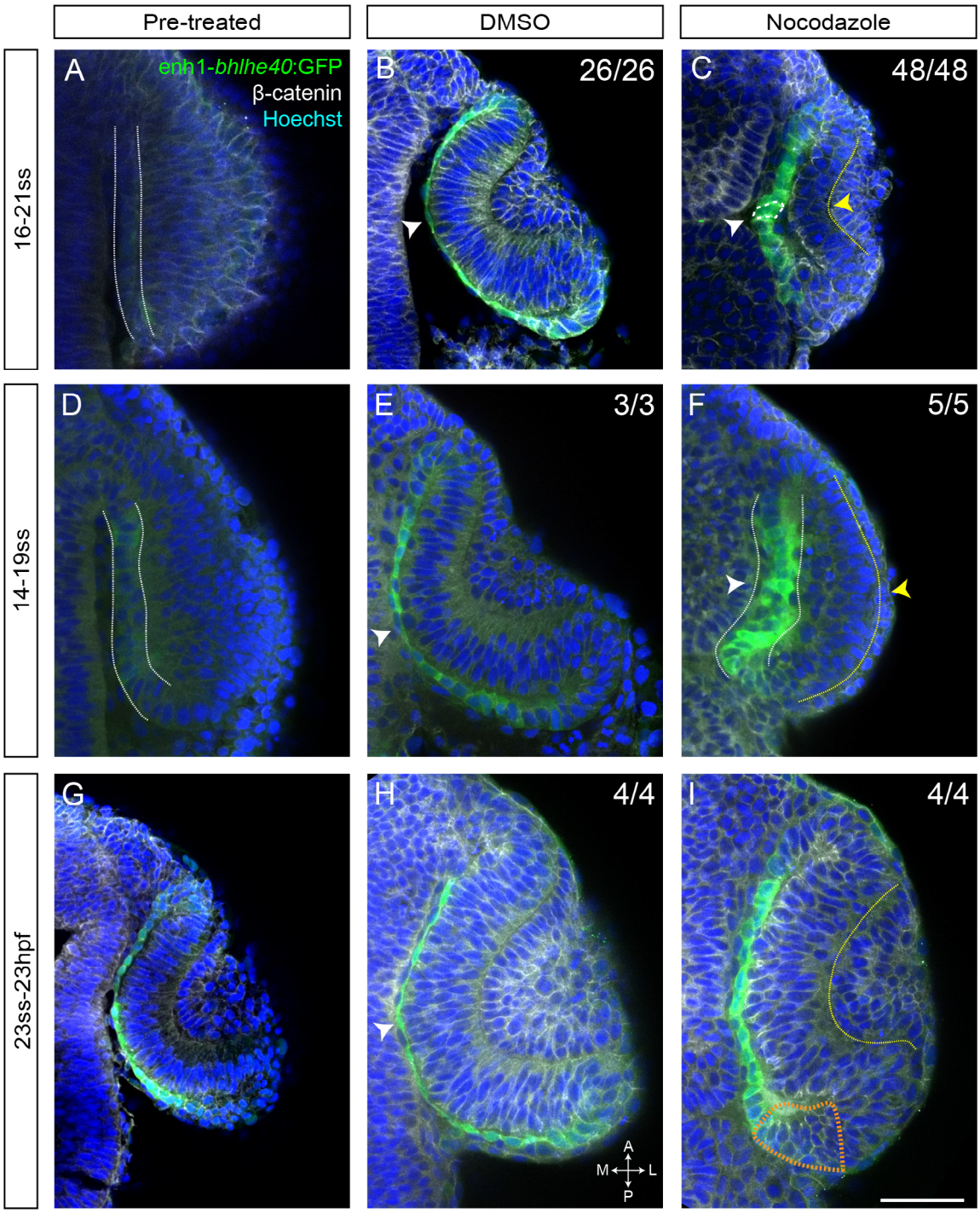

Figure 21: MT depolymerization interferes with RPE shape changes.

(A) Embryo at t = 0. RPE cells form a monolayer of cuboidal cells. **(B)** Control embryo incubated in DMSO. RPE cells became flat (white arrowhead) and the eye folds to form the OC. **(C)** Nocodazole treated embryo. RPE cells present a columnar-like morphology with a longer A-B axis (white arrowhead). NR is visibly thinner but present signs of basal constriction (yellow arrowhead). **(D)** Embryo at t = 0. RPE cells are organized as a pseudostratified epithelium. **(E)** Control embryo incubated in DMSO. RPE cells are flat although still not squamous (white arrowhead). **(F)** Nocodazole treated embryo. RPE cells do not flatten or form a monolayer (white arrowhead), whereas the NR does not undergo basal constriction (yellow arrowhead). **(G)** Embryo at t = 0. RPE cells form a monolayer of flat cells and NR basal constriction is at an advanced stage. **(H)** Control embryo incubated in DMSO. RPE cells are squamous and OC folding seems almost completed. **(I)** Nocodazole treated embryo. RPE A-B axis seems longer than in the control embryos. The tissue is also less extended and NR cells are misplaced in the outer layer (orange dashed contour). enh1-*bhlhe40*:GFP embryos were fixed at the needed stage and labeled with anti-GFP (green), anti-β-catenin (white) and Hoechst (blue). All the images are dorsal views of one eye. The frequency of embryos with the illustrated phenotype is indicated in the top right corner of each panel. White dashed lines delineate RPE cells and yellow ones the basal region of the NR. Scale bar: 50 µm.

after Nocodazole treatment, although less severe (Figure 22A,B). RPE cells were not able to become squamous showing a cuboidal-like morphology that was associated with a less folded eye, corroborating the need of a proper MT cytoskeleton for RPE cell flattening. There was statistically significant differences in length of the A-B axis in RPE cells between embryos injected with the control UAS:GFP and the UAS:*STMN1* vector (Figure 22C; Mann-Whitney U test: z=-3.130, p<0.01, mean rank of 4 for UAS:GFP and of 11 for UAS:*STMN1*). Besides, as expected from RPE morphology, we also found statistically significant differences in the eye invagination angle between the two groups (Figure 22D; Mann-Whitney U test: z=-2.875, p<0.01, mean rank of 4.29 for UAS:GFP and of 10.71 for UAS:*STMN1*). Together the previous data indicate the involvement of the MT cytoskeleton in the morphogenesis of the RPE.

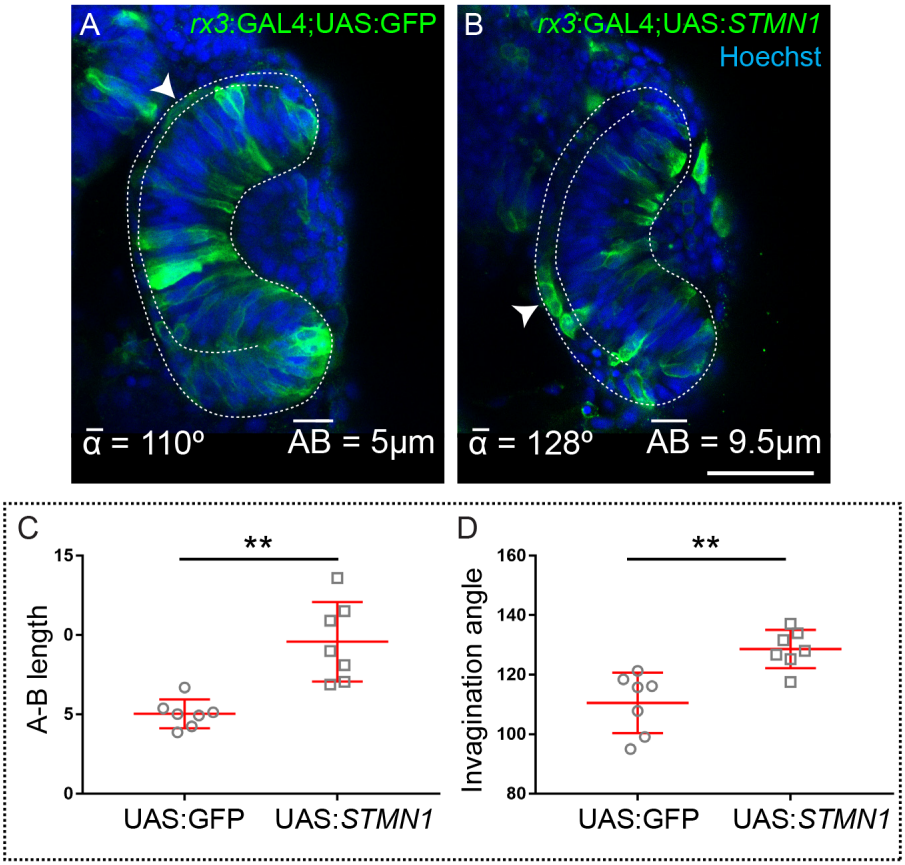

Figure22: Overexpression of STMN1 in the eye induces a nocodazole-mediated phenotype.

(A) *rx3*:GAL4 embryo injected with the UAS:GFP vector (n=7). **(B)** *rx3*:GAL4 embryo injected with the UAS:*STMN1* vector (n=7). When *STMN1* is overexpressed in the eye RPE flattening is prevented and the cells present a cuboidal like shape (white arrowheads). Embryos were fixed at 24 hpf stage labeled with anti-GFP (green) and Hoechst (blue). **(C)** RPE A-B length in *rx3*:GAL4 embryos injected with UAS:GFP or UAS:*STMN1* vectors. Data represent mean ± SD. Differences in A-B length between the two groups are statistically significant (p<0.01). **(D)** Invagination angle in *rx3*:GAL4 embryos injected with UAS:GFP or UAS:*STMN1* vectors. Data represent mean ± SD. Differences in invagination angle between the two groups are statistically significant (p<0.01). Both images are dorsal views of one eye. Average invagination angle and length of the A-B axis in RPE cells are indicated at the bottom. Scale bar: 50 µm.

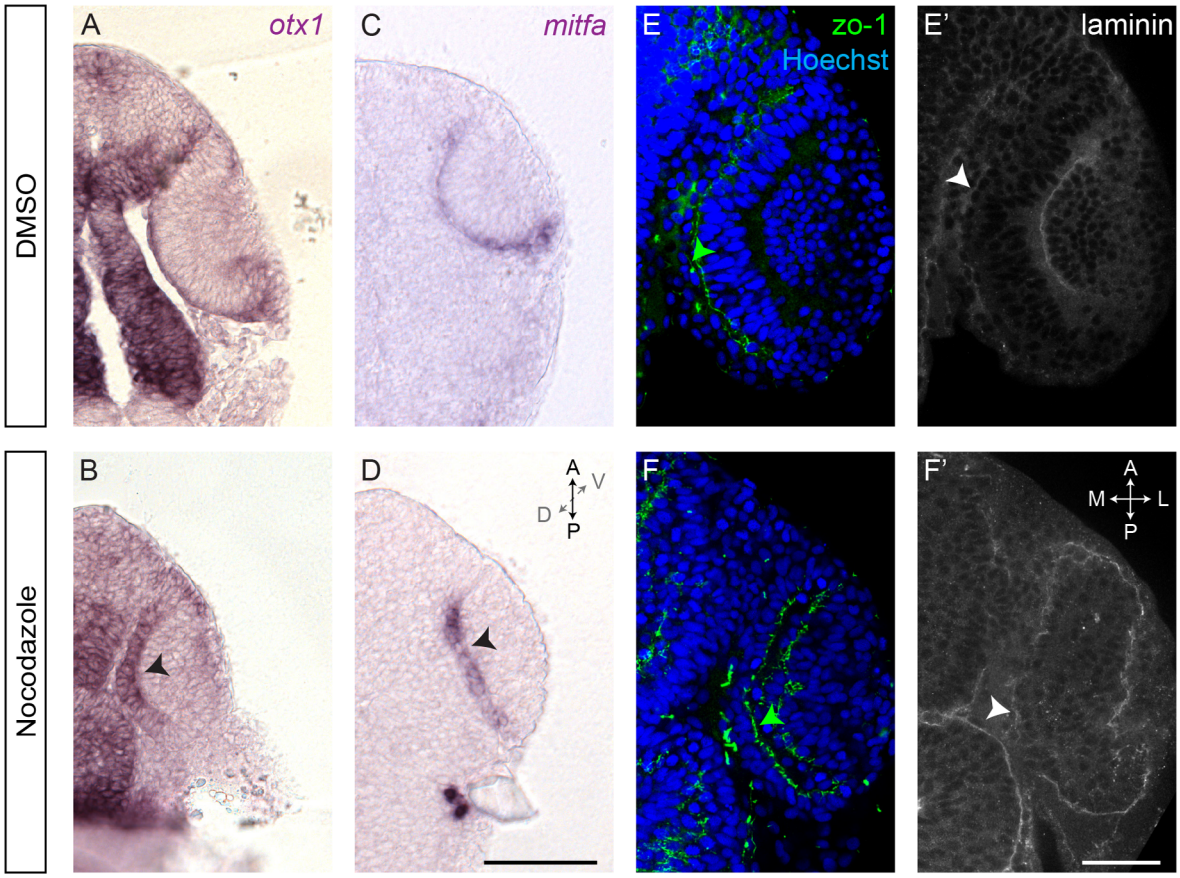

Figure 23: RPE specification and cell polarity are maintained in absence of cell flattening.

(A) DMSO and **(B)** Nocodazole-treated embryos hybridized with *otx1* specific probe. **(C)** DMSO or **(D)** Nocodazole-treated embryos with *mitfa* specific probe. After Nocodazole treatment both mRNA are specifically detected in the RPE (black arrowheads) despite RPE cells remained elongated in their A-B axis. **(E, E')** Wild type embryos labeled with zo-1 (green/apical), laminin (white/basal) and Hoechst (blue) after DMSO or **(F, F')** Nocodazole treatment. In both cases A-B polarity is maintained (green and white arrowheads), even after depolymerizing MTs when RPE cells do not flatten correctly. **A-D** Images are dorsal views of flat mounted embryos. **E-F'** Images are dorsal sections of one eye. Scale bars: 100 µm in **A-D** and 50 µm in **E-F'**.

To assess whether Nocodazole-induced conversion to a progenitor-like morphology was indicative of an alteration in tissue specification, we analyzed the expression of the RPE differentiation markers *otx1* and *mitfa*. The expression of both genes was detected by ISH after Nocodazole treatment between 16 and 21 ss. In controls both mRNA labeled the thin outer layer in the OC (Figure 23A,C), whereas, in the treated embryos, they labeled a thicker and shorter layer in which cells were clearly elongated along the A-B axis (Figure 23B,D). The GFP reporter of enh1-*bhlhe40*:GFP line was also clearly visible after depolymerization of MTs, indicating that RPE specification occurred normally. A-B polarity was also properly maintained despite of the morphological alterations when analyzed with the specific markers zo-1 (apical; Figure 23E,F) and laminin (basal; Figure 23E',F').

These observations indicate that RPE morphology can be uncoupled from its proper specification and polarity orientation.

4. In search of new candidates involved in RPE specification

As already indicated in the introduction, our current knowledge of the gene regulatory network controlling RPE specification is still limited (Introduction section 5). To overcome this limitation, we performed RNA-seq analysis in the attempt of identifying new genes that could enlarge the network currently proposed to control RPE specification. For this purpose we used two transgenic zebrafish lines: enh1-*bhlhe40*:GFP and *vsx2.2*:GFP-caax (Gago-Rodrigues et al., 2015) which labels retinal progenitors at OV stages and NR cells at OC stages. Both *rx* and *vsx* genes, initially expressed in all retinal progenitors, are down-regulated in RPE cells while maintained in NR ones when they become specified. Therefore, we used *vsx2.2*:GFP-caax embryos at 16 hpf stage (14 ss) to isolate retinal progenitors and enh1-*bhlhe40*:GFP embryos to isolate RPE cells at two differentiation stages: 18 hpf (18 ss) and 23 hpf. At 18 hpf the RPE is composed of cuboidal cells whereas at 23 hpf they are already flat cells in an almost completely formed OC. The total RNA was extracted from isolated progenitor or RPE cells and used for deep sequencing (RNA-seq analysis). We were mostly interested in the differentially expressed genes (DEGs) at 16 hpf vs 18 hpf stage and 16 hpf vs 23 hpf stage. This work was performed in collaboration with Lorena Buono (Juan Ramón Martínez-Morales' laboratory, CABD) who sorted the progenitor cells (v*sx2.2*:GFP-caax) and performed the bioinformatics analyses.

Once we obtained the list of DEGs genes in 18 hpf and 23 hpf RPE cells compared with that of 16 hpf progenitors we validated the obtained transcriptome searching for enrichment of the genes used as markers to isolate the two cell populations. As expected, in both comparisons, the *bhlhe40* gene was up-regulated in the RPE whereas *vsx2* was down-regulated. We next analyzed the presence of other genes known to change their expression levels during RPE development. At 18 hpf, *rx* and *vsx1* were also down-regulated in the RPE. However, the core genes known to be involved in RPE specification were not detected until 23 hpf (*otx2b* and *mitfa*; see fold change values in Table 11).

16 hpf vs 18 hpf		**16 hpf vs 23 hpf**	
Gene	log2(fold change)	Gene	log2(fold change)
bhlhe40	1.68805	***bhlhe40***	2.98279
rx1	-1.03416	*otx2b*	1.0648
rx2	-1.97535	*mitfa*	4.17987
rx3	-1.70647	*rx1*	-1.43063
vsx1	-1.01992	*rx2*	- 0.976121
vsx2	-1.89106	*rx3*	-2.15439
		vsx1	-1.9182
		vsx2	- 0.813524

Table 11: Values of expression fold changes for genes differentially expressed in progenitors and RPE differentiated cells. Genes up-regulated in the RPE are shown in green and genes up-regulated in progenitors in white.

This initial analysis confirmed the specificity of the isolated transcriptomes. We therefore next analyzed the transcriptomes using a gene ontology (GO) enrichment analysis with the GOrilla tool (Eden et al., 2009) with the goal of identifying groups of genes with specific functions that were either up or down-regulated during RPE specification. At 18 hpf, there were several categories of up-regulated genes related to pigmentation and generation of reactive oxygen species (Figure 24). Genes belonging to the first category, such as *tyr*, *tyrp1b*, *dct* or *slc45a2*, were already up-regulated at early stages although pigmentation is visible only later in development. Thus, the pigmentation cascade is activated as part of the RPE specification process. Genes participating in the biosynthesis of oxygen reactive species, such as *nos1*, *nos2b* and *duox,* were also up-regulated likely because the oxygen-enriched environment that surrounds the RPE. At 23 hpf both of these categories of genes continue to be up-regulated and new GO classes appear, including chloride channels or inorganic anion transport molecules (Figure 25). These categories are related with RPE physiological functions and confirm that RPE specification is fully ongoing at early stages. Notably, the list of GO classes that were found down-regulated in the RPE as compared to progenitor cells was quite large. In both comparisons (16 vs 18 hpf and 16 vs 23 hpf), we found categories related to RNA processing and metabolism, translation, or nitrogen compound metabolism (Figure 26 and 27). Genes related with the regulation of the cell cycle and nuclear pore complex assembly appeared down-regulated at 23 hpf, in good agreement with our observations that OC folding occurs with little contribution of RPE proliferation.

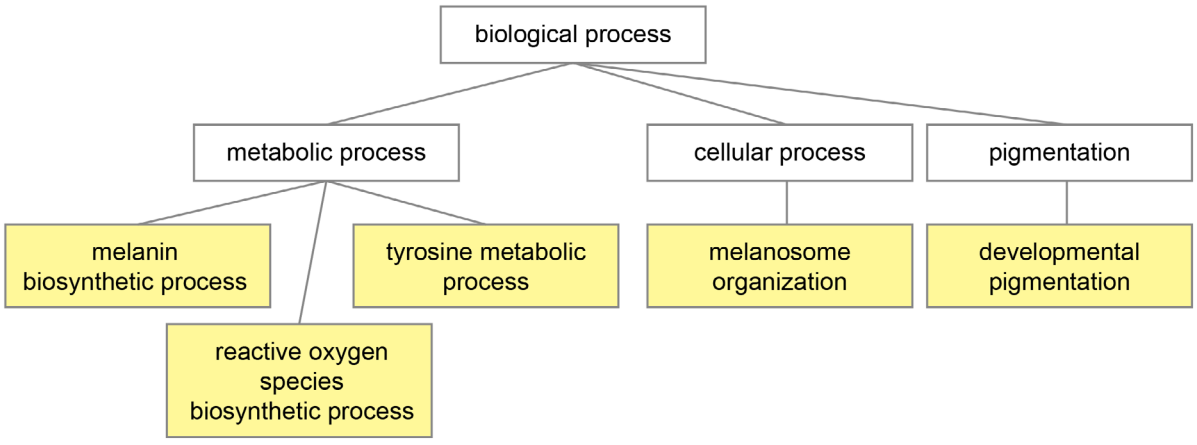

Figure 24: Enriched GO terms of genes up-regulated in the 18 hpf RPE when compared with 16 hpf retinal progenitors.

Simplification of the figure generated by the GOrilla tool (Appendix I), showing the main GO terms detected in the RPE up-regulated genes at 18 hpf stage. Yellow boxes are categories with p-values from 10^{-3} to 10^{-5}.

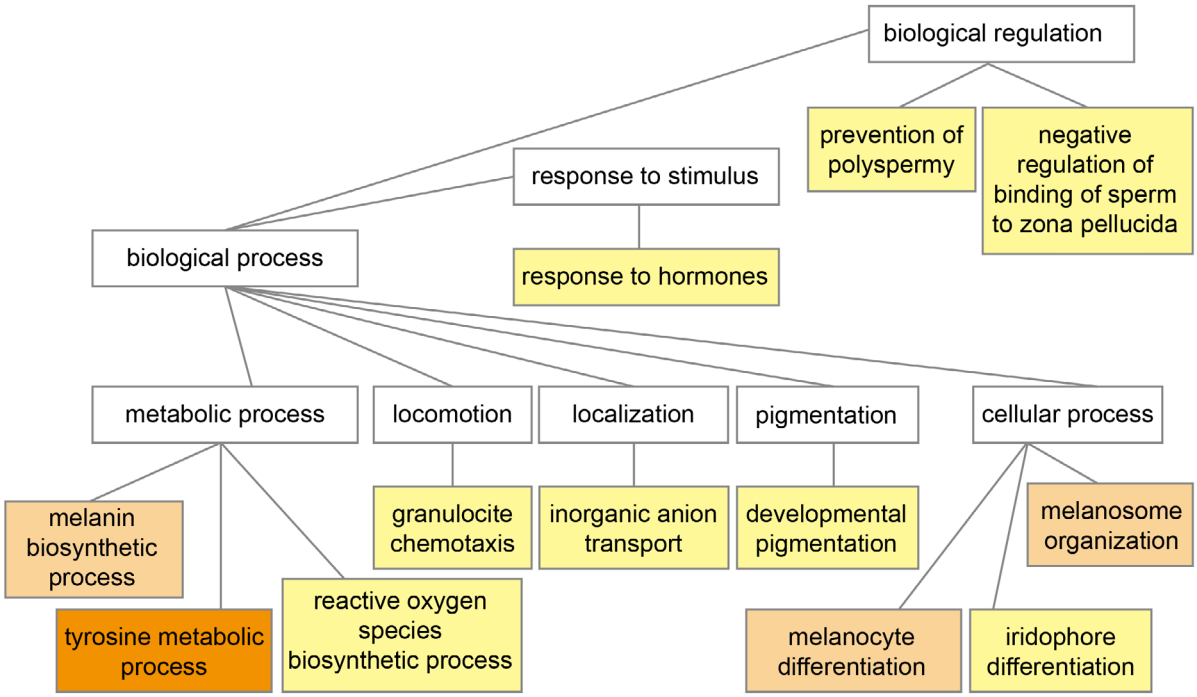

Figure 25: Enriched GO terms of genes up-regulated in the 23 hpf RPE when compared with 16 hpf retinal progenitors.

Simplification of the figure generated by the GOrilla tool (Appendix I) showing the main GO terms detected in the RPE up-regulated genes at 23 hpf stage. Yellow boxes are categories with p-values from 10^{-3} to 10^{-5}, light orange from 10^{-5} to 10^{-7} and dark orange from 10^{-7} to 10^{-9}.

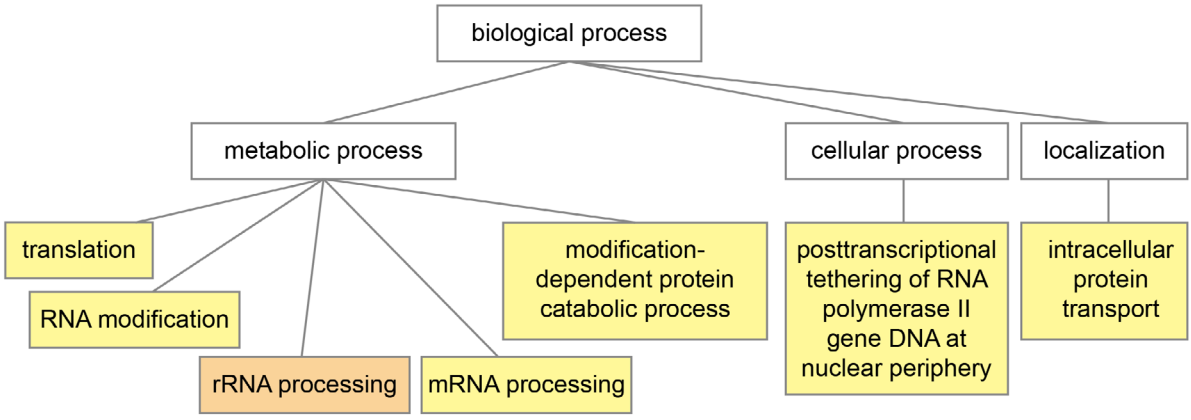

Figure 26: Enriched GO terms of genes down-regulated in the 18 hpf RPE when compared with 16 hpf retinal progenitors.

Simplification of the figure generated by the GOrilla tool (Appendix I) showing the main GO terms detected in the RPE down-regulated genes at 18 hpf stage. Yellow boxes are categories with p-values from 10^{-3} to 10^{-5} and light orange from 10^{-5} to 10^{-7}.

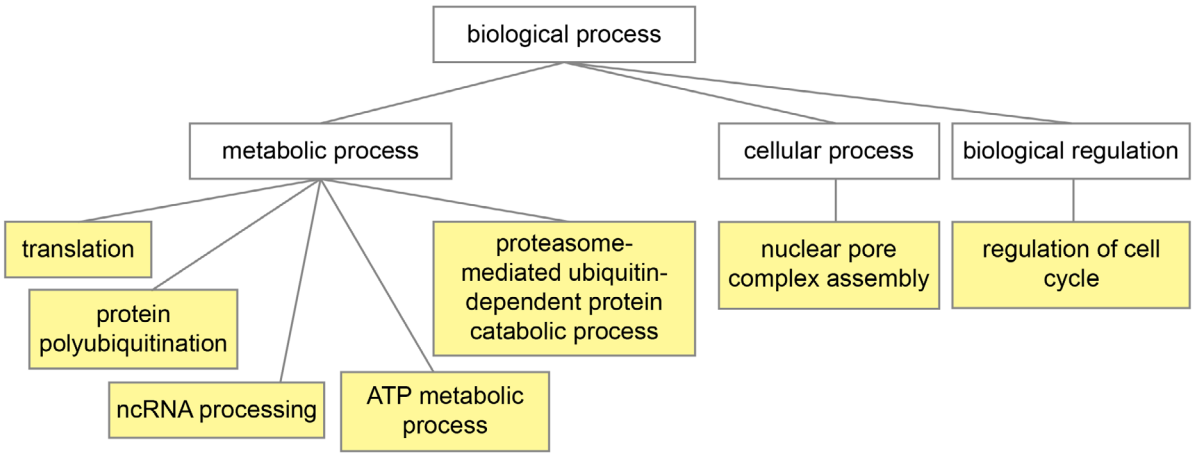

Figure 27: Enriched GO terms of genes down-regulated in the 23 hpf RPE when compared with 16 hpf retinal progenitors.

Simplification of the figure generated by the GOrilla tool (Appendix I) showing the main GO terms detected in the RPE down-regulated genes at 23 hpf stage. Yellow boxes are categories with p-values between 10^{-3} to 10^{-5}.

Among the curated list of genes, we searched for additional genes already described as related to RPE development. We mainly focused in transcription factors, molecules involved in cell-to-cell adhesion and cytoskeletal/ECM proteins, as these classes of genes are the likely motors of RPE transformation during OC folding. As already mentioned, comparison of the transcriptomes from retinal progenitor cells (16 hpf) with either 18 and 23 hpf RPE cells revealed the increased expression of several components of the pigmentation cascade (Table 12A) so that genes related with melanin production such as *tyr* (tyrosine) appear earlier than transcription factors or genes involved in melanosome transport such as *mitfa* or *rab27a*. Genes encoding components of the tight junction, adherens junctions and desmosome were also found, in agreement with the epithelial nature of the RPE and its role in the establishment of the blood barrier (Table 12B). Among the most prominent components, we found ocludins, claudins, E-cadherin (among other cadherins and protocadherins), plakophilins (which link cadherins to intermediate filaments), desmoplakins and desmoglein. Regarding ECM proteins (Table 12C) the most prominent changes between progenitors and RPE cells were related to collagen and laminin subunits composition and the down regulation of fibronectin (*fn1a* and *fn1b*).

Data kindly provided by Lorena Bueno and obtained with the tool "Classification System" of the PANTHER software (Mi et al., 2013) further pointed to a set of transcription factors that are likely important for the initial specification of the RPE. Most of them have not been previously investigated as determinants of RPE identity and will therefore be the objects of further validation using a screening approach based on gene knockout with the CRISPR/Cas9 technology and injecting several guides for the same gene (Wu et al., 2018). A list of the most relevant transcription factors that appeared in the transcriptome analysis as potentially relevant in RPE development is resumed in Table 13.

A. Pigmentation					
Transcript ID	Gene	Stage - Fold change			
ENSDARG00000006008	*dct*	18 hpf	5.50135	23 hpf	9.38421
ENSDARG00000056151	*tyrp1b*	18 hpf	4.98221	23 hpf	10.0066
ENSDARG00000002593	*slc45a2*	18 hpf	4.93576	23 hpf	8.10749
ENSDARG00000039077	*tyr*	18 hpf	4.37802	23 hpf	8.87469
ENSDARG00000033760	*pmelb*	18 hpf	3.62729	23 hpf	7.59104
ENSDARG00000029204	*tyrp1a*	18 hpf	2.7028	23 hpf	6.83287
ENSDARG00000061303	*oca2*	18 hpf	2.62916	23 hpf	7.49861
ENSDARG00000038991	*nsfb*	18 hpf	2.45987	23 hpf	2.31188
ENSDARG00000044781	*bace2*	18 hpf	1.9661	23 hpf	4.85637
ENSDARG00000007654	*nsfa*	18 hpf	1.45488	23 hpf	2.39337
ENSDARG00000069989	*bnc2*	18 hpf	1.35067	23 hpf	1.37017
ENSDARG00000061635	*myo5aa*	18 hpf	1.20883	23 hpf	3.24801
ENSDARG00000003732	*mitfa*	23 hpf		4.17987	
ENSDARG00000020237	*mc1r*	23 hpf		3.13239	
ENSDARG00000098745	*tfec*	23 hpf		1.94816	
ENSDARG00000026170	*hps1*	23 hpf		1.69744	
ENSDARG00000103935	*rab27a*	23 hpf		1.52763	
ENSDARG00000013581	*hps6*	23 hpf		1.12713	
ENSDARG00000026170	*hps1*	23 hpf		1.69744	
B. Cell adhesion					
ENSDARG00000090268 *(of 7 total keratins at 23*	*krtt1c19e hpf)*	18 hpf	4.10815	23 hpf	8.1762
ENSDARG00000090598	*pkp1a*	18 hpf	3.27316	23 hpf	3.75511
ENSDARG00000052705	*pkp1b*	18 hpf	2.85109	23 hpf	2.88545
ENSDARG00000051861	*pkp3a*	18 hpf	2.83105	23 hpf	3.93601
ENSDARG00000076945	*dsg2.1*	18 hpf	2.80353	23 hpf	3.3166
ENSDARG00000005108	*oclna*	18 hpf	2.55786	23 hpf	3.55202
ENSDARG00000003091	*oclnb*	18 hpf	2.54716	23 hpf	3.68841
ENSDARG00000040045 *(of 11 total cldn at 23*	*clnd1 hpf)*	18 hpf	2.37043	23 hpf	3.84156
ENSDARG00000022309	*dspa*	18 hpf	2.07345	23 hpf	1.92337
ENSDARG00000044968	*vcla*	18 hpf	1.7148	23 hpf	1.76177
ENSDARG00000102750 *(of 8 total cdh and 7*	*cdh1 pcdh)*	18 hpf	1.50446	23 hpf	1.94187
ENSDARG00000002909	*tjp3 (zo-3)*	18 hpf	1.49175	23 hpf	2.06681
ENSDARG00000076426	*dsg2l*	18 hpf		1.48668	
ENSDARG00000099323	*dlg2*	18 hpf		2.25883	
ENSDARG00000102216	*dlg1l*	18 hpf		1.1273	
C. ECM					
ENSDARG00000039133	*lamb4*	18 hpf	3.07016	23 hpf	4.51166
ENSDARG00000045524	*lamb1b*	18 hpf	2.21665	23 hpf	1.72046
ENSDARG00000012422 *(of 15 total col at 23 hpf)*	*col11a2*	18 hpf	4.15777	23 hpf	4.80306
ENSDARG00000093572	*lamc3*	18 hpf		2.04647	
ENSDARG00000033950	*lamb2l*	18 hpf		1.03711	

Table 12: (A) Group of genes found up-regulated in RPE populations at 18 hpf and 23 hpf related with pigmentation, **(B)** cell adhesion and **(C)** ECM.

18 hpf			23 hpf		
Transcript ID	Gene	Fold change	Transcript ID	Gene	Fold change
ENSDARG00000059362	*ptrfb*	4.64742	ENSDARG00000003991	*fhl2b*	4.50817
ENSDARG00000069675	*her8.2*	4.26755	ENSDARG00000015506	*klf5a*	3.86355
ENSDARG00000061391	*grhl1*	3.30818	ENSDARG00000055395	*foxq1b*	3.81265
ENSDARG00000015506	*klf5a*	3.02359	ENSDARG00000030896	*foxq1a*	3.69845
ENSDARG00000029766	*nr1i2*	2.76678	ENSDARG00000029766	*nr1i2*	3.60206
ENSDARG00000011956	*dlx4a*	2.7567	ENSDARG00000077982	*elf3*	3.47376
ENSDARG00000055926	*foxi3a*	2.53773	ENSDARG00000069675	*her8.2*	3.4368
ENSDARG00000008697	*epas1a*	2.52957	ENSDARG00000009550	*foxi3b*	3.36714
ENSDARG00000007097	*her13*	2.31256	ENSDARG00000004712	*tbr1b*	3.23185
ENSDARG00000009550	*foxi3b*	2.23062	ENSDARG00000061391	*grhl1*	3.1683
ENSDARG00000053650	*foxb1b*	2.17969	ENSDARG00000004060	*bhlhe40*	2.98279
ENSDARG00000078552	*grhl3*	2.09108	ENSDARG00000040432	*klf2b*	2.97727
ENSDARG00000062510	*bcl11ba*	1.77998	ENSDARG00000015876	*npas1*	2.84221
ENSDARG00000098730	*eng1b*	1.77822	ENSDARG00000036051	*irx4b*	2.78897
ENSDARG00000004060	*bhlhe40*	1.68805	ENSDARG00000023537	*ahr1b*	2.7532
ENSDARG00000017168	*nr2f1b*	1.64252	ENSDARG00000011956	*dlx4a*	2.7416
ENSDARG00000039569	*emx1*	1.59903	ENSDARG00000008697	*epas1a*	2.73964
ENSDARG00000054031	*mxd4*	1.53	ENSDARG00000059362	*ptrfb*	2.72814
ENSDARG00000039701	*emx2*	1.5192	ENSDARG00000055926	*foxi3a*	2.64459
ENSDARG00000052695	*nr2f1a*	1.51869	ENSDARG00000039569	*emx1*	2.43673
ENSDARG00000059279	*tfap2a*	1.51784	ENSDARG00000055493	*hic1*	2.22568
ENSDARG00000044356	*tp63*	1.50952	ENSDARG00000063153	*bcl11ab*	2.20389
ENSDARG00000077982	*elf3*	1.4836	ENSDARG00000078552	*grhl3*	2.17536
ENSDARG00000102082	*nr3c2*	1.41373	ENSDARG00000021833	*ahr2*	2.14102
ENSDARG00000021833	*ahr2*	1.39427	ENSDARG00000041691	*bhlhe41*	2.08946
ENSDARG00000071560	*dlx4b*	1.38628	ENSDARG00000069988	*arid5b*	2.02385
ENSDARG00000009280	*smyd1a*	1.37609	ENSDARG00000075274	*tead4*	1.97724
ENSDARG00000069989	*bnc2*	1.35067	ENSDARG00000029497	*tfcp2l1*	1.88176
ENSDARG00000040432	*klf2b*	1.33817	ENSDARG00000056638	*pir*	1.8433
ENSDARG00000102025	*znf644b*	1.33809	ENSDARG00000059279	*tfap2a*	1.81894
ENSDARG00000003469	*neurod4*	1.33207	ENSDARG00000079922	*klf4*	1.80976
ENSDARG00000056638	*pir*	1.32077	ENSDARG00000039095	*nkx2.3*	1.78774
ENSDARG00000023537	*ahr1b*	1.31139	ENSDARG00000002026	*qkib*	1.7654
ENSDARG00000026395	*rfx4*	1.30274	ENSDARG00000043483	*otx5*	1.7468
ENSDARG00000068409	*vgll4l*	1.2803	ENSDARG00000079201	*TSHZ2*	1.73153
ENSDARG00000100232	*glis2b*	1.27719	ENSDARG00000015064	*esrrd*	1.68563
ENSDARG00000035735	*gsx1*	1.23964	ENSDARG00000087303	*cebpd*	1.609
ENSDARG00000059483	*tead1b*	1.17988	ENSDARG00000068409	*vgll4l*	1.59929
ENSDARG00000059483	*tead1b*	1.17988	ENSDARG00000031777	*pparaa*	1.59118
ENSDARG00000074030	*myt1a*	1.15737	ENSDARG00000007097	*her13*	1.52911
ENSDARG00000079922	*klf4*	1.12598	ENSDARG00000054031	*mxd4*	1.492
ENSDARG00000031138	*irx3b*	1.10591	ENSDARG00000100497	*hic2*	1.44924
ENSDARG00000037196	*ARID5B*	1.0899	ENSDARG00000095170	*lrrfip1b*	1.44919
ENSDARG00000061509	*tbx3b*	1.06929	ENSDARG00000017168	*nr2f1b*	1.42974
ENSDARG00000036868	*tbpl1*	0.998784	ENSDARG00000068168	*hes2.2*	1.38865
ENSDARG00000022569	*nkx6.1*	0.989023	ENSDARG00000069989	*bnc2*	1.37017
ENSDARG00000032039	*mxd1*	0.983951	ENSDARG00000006640	*eomesa*	1.35385
ENSDARG00000020417	*emx3*	0.977172	ENSDARG00000086173	*relb*	1.3018

ENSDARG00000008886	*msx1b*	0.966528	ENSDARG00000101959	*etv1*	1.30129
ENSDARG00000074526	*zbtb16b*	0.953711	ENSDARG00000104090	*june*	1.29586
ENSDARG00000074319	*sall1a*	0.912506	ENSDARG00000008886	*msx1b*	1.22701
ENSDARG00000100497	*hic2*	0.902389	ENSDARG00000003469	*neurod4*	1.22481
ENSDARG00000077840	*meis2b*	0.79308	ENSDARG00000037196	*ARID5B*	1.16353
			ENSDARG00000003165	*nr2f6b*	1.15637
			ENSDARG00000071560	*dlx4b*	1.14038
			ENSDARG00000076068	*crtc1a*	1.08566
			ENSDARG00000011235	*otx2*	1.06377
			ENSDARG00000101628	*ascl1b*	1.06074
			ENSDARG00000052695	*nr2f1a*	1.00136
			ENSDARG00000032039	*mxd1*	0.993912
			ENSDARG00000033172	*nr2f5*	0.940319
			ENSDARG00000039701	*emx2*	0.912486

Table13: Transcription factors upregulated in the RPE at 18 and 23 hpf when compared with retinal progenitors.

bhlhe40 gene itself was up-regulated at 18 hpf and 23 hpf when comparing with progenitors at 16 hpf with a fold change of 1.69 and 2.98 respectively. This was expected since its expression in the RPE starts around 15 ss (Yao et al., 2006; previous results). *bhlhe40* encodes a recently RPE-associated transcription factor, which seems to bind the *mitf* promoter (Feige et al., 2011). This observation together with its restricted expression pattern suggested a possible implication in RPE specification. There is already available information regarding *bhlhe40* knockdown experiments in zebrafish which induce alterations in the circadian locomotor activity in larvae, a function related with the expression of the gene in the pineal gland (Ben-Moshe et al., 2014). However, its role in eye development has not been studied. To address this issue we generated the corresponding mutant using the CRISPR-Cas9 technology.

5. Bhlhe40 transcription factor is dispensable during RPE morphogenesis

The *bhlhe40* gene is located in the minus strand of the 11 chromosome and it is composed of 5 exons. Only one transcript of 2804 bp has been identified which gives rise to a 403 aa length protein with three different domains. The first domain is the bHLH domain required for dimerization and specific binding to the DNA which is followed by an Orange domain, characteristic of transcriptional repressors and responsible for dimerization with other proteins. The presence of these two domains in tandem is characteristic of the bHLH-O family of transcriptional repressors to which the Bhlhe40 protein belongs (Sun et al., 2007, Davis and Turner, 2001). Finally, a proline-rich domain is located at the C-terminal region through which the protein interacts with the HDAC proteins as co-repressors (He et al., 2009, Sun and Taneja,

2000). The zebrafish gene shares about 60% identity with its orthologues in human, mouse and rat and this homology raises up to 97% when the bHLH domain alone is considered (Sun et al., 2007, Yao et al., 2006). We generated two different mutations in the *bhlhe40* gene (Figure 28A). One mutation was a 5 bp deletion in exon 2 (E2 mutant; Figure 28B), which generated an early

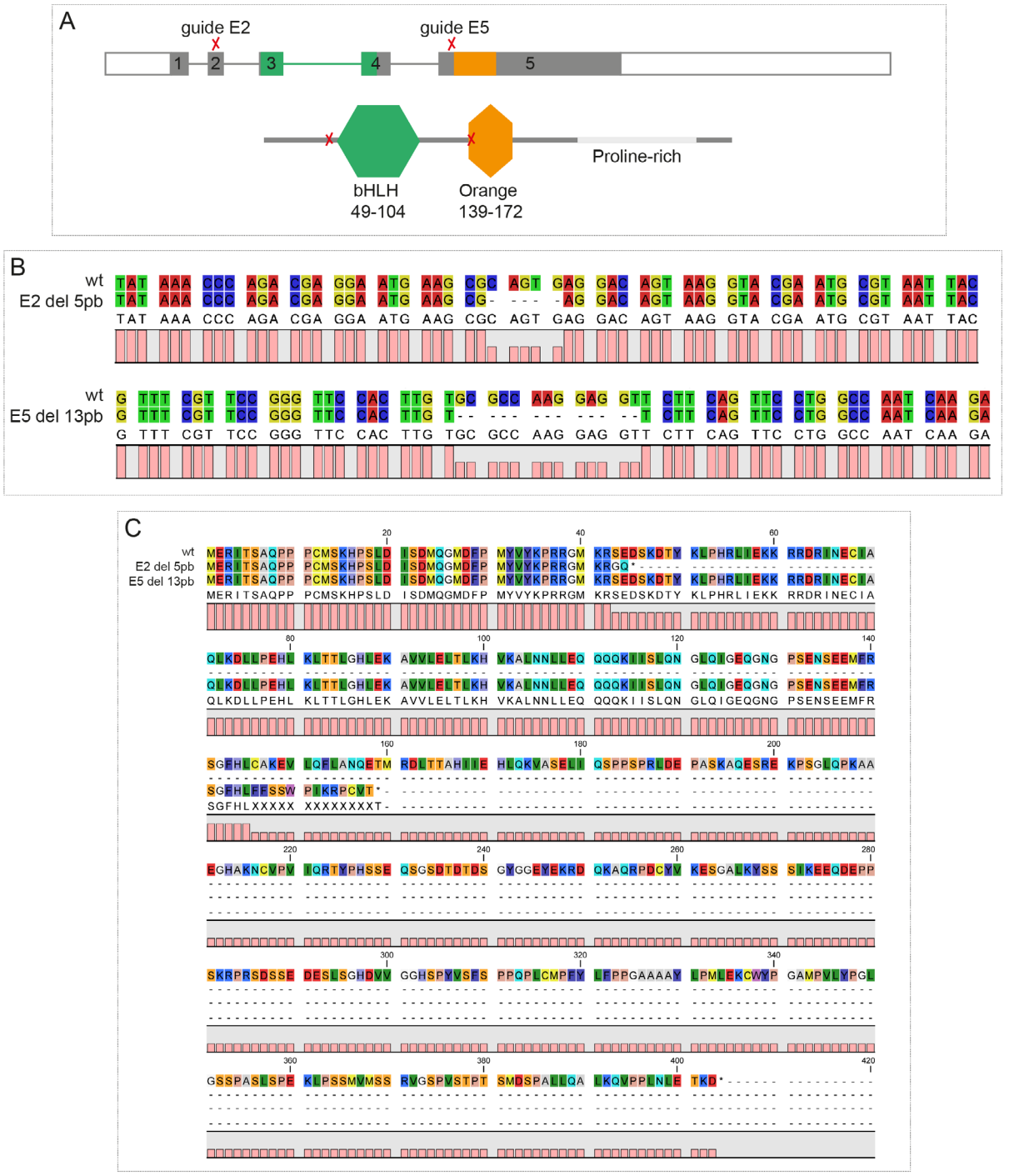

Figure 28: *bhlhe40* mutant design.

(A) Schematic representation of *bhlhe40* mRNA and protein structures in which the mutated regions are represented. **(B)** Sequence alignment between the wild type and the mutant gDNAs (E2 above, E5 below). **(C)** Sequence alignment between the wild type and the mutant proteins. Alignments were done with CLC Sequence Viewer 8.0.

stop codon. The resulting protein was a truncated version containing the first 42 aa plus 2 de novo aa (Figure 28C). We designed guides to induce DNA breaks around the exon 2 to avoid the possibility that the transcriptional machinery would have found an alternative transcription initiation site but with the security that the resulting truncated protein would lack the bHLH domain. According to this strategy, the resulting sequence had no alternative start site that could generate an "in phase" transcript. The second mutation we obtained was a deletion of 13 bp at the beginning of exon 5 (E5 mutant; Figure 28B) that also caused an early stop codon. The resulting protein had 158 aa from which the last 13 were changed with respect to the wild type protein (Figure 28C). It contained the bHLH domain but only 6 aa from the Orange domain. With this mutant, we intended to generate a potential dominant negative version that would bind to DNA without interacting with cofactors through the Orange domain.

The two mutant lines grew to adulthood, and maternal zygotic mutants were also recovered and analyzed. At 24 hpf no evident eye defects were found when comparing wild type (Figure 29A) and mutant embryos (Figure 29B,C). In all cases the OC was normally formed and the general morphology of the embryo appeared normal. Similar results were observed at 48 hpf when eye had a normal shape, size and pigmentation levels (Figure 29D-F). The morphology of the adult eye was also normal (Figure 29G-I) and the NR presented a normal layer composition (Figure 29G'-I'). In sum, all eye structures were properly formed and maintained despite *bhlhe40* knockout, indicating that this transcription factor is dispensable for eye morphogenesis.

As *bhlhe40* gene does not seem to be required for RPE morphogenesis, we next explored its potential contribution to RPE homeostasis and/or its functions as an essential structure for photoreceptor survival. Indeed, in eyes with impaired RPE functions a strong light stimulus would enhance photoreceptor damage. To assess a potential impairment of RPE functions, we exposed 5 days post fertilization (dpf) larvae to a light source of more than 90000 lux during 30 min and allowed them to recover for 2 days. This procedure caused a photolesion that led to photoreceptors' death. To assess this death, we analyzed the presence of photoreceptors using the zpr1 antibody that labels red/green double cones. In the wild type larvae exposed to intense light, photoreceptors showed an aberrant morphology with a rounder shape and a shorter outer segments (Figure 30A,B), as compared to those of untreated larvae. Immunostaining was more intense in the outer segment as compared to controls in which it was localized mostly the inner segment. The E2 mutants presented a very similar phenotype with no apparent enhanced damage to the photoreceptors (Figure 30C,D). Hence, the mutants do not show an increased photosensitivity and the function of *bhlhe40* gene in the RPE does not seem to be required for photoreceptor homeostasis.

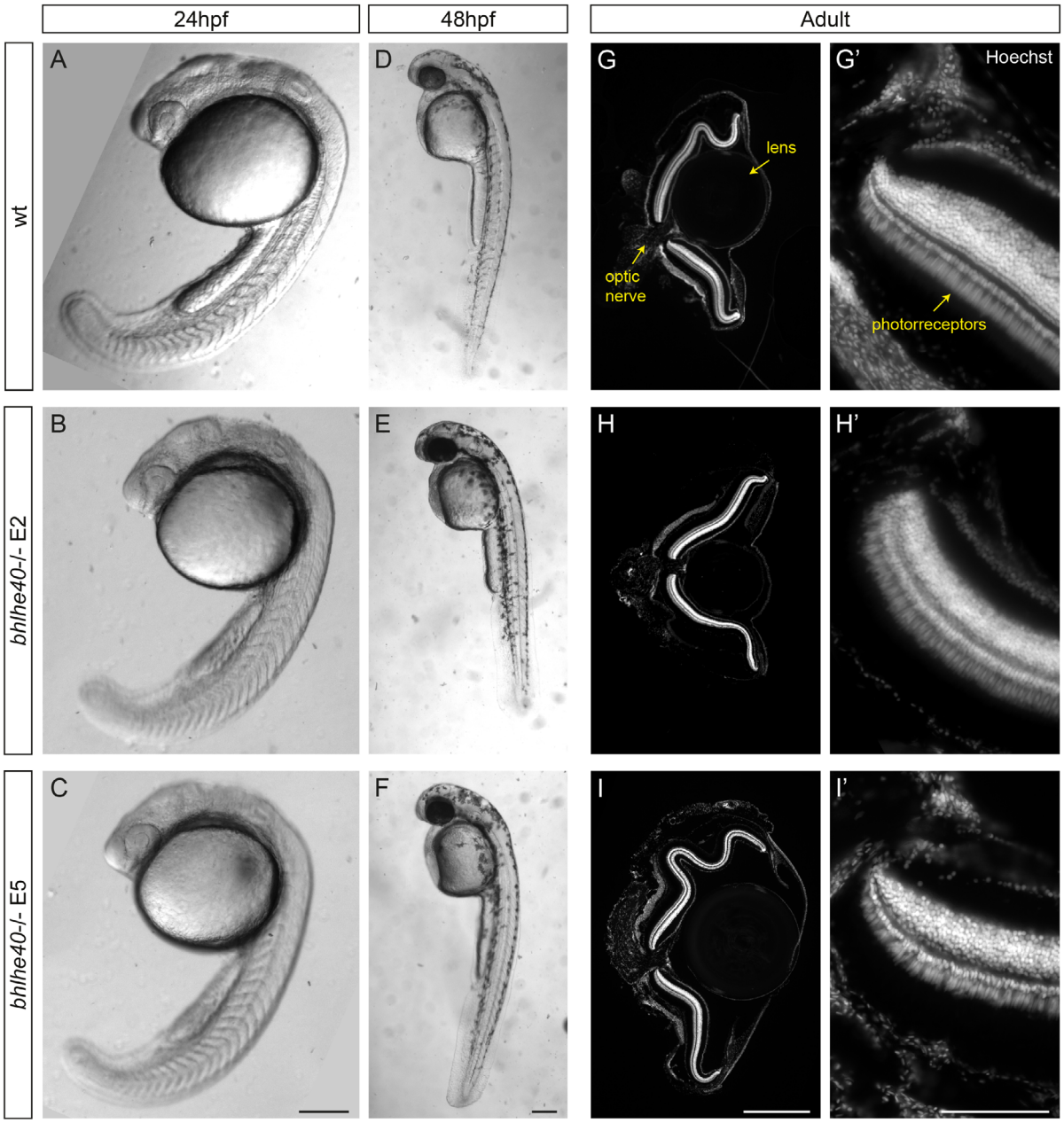

Figure 29: *bhlhe40* mutants have no evident eye morphogenesis defects.

(A) Lateral view of wild-type, **(B)** *bhlhe40* E2 mutant and **(C)** *bhlhe40* E5 mutant embryos at 24 hpf. In all embryos the eyes have a similar level of development with an OC formed although still not closed. **(D)** Lateral view of wild-type, **(E)** *bhlhe40* E2 mutant and **(F)** *bhlhe40* E5 mutant embryos at 48 hpf. All embryos show normal OCs and pigmentation levels. **(G,G')** Cryosections of wild-type, **(H,H')** *bhlhe40* E2 mutant and **(I-I')** *bhlhe40* E5 mutant adult eyes at different magnifications. General eye structure and layers are properly formed and maintained in both mutants. Scale bars: 200 µm in **A -F**, 500 µm in **G-I** and 100 µm in **G'-I'**.

Genetic compensation is a frequent event in zebrafish, after selective gene mutations (El-Brolosy et al., 2019, El-Brolosy and Stainier, 2017). The absence of a phenotype related to OC morphogenesis in the *bhlhe40* mutants could be due to compensation by related genes. This gene has 26 homologue genes in zebrafish, which are also bHLH-orange transcription factors, sharing low percentages of identity (between 15 and 40%). The closest homologue is the *bhlhe41* (Basic Helix-Loop-Helix Family Member E41) gene, also known as *dec2*, *sharp1* or *bhlhb3*. The

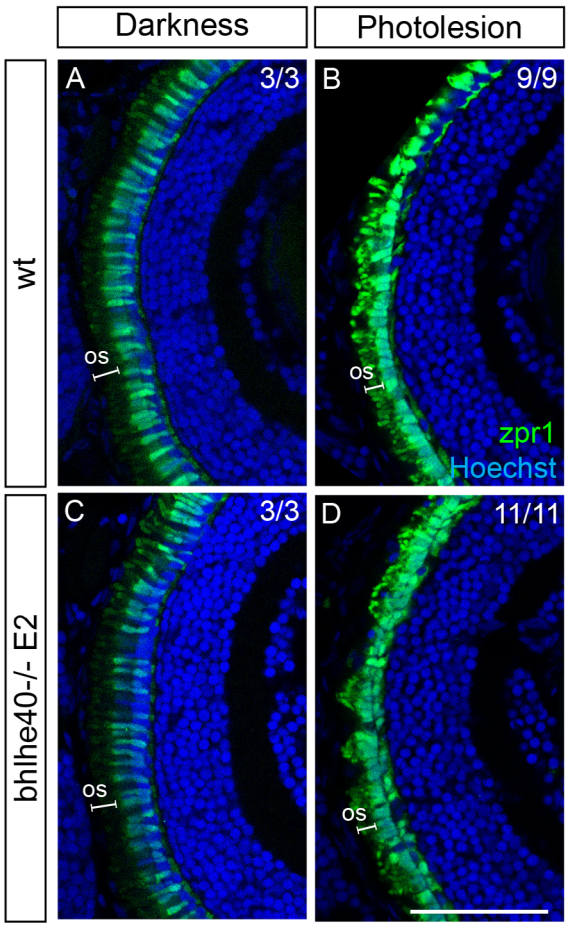

Figure 30: Mutant and wild type larvae have similar levels of photosensitivity.

(A) Control wild type larva. **(B)** Control *bhlhe40* E2 mutant larva. **(C)** Wild type larva after photolesion. **(D)** *bhlhe40* E2 mutant larva after photolesion. Both wild type and mutant larvae respond in a similar way to high light intensity exposure. Photoreceptor's nuclei are pyknotic and the outer segments (os, white bars) of photoreceptors are clearly disorganized. All images are frontal cryosections labeled with zpr1 antibody (green; red/green double cone photoreceptors marker) and Hoechst (blue). Scale bar: 50 µm.

two derived proteins share 53% identity in their overall amino acid sequence, and 92% and 51% identity when comparing the bHLH and Orange domains, respectively. The expression pattern described for the *bhlhe41* gene differs from what we have observed for *bhlhe40,* although both genes are expressed in the pineal gland and have been related with circadian rhythms (Abe et al., 2006). ISH studies did not detect *bhlhe41* expression in the zebrafish RPE (Chen et al., 2010, Yao et al., 2006, Ben-Moshe et al., 2014), although the gene is found up-regulated in RPE cells at 23 hpf (2,09 fold change as compared to 16 hpf progenitor cells) in our RNA-seq analysis. Furthermore, both *Bhlhe40* and *Bhlhe41* increase their expression during mouse RPE maturation (Cohen-Tayar et al., 2018) and are found up-regulated in hiPSCs (human induced pluripotent stem cells) differentiated into RPE together with *MITF* (Chuang et al., 2018). Therefore, and although it has been suggested that the two genes have no redundant functions (Chen et al., 2010), we decided to analyze *bhlhe41* expression levels in the *bhlhe40* mutants. First, we performed an ISH against *bhlhe41* to see if there are differences in the pattern or the intensity of the signal. At 24 hpf *bhlhe41* mRNA was detected in the midbrain, hindbrain and pronephric duct as previously described (Chen et al., 2010; Figure 31A). In the E2 and E5 mutants, this expression pattern was maintained and no differences were found (Figure 31B,C). We also performed semi-quantitative PCR analysis in 24 hpf embryos and 5 dpf larvae. In wild type and mutants the amplified bands had a similar level of intensity (Figure 31D). This indicates that *bhlhe41* transcripts are not up-regulated when Bhlhe40 is absent, which however cannot completely discard a compensatory activity of the *bhlhe41* gene. To rule out this possibility, we attempted to inactivate the *bhlhe41* gene on the *bhlhe40* mutant background

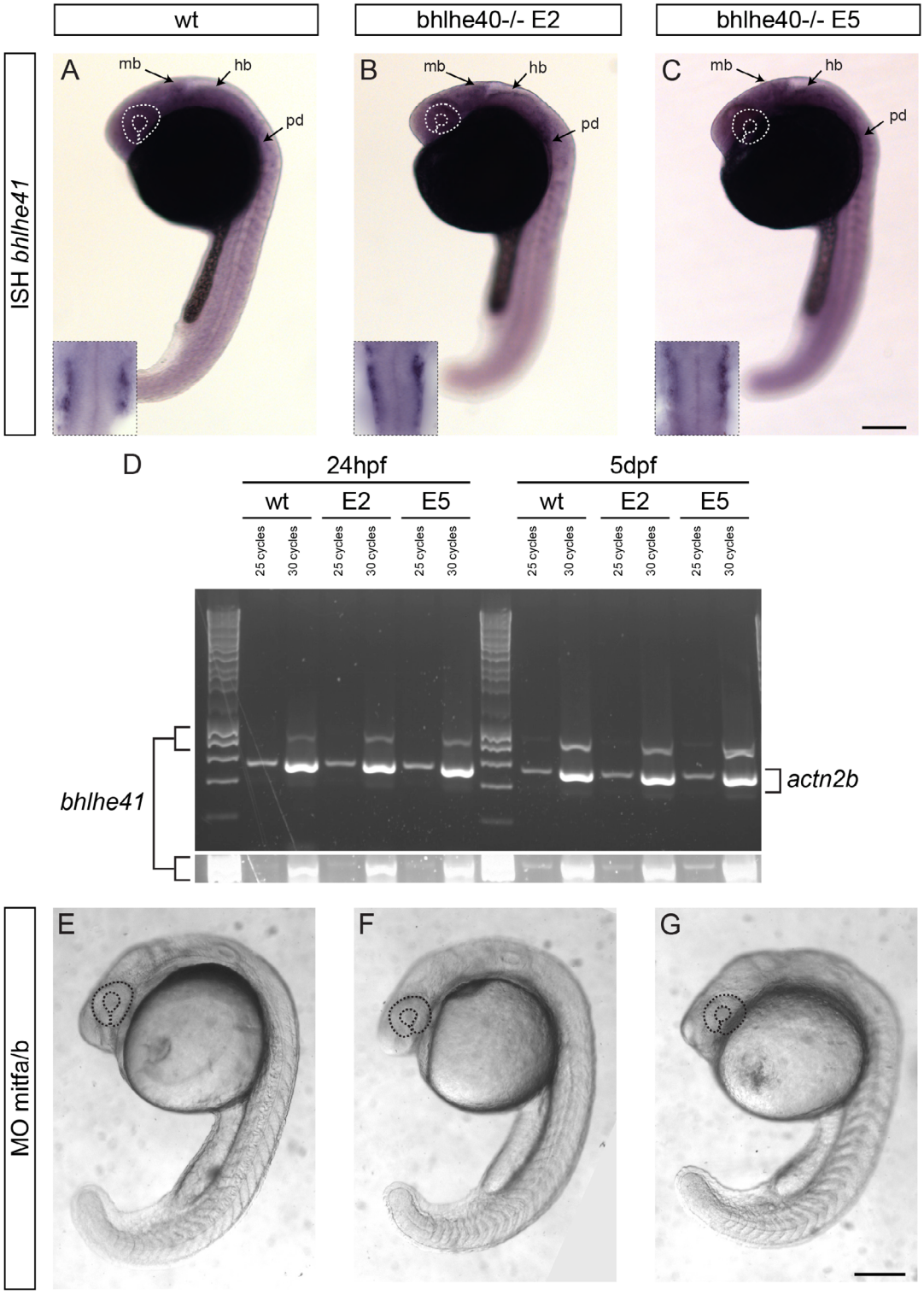

Figure 31: Analysis of genetic compensation in *bhlhe40* mutants.

(A) *bhlhe41* ISH in wild type, **(B)** E2 *bhlhe40* mutant and **(C)** E5 *bhlhe40* mutant embryos. There are no evident differences in the expression pattern between wild type and mutant embryos. *bhlhe41* is expressed in the midbrain (mb), hindbrain (hb) and pronephric ducts (pd). In the lower left corner pronephric duct signal is shown from a dorsal view. **(D)** Semiquantitative PCR of *bhlhe41* and *actn2b* (control) in wild type and *bhlhe40* mutant embryos at 24 hpf and 5 dpf (heads). No differences in *bhlhe41* expression levels are detected. **(E)** Injection of *mitfa* and *mitfb* MOs in wild type, **(F)** E2 *bhlhe40* mutant and **(G)** E5 *bhlhe40* mutant embryos. Despite MOs injection embryos developed normally. **A-C** and **E-G** are lateral views of 24 hpf embryos. All the images are lateral views of the whole embryo. Scale bars: 200 µm in **A-C** and **E-G**.

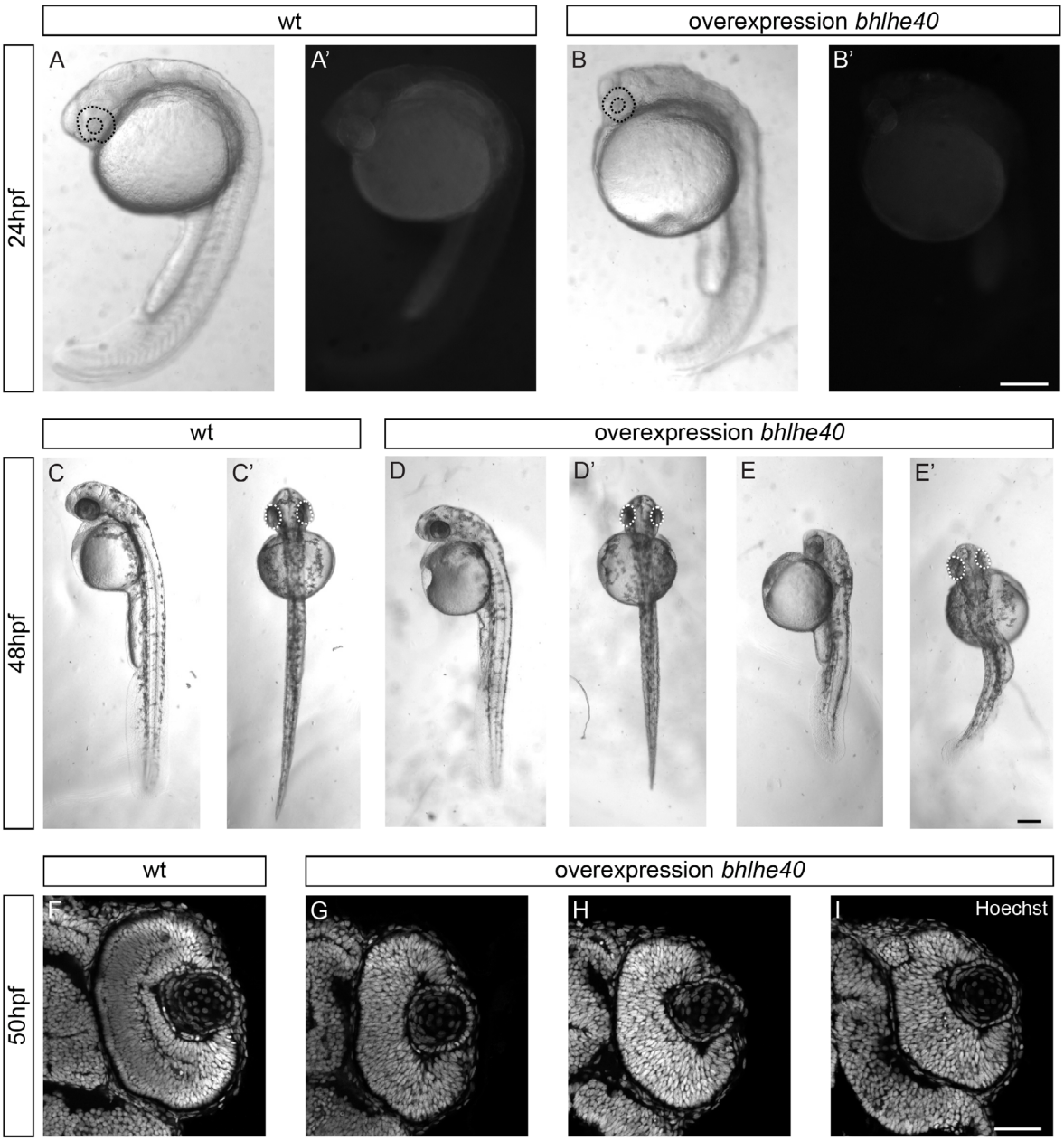

Figure 32: Overexpression of *bhlhe40* causes a reduction of the eye and embryo size.

(A) Bright field and **(A')** GFP fluorescence lateral view of an enh1-*bhlhe40* embryo at 24 hpf. **(B)** Bright field and **(B')** GFP fluorescence lateral view of an enh1-*bhlhe40* embryo injected with *bhlhe40* mRNA at 24hpf. Embryos in which *bhlhe4*0 is overexpressed show decreased size and smaller eyes. **(C)** Lateral and **(C')** dorsal view of an enh1-*bhlhe40* embryo at 48 hpf. **(D,E)** Lateral and **(D',E')** dorsal view of enh1-*bhlhe40* embryos injected with *bhlhe40* mRNA at 48 hpf. **(F)** Frontal cryosections of an enh1-*bhlhe40* embryo at 60 hpf. **(G-I)** Frontal cryosections of enh1-*bhlhe40* embryos injected with *bhlhe40* mRNA at 60 hpf. Embryos in which *bhlhe4*0 is overexpressed show decreased size, smaller eyes and defects in the tail. Scale bars: 200 µm in **A-E**' and 50µm in **F-I**.

using three different guides at the same time, a strategy successfully used by Wu et al. (2018). Unfortunately, none of the 4 guides (Material and Methods section 20) we used successfully altered the *bhlhe41* gene.

As it was mentioned before, a functional relation between *bhlhe40* and *mitf* was described under hypoxia. Feige et al. (2011) describe the presence of *BHLHE40* binding sites in the

promoter of the M-MITF isoform. Alternative promoters and alternative splicing are relevant in mammals for the regulation of several MITF isoforms. The *mitf* regulatory landscape seems more complex in mouse or human than in zebrafish, in which the gene is duplicated but a single isoform for both *mitfa* and *mitfb* were identified (Lane and Lister, 2012, Lister et al., 2001). However, a possible *bhlhe40*-mediated regulation of *mitf* genes could exist also in zebrafish. We explored this possibility injecting morpholinos against *mitfa* and *b* previously used by Lane and Lister (2012) in the *bhlhe40* mutants. This approach should address whether the two genes cooperate during RPE development and whether *mitf* could compensate *bhlhe40* functions in the mutants. Knockdown of *mitfa* and *b* however caused no effect on the mutants (Figure 31E-G).

Finally, we decided to address the possible function of *bhlhe40* by overexpressing its mRNA in zebrafish embryos. We observed that overexpression of *bhlhe40* caused the shortening of the embryonic antero-posterior axis detectable at 24 hpf (Figure 32A,B) associated in some cases to tail defects (Figure 32E,E'). More notably, eyes were visibly smaller both at 24, 48 and 60 hpf (Figure 32C-I) and in some cases the defects were asymmetric (Figure 32D',E'). These eye phenotypes were detected in about 70% of the injected embryos whereas the remaining 30% were undistinguishable from wild type. GFP reporter expression from the enh1-*bhlhe40*:GFP line was detectable in both control and *bhlhe40* overexpressing embryos (Figure 32A',B').

Together these results suggest that *bhlhe40* might normally down-modulate cell proliferation, which is in agreement with the idea that RPE proliferation is quite reduced as compared to the NR. The phenotype could be also explained by a control of cell death; however, this is unlikely since differential cell death was not detected in injected embryos.

DISCUSSION

The work described in this thesis provides insights into the mechanisms controlling the transformation of zebrafish RPE cells from a columnar/neuroepithelial to a flatten morphology, a process that occurs concomitantly to RPE specification. Cell shape change mediated by myosin II and MTs is the main process contributing to RPE expansion. Indeed, proliferation, which is a mayor mechanism for tissue growth, is negligible during RPE flattening. Notably, this RPE cell shape change represents a motor for OC folding together with the already described contribution of NR basal constriction. The list of DEGs in the RPE versus retinal progenitors, generated during this thesis, further identifies new potential candidate genes that can be added to the regulatory network driving the specification of this epithelium. Notably, this analysis underscores the importance of cytoskeletal and tight and adherens junction components as key factors underlying RPE specification/differentiation, further supporting the contention that morphological transformation of RPE cells is an important part of its initial development. The generation of a transgenic line, in which GFP reporter expression driven by a specific *bhlhe40* enhancer identifies nascent RPE cells, enabled reaching this conclusion. However, and despite a specific up-regulation during early steps of RPE specification, the *bhlhe40* does not seem to be required for RPE development or homeostatic functions, likely because others and yet unidentified related genes may compensate for its activity.

1. Zebrafish RPE reporter lines

The transgenic line enh1-*bhlhe40*:GFP had just been generated in the laboratory when the present work started. At that time, the scientific community did not count with zebrafish lines that specifically labeled the RPE at very early stages of its specification. This transgenic line shows specific GFP expression in RPE cells from 14 ss/16 hpf and, later in development, it also labels neural crest cells and the pineal gland. Thus the discovery of the enhancer 1 gave us the advantage of visually identifying RPE cells as they acquired their identity thereby enabling the study of early RPE morphogenesis. As we were performing this analysis, other two RPE reporter lines have been described. The first one, known as 4xGTIIC:eGFP, represents the reporter of the transcriptional activity of factors of the Tead family (Miesfeld and Link, 2014). In this line, four consecutive consensus Tead binding sites drive GFP expression. Tead transcription factors need the interaction with other cofactors to activate transcription, including Yap/Taz, which are expressed in zebrafish RPE cells (Miesfeld et al., 2015). The 4xGTIIC:eGFP line expresses GFP in the RPE from 18 ss/18 hpf, thus later than the enh1-*bhlhe40*:GFP line. An additional disadvantage of the 4xGTIIC:eGFP line for the study of RPE development is its expression in other structures including the lens ectoderm, *foxc1b*-positive mesenchymal cells of the head, the

midbrain/hindbrain boundary and, at later stages, also the heart and the somites (Miesfeld et al., 2015, Miesfeld and Link, 2014). The second described RPE reporter line, known as -2.7 kb *tfec*:eGFP, is a transgenic line in which the 2.7 kb upstream the *tfec* gene drives GFP expression (Miesfeld et al., 2015). In this case GFP expression in the RPE is detected at 10 ss stage (14 hpf), when both cell layers of the OV are still pseudostratified, therefore slightly earlier that the line we generated. However, the *tfec* gene is expressed also in neural crest cells so that the transgenic line does not allow distinguishing between these two populations or from the wide region of the diencephalon where reporter expression is also found.

Taking these observations together, the enh1-*bhlhe40*:GFP can be considered as the best available tool to study early RPE development as it is highly specific and marks the nascent RPE at the appropriate time.

The enh1-*bhlhe40*:GAL4 transgenic line generated in this work, in contrast, did not show the expected RPE restricted expression. When the UAS:GFP vector was injected, GFP expression was detected in both the NR and the RPE. The unexpected transgene expression in the NR was incompatible with the goal of driving gene expression exclusively in the RPE. We interpret the observed pattern for the GAL4 line as a result of a position effect due to the site of integration of the transgene. The chromosomal environment around the transgene may affect its expression and differences can be found in different fishes with different sites of insertion (Stuart et al., 1990). These position effects can be avoided using insulators, DNA sequences that avoid the transgene response to surrounding regulatory sequences (Bessa et al., 2009, Chung et al., 1993). Unfortunately the GAL4 line was generated without *β-globin* 5′ HS4 insulators present at both sides of the transgene enh1-*bhlhe40*:GFP (Allen and Weeks, 2005, Bessa et al., 2009) because the approach used for the generation of the GAL4 line did not initially allowed the inclusion of insulators. When analyzing potential founders (F0) for the GAL4 line we used the marker for effective transgenesis (*cmlc2*:EGFP) that drives GFP expression in the heart. Fishes whose progeny (F1) had GFP expression in the heart were selected assuming GAL4 expression in the RPE. Then, it was not until we injected the UAS:GFP vector in F2 embryos that we could verify the actual GAL4 eye expression pattern. In the future, additional founders should be screened expecting to find the transgene in another chromosomal position with a more restricted RPE pattern. Additionally, we could use the enh1-*bhlhe40*:GFP line to generate a GAL4 knock-in fish using CRISPR/Cas9 technology as previously described by Kimura et al. (2014) and successfully used by some collaborators. The GAL4 gene would be introduced in the already integrated transgene after the enhancer 1, and before the GFP, so that the site of integration would be maintained and the lack of position effects ensured.

2. Cell flattening as a mechanism of epithelial morphogenesis

As stated in the introduction, tissue and organ morphogenesis involves a number of different events. Our *in vivo* studies suggest that cell death and cell migration do not take place during RPE morphogenesis since neither apoptotic events nor cell movements are detected. We have therefore focused our attention to cell proliferation and cell shape changes.

The regulation of the growth of the inner and outer layers of the OV/OC has been proposed as a mechanism underlying OC folding in mouse embryos (Okuda et al., 2018, Carpenter et al., 2015). For example, in the *Wls* mouse mutants (Wnt ligand transporter wntless), RPE proliferation is reduced and, as a consequence, this tissue consists of half the cell number of wild type RPE (Carpenter et al., 2015). Since fewer RPE cells are generated, there is a reduction of RPE extension associated with less folded eyes, despite the presence of a normal NR (Carpenter et al., 2015). Similarly, Okuda et al. (2018) developed models to address OC folding and their simulations indicate that a specific proportion of RPE versus NR cell number is required for proper folding.

In this thesis, we analyzed to what extent proliferation is important for zebrafish RPE development, taking advantage of our RPE reporter line and BrdU incorporations. In apparent contrast with the above studies, we found that, following RPE specification, between 16 ss/17 hpf to 20 ss/19 hpf, there is a 30% reduction of the proliferation rate, which coincides with the formation of the first flat cells. This suggests that proliferation does not contribute in a very significant manner to RPE surface expansion. RPE proliferation in zebrafish has been previously analyzed by Cechmanek and McFarlane (2017) using immunostaining of PH-H3. PH-H3 is a marker of mitosis, a very short phase of the cellular cycle. Since zebrafish RPE cell number is very low, important information may be missed when only labelling mitosis. We determined that, at 18 ss, 34% of RPE cells are proliferating whilst only 2-4% are apparently undergoing mitosis (Cechmanek and McFarlane, 2017). Notably, in our study *ccnd1*-mediated over-proliferation of OV cells retained RPE cells in a cuboidal shape and in a dorsal position, supporting a minor contribution of proliferation to zebrafish RPE expansion, in which a minority of cells (around 20%) will undergo proliferation between 20 ss and 48 hpf stages to allow the tissue to adapt to the continuous NR growth. The difference between our results and the observations in mouse embryos likely reflects species differences. Indeed, RPE cells in mouse do not acquire a squamous conformation as in zebrafish and thus matching of the NR apical surface can be acquired only with the incorporation of new cells.

This possibility is supported by our analysis of RPE shape changes in zebrafish, the final squamous morphology of which stands out in comparison with the cuboidal shape of the RPE in mouse and chicken. While flattening, from 14 ss/16 hpf to 26 ss/22 hpf, RPE cells increase

three-fold their surface but decrease the length of their A-B axis by half, finally without a change in cell volume. Thus, if proliferation has a minor effect on RPE morphogenesis, the increase in surface derived from the flattening process is responsible for RPE expansion. We show that when the RPE does not flatten properly, because of myosin II specific inhibition, the eye is less folded resembling the mouse phenotype caused by reduced proliferation. Thus, in both organisms normal OC morphogenesis is accompanied by RPE expansion. Whilst in mouse this is achieved by the generation of new RPE cells, in zebrafish the tissue expands changing cell shape from columnar to squamous (Figure 33). The final goal–RPE expansion–is thus common to both organisms, although the mechanism to achieve it is different. This difference may be due, for example, to time. OC morphogenesis is very fast in zebrafish when compared to the mouse and thus cell stretching may be more efficient and rapid than proliferation.

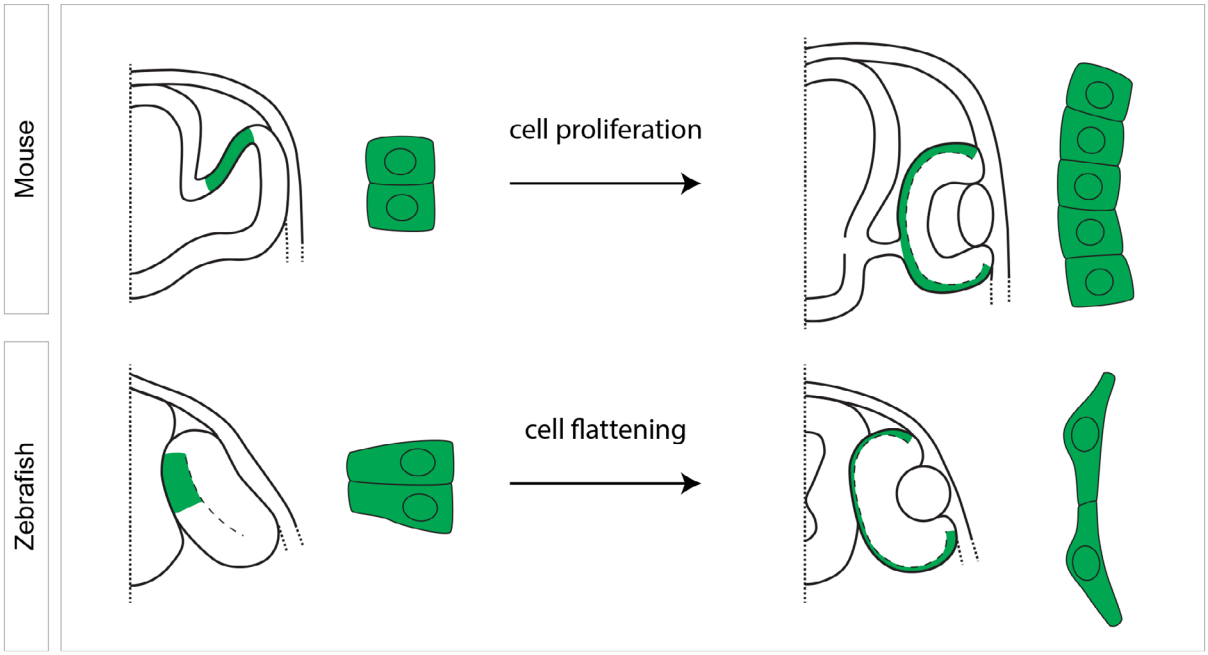

Figure 33: Proposed models for RPE expansion in mouse and zebrafish.

Differential mechanisms by which the mouse (upper row) and zebrafish (bottom row) RPE appear to expand their surface during eye morphogenesis. In mouse, proliferation is the likely main factor of RPE extension, whereas in zebrafish RPE extends by cell stretching.

Actomyosin mediated RPE stiffness was proposed to mediate mouse eye folding together with proliferation. Mouse RPE cells show increased levels of phospho-myosin II in comparison with the NR and increased stiffness, as measured by ATM (atomic force microscopy) (Carpenter et al., 2015, Eiraku et al., 2011). Actomyosin activity seems also to be important for zebrafish RPE morphogenesis based on our results, although the subcellular mechanism we proposed may be different. Cortical Myosin II in the presence of cross-linker molecules can increase cell

stiffness *in vivo* by pulling on actin filaments (Rauzi and Lenne, 2011), a process that could operate in the cuboidal mouse RPE. Since zebrafish RPE cells are flat, instead of generating stiffness from the cortex, actomyosin would be organized in stress fibers. A flat morphology in other contexts is associated with increased stiffness and the presence of stress fibers that compress the nucleus (Vishavkarma et al., 2014, Tee et al., 2011). Myosin II plays an essential role in the compressive activity of stress fibers and its inhibition with Blebbistatin causes a loss of the flat cell morphology together with a decrease in cell stiffness (Vishavkarma et al., 2014, Tee et al., 2011). We did not find evident accumulations of myosin in RPE cells and we were not able to detect stress fibers around the nucleus of the cells when they were flat, likely because the membranes are very close to the nucleus, making the resolution of the cytoskeletal components difficult with confocal microscopy. However, since Blebbistatin treatments induce a round morphology in RPE cells, we propose that myosin II inhibition compromise RPE stiffness and OC folding by interfering with stress fibers assembly in zebrafish (Figure 34A).

The idea that zebrafish RPE cells are stiff is supported also by the following observations. Morphants or mutants in which the RPE is discontinuous show NR out-pocketing right where the gaps are (Figure 4E in Miesfeld et al., 2015, Figure 3B in Lane and Lister, 2012, and laboratory observations), indicating that the zebrafish RPE has the mechanical role of containing the NR. In agreement, our RNAseq analysis detected up to 7 keratins up-regulated in RPE versus progenitor cells. Keratins are structural components of intermediate filaments, which are known to confer cell stiffness (Seltmann et al., 2013). Besides, the *tfap2a* gene, a well-known regulator of the expression of keratin genes (Leask et al., 1991) is also up-regulated in the RPE.

To directly test the stiffness of the zebrafish RPE, we should measure it in the embryos for example using Brillouin Microscopy. This approach seems a great option since it has been successfully used in zebrafish (Schlüßler et al., 2018). It would be also interesting to analyze the composition of the ECM in the outer layer versus the inner layer, since ECM components may confer higher substrate stiffness and allow RPE flattening, whilst a softer environment would be maintained for the NR.

Carpenter et al. (2015) propose RPE proliferation and stiffness as two late processes contributing to OC folding in mouse, taking place from E10.5. This implies that RPE morphogenesis is not per se sufficient to trigger OC folding and other mechanisms are required. Indeed, altered RPE development is associated with less folded OCs but not to the absence of folding. The apical relaxation of NR cells and the apical and basolateral constriction in rim cells described in organoids studies are additional mechanisms proposed to promote mouse OC folding (Okuda et al., 2018, Eiraku et al., 2011). Similarly, our results, in line with previous studies (Sidhaye and Norden, 2017, Nicolas-Perez et al., 2016) show that impairment of NR

basal constriction is important for OC folding. The contribution of this mechanism is also more evident than the lack of RPE stretching, at least according to our measures of OC folding after specific and equal interference with either NR or RPE cytoskeleton. Impairment of NR basal constriction leads to less folded eyes than interfering with RPE stretching, thus we propose that in zebrafish RPE flattening and stiffness contribute to the global folding complementing the force exerted by NR basal constriction.

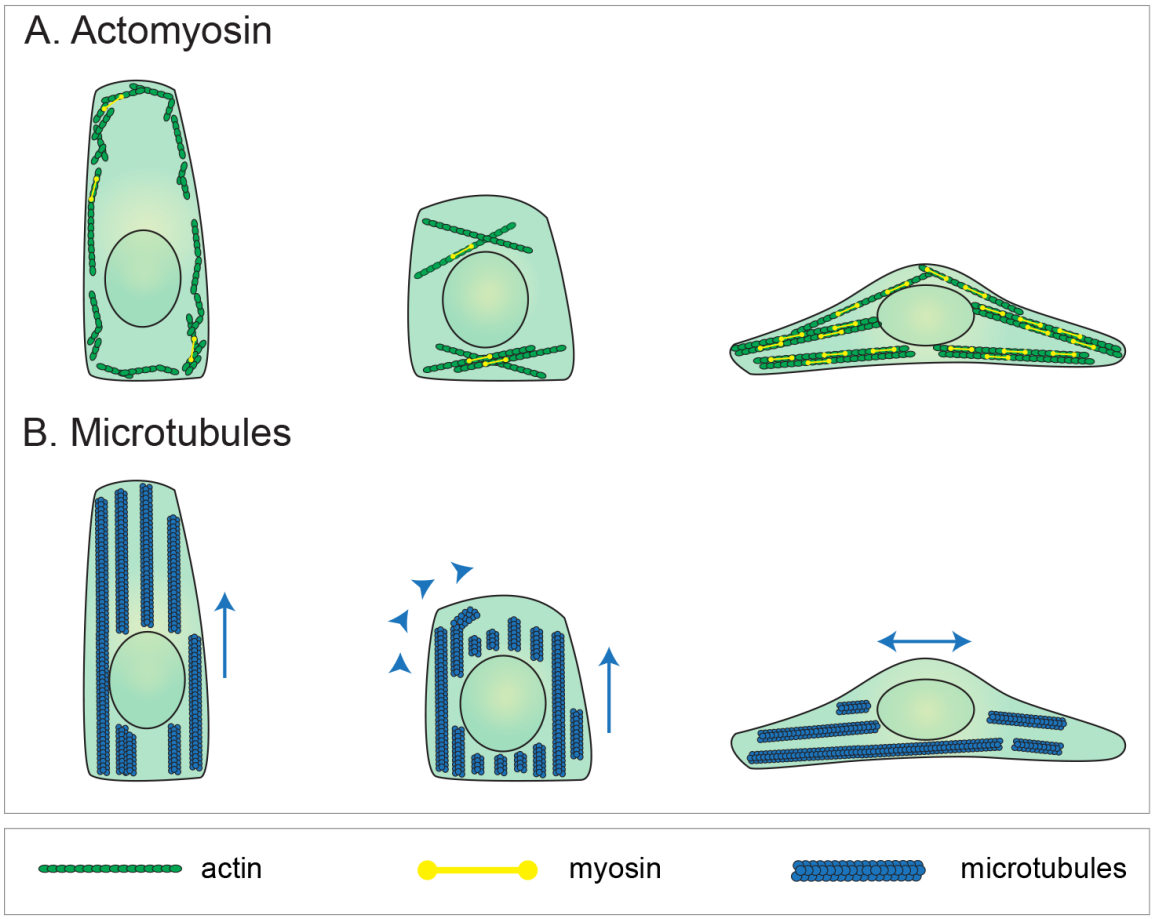

Figure 34: Proposed cytoskeleton contribution to RPE cell flattening.

(A) Proposed actomyosin distribution, which would form stress fibers that compress the nucleus to enable RPE cell flattening. **(B)** Proposed MT rotation that would help the reduction in A-B length and extension in surface of RPE cells also contributing to the flattening process.

During this study we also analyzed MT dynamics. MTs are essential structures in epithelial cells for acquisition of proper polarity, organelles positioning, distribution of membrane proteins and vesicles' transport. At OV stages, when the RPE is pseudostratified or cuboidal, MTs have their plus end located in the basal region of the cells and the minus terminal in the apical region, an organization also found in the NR. Notably, when the RPE acquires a flat morphology MTs organization changes and progresses laterally suggesting that the cytoskeleton has rotated 90º (Figure 34B). If MTs are depolymerized using Nocodazole, RPE cells lose their morphology

and return to a progenitor-like configuration. Based on these observations we propose that RPE cells may rotate their MT cytoskeleton, complementing the role of myosin II activity to promote flattening. This process has been described during *Drosophila* amnioserosa morphogenesis (Pope and Harris, 2008). These cells also change from a columnar to a squamous morphology by undergoing a 90° rotation of the cellular components initiated by an autonomous bending of the growing MTs. While growing, the MTs encounter an actin accumulation exerting resistance that forces them to bend and grow in the perpendicular axis. Notably, in this epithelium MT rotation is accompanied by remodeling of the adherens junctions, in a process dependent on myosin activity (Pope and Harris, 2008). Thus a potential role of myosin II in RPE flattening may also be the modification of cell-cell adhesion. To elucidate if a similar process is occurring in RPE flattening MTs dynamics should be analyzed in more detail.

3. Eye populations undergo active and independent morphogenetic mechanisms

The opportunity to interfere with myosin II either in the NR or RPE independently gave us the opportunity to demonstrate that the RPE cells change their shape in a cell autonomous manner and though an active process. Embryos incubation with Blebbistatin has a simultaneous effect on both the RPE and the NR, impeding cell flattening in the first one and basal constriction in the second one. This prevents to discern if RPE cell shape changes are cell autonomous or promoted by the rearrangement occurring in the NR. This was a possibility that needed to be considered because applying pressure to a specific point of a cell monolayer in culture causes radial stretching of the cells (Aragona et al., 2013). This resembles what happens to the RPE cells located in the most central region of the folding OC suggesting that NR basal constriction may generate pressure over the RPE promoting its flattening, although this possibility is unlikely since RPE shape changes start before NR invagination. Our results ruled out a potential dependence of RPE flattening on NR basal constriction. NR-specific ABleb treatments show that RPE cells still flatten when NR basal constriction is impaired. Moreover, myosin II inhibition in the RPE interferes with the flattening process despite NR basal constriction occuring normally. These results indicate that both events are independent. We also propose RPE flattening and rim involution as independent processes because during these experiments we rarely observed accumulation of NR in the outer layer as occurs when interfering with rim movements (Figure 4D and 5C in Sidhaye and Norden, 2017). This observation complements those showing that the RPE develops normally when rim movements are impaired (Sidhaye and Norden, 2017).

All these observations taken together indicate that cell shape changes taking place during OC morphogenesis are independent of each other despite RPE and NR forming a continuous

through the rim. In contrast, in embryos at OC stages treated with Nocodazole NR cells initially located in the inner layer end up in the outer layer. This is coupled with a retraction of the RPE that reduces its surface. One interpretation of these results would be that the RPE pulls NR cells back. However, Nocodazole treatments are not spatially restricted and all tissues are affected by MT depolymerization. Therefore, we cannot assume that this phenotype is due to MT interference only in the RPE.

4. New regards about RPE specification

Our RNAseq analysis and the phenotype of zebrafish mutants of RPE regulators such as Otx or Yap suggest an early determination of RPE fate and loss of progenitor's potentiality. In mouse, interference with RPE determinant genes results in the development of an ectopic NR-like tissue in the outer layer (Kim et al., 2016, Martinez-Morales et al., 2001). This phenotype has never been observed in zebrafish, which instead show less severe defects with a discontinuous or smaller RPE layer (Miesfeld et al., 2015, Lane and Lister, 2012). This species-specific difference might relate again with the shorter developmental time characteristic of the zebrafish. To accomplish with fast development, the zebrafish RPE may undergo a very early and irreversible determination not easily modified by the lack of single gene function as in mouse. Observations derived from our RNA-seq analysis support this possibility. There are no major differences in the RPE up-regulated genes between 18 hpf (cuboidal) and 23 hpf (flat) time points. Furthermore, the GO categories that are found enriched in the RPE at 18 and 23 hpf stages compared to progenitors relate to genes involved in RPE mature functions with little differences between the two RPE stages. For instance, main pigmentation genes are already expressed at 18 hpf despite the fact that pigmentation is firstly detected at 24 hpf. This indicates that genes necessary for RPE functions are turn on very early as a whole and not stepwise, making tissue identity difficult to perturb. This suggests that specification and differentiation of the RPE occurs likely simultaneously. This possibility is also supported by the very early decrease in the rate of RPE progenitor proliferation, which takes place between 16 ss/17 hpf and 20 ss/19 hpf and last until 48 hpf.

In Nocodazole treatments between 16 and 21 ss, RPE cells revert from a cuboidal morphology to a columnar-like shape, but their identity is conserved as the cells maintain the expression of typical markers such as *otx1* and *mitfa*. Notably, *otx1* expression normally starts before the beginning of the drug treatment (16 ss) and therefore its expression might not be surprising. However, *mitfa* is firstly detected when the treatment starts, indicating that acquisition of cell identity occurs independently of its morphology. This is also supported by the observation that GFP from the enh1-*bhlhe40*:GFP line is undisturbed after Nocodazole treatments, even at

very early stages. The relation between cell behaviors and the acquisition of cell identity has been analyzed during earlier stages of eye formation. In this context Cavodeassi et al. (2013) demonstrated that once the different cell identities are acquired in the anterior neural plate (g. e. eye versus telencephalon) the mechanisms controlling cell segregation are activated. Indeed, if the genes controlling this segregation (*ephrins* and *eph*) are manipulated, cells misbehavior does not impact on cell identity. We propose that the same process may occur in the RPE. RPE specification is achieved first and activates the mechanisms leading to cell flattening.

5. Does bhlhe40 contribute to RPE development or function?

Early *bhlhe40* expression suggested a potential role of this gene in RPE development. To check this possibility, we generated the corresponding mutant in zebrafish. We generated two different mutant lines, both of which generate truncated proteins: the E2 line produces a protein with no known functional domains whereas the E5 line produces a protein containing the bHLH domain but no Orange domain or proline-rich region. Both embryonic and adult E2 and E5 eyes are properly formed with no evident morphological defects. The apparent absence of a phenotype can be interpreted as the result of (1) genetic compensation by other related genes, (2) a secondary role of the *bhlhe40* gene in zebrafish when compared with other species (as it occurs for *mitf* genes) or (3) due to the activity of *bhlhe40* in RPE functions other than its morphogenesis/specification.

The *bhlhe41* gene is the closest homolog of the *bhlhe40* gene and they could compensate each other function since both bind to the same E-box sequences in the genome (Yamada and Miyamoto, 2005). Both genes are expressed in the RPE according to our RNAseq data of 23 hpf RPE, although *bhlhe41* has not been detected in the RPE with ISH (Chen et al., 2010). The expression levels of *bhlhe41* in the mutants do not vary; however, this gene could still be compensating *bhlhe40* absence. Since we were not able to knockout *bhlhe41* in the *bhlhe40* mutants we cannot confirm a compensatory event. We used several guides against the first exons of the gene trying to knockout it with CRIPSR/Cas9 technology (Wu et al., 2018), but they were not efficient in generating mutations. Other way to generate knockouts in zebrafish is to delete the promoter of the gene using also CRISPR (El-Brolosy et al., 2019), which for this gene is located in the same region as the first four exons if we check the genomic maps containing enhancer histone marks (Bogdanovic et al., 2012a). As a last alternative, *bhlhe41* proper splicing can be abrogated with a morpholino that is reported in the literature (Srdanović et al., 2017), an experiment that may be performed in the future.

Information available in other species can help us find a potential role for the *bhlhe40* gene in the RPE and also to check if, similar to *mitf* genes, it may have a less determinant role

in RPE specification than in other species. However, no vision defects have been reported in the corresponding mouse mutant, ruling out a *bhlhe40* role in RPE morphogenesis also in this model. *Bhlhe40* and *Bhlhe41* double mouse mutants have sleep alterations and both molecular and behavioral characteristics close to psychiatric disorders (Baier et al., 2014). In human several mutations in the proline rich region of the *BHLHE41* gene are associated with a reduction of sleep hours (Cardinale et al., 2014, He et al., 2009). In zebrafish, knockdown of *bhlhe41* have been also related with sleep alterations (Srdanović et al., 2017). These alterations have been related with the well-known function of *Bhlhe40* and *Bhlhe41* as members of the mammalian circadian clock (Honma et al., 2002). Indeed, previous analysis of the *bhlhe40* morphant showed that the absence of this transcription factor alters the regulation of locomotor activity by light (Ben-Moshe et al., 2014). This is mainly due to *bhlhe40* activity in the pineal gland where its expression is increased after light exposure. Although the authors do not mention a *bhlhe40* role in the eye, in their ISH images an increase in expression levels can be also seen in the RPE after light pulse (Figure 2A in Ben-Moshe et al., 2014). Therefore, *bhlhe40* is likely to have a light related role in the eye in which several processes operate under circadian regulation. There is no differential sensitivity of the photoreceptor cells of wild type and *bhlhe40* mutant larvae when exposed to intense light, suggesting that *bhlhe40*-deficient RPE, at least in this condition, have functional properties similar to those of the wild type. However, *bhlhe40* could be still involved in the long term regeneration of these cell types since in zebrafish both photoreceptors and RPE are able to regenerate after a lesion (Hanovice et al., 2019, Otteson and Hitchcock, 2003). *Bhlhe40* single mouse mutant also presents neuronal alterations in the hippocampus with increased excitability and reduced synaptic plasticity (Hamilton et al., 2018) and have defects in large peritoneal macrophage self-renewal (Jarjour et al., 2018). Our maternal zygotic adult mutants grew up normally and are fertile, but we cannot discard that they present behavioral or sleep-related alterations.

Since the mutant shows no morphogenetic defects, we analyzed the effect of *bhlhe40* overexpression trying to assess whether Bhlhe40 may be important for RPE specification or morphogenesis. This approach causes eye defects with some variability. The embryos show smaller eyes, sometimes closer and occasionally just one eye. In addition, the general size of the embryo seems to be reduced, suggesting a potential role of this transcription factor in proliferation. In cell cultures, but also in lung cancer, BHLHE40 has been found to directly bind E-box sequences present in the promoter of *CCDN1* inhibiting its expression (Liu et al., 2013, Bhawal et al., 2011) and *BHLHE40* overexpression causes a reduction in cell proliferation (Bhawal et al., 2011). BHLHE41 has a similar capacity of binding *CCND1* promoter (Bhawal et al., 2011, Li et al., 2011). ID1, a HLH protein involved in cell cycle regulation, is also repressed

by BHLHE40 in cell culture (Qian and Chen, 2008). ID proteins are generally present in undifferentiated and proliferative tissues (Roschger and Cabrele, 2017). Repression of Id1 by Bhlhe40 in zebrafish RPE may be necessary since in the RNAseq data we found that this transcription factor is down-regulated in the RPE at both stages analyzed. Thus, Bhlhe40 may have a specific role in reducing RPE proliferation rate at the onset of RPE specification.

bhlhe40 overexpression affects the whole embryo. Not only eyes were smaller but also other regions of the embryos. A more detailed analysis of the role of this gene will involve overexpression of *bhlhe40* only in the eye, allowing us to analyze an eye specific response. This experiment is readily feasible by making use of the GAL4/UAS system and the *rx3*:GAL4 line.

In summary, we propose that apart from the circadian functions of *bhlhe40* already described in the pineal gland, this gene may be related with the reduction of proliferation detected in the RPE. Further analysis will be needed to prove this hypothesis.

CONCLUSIONS

1. The Tg(enh1-*bhlhe40*:GFP) line constitutes a novel tool to follow zebrafish RPE morphogenesis *in vivo* from nearly its specification.

2. Zebrafish RPE morphogenesis is directly promoted by cell shape changes with general cell volume conservation and overall reduction in the proliferation rate.

3. Cell shape changes of the RPE are active events dependent on myosin II activity and MTs dynamics.

4. Zebrafish RPE morphogenesis contributes to OC folding complementing the force imposed by basal constriction of the NR.

5. Zebrafish RPE specification is abrupt leading to a fast and irreversible divergence from retinal progenitor cells and occurs in absence of cell shape changes.

6. The *bhlhe40* gene is apparently dispensable for zebrafish eye morphogenesis and general embryo development.

REFERENCES

ABE, T., ISHIKAWA, T., MASUDA, T., MIZUSAWA, K., TSUKAMOTO, T., MITANI, H., YANAGISAWA, T., TODO, T. & IIGO, M. 2006. Molecular analysis of Dec1 and Dec2 in the peripheral circadian clock of zebrafish photosensitive cells. *Biochemical and Biophysical Research Communications,* 351**,** 1072-1077.

ADIJANTO, J., CASTORINO, J. J., WANG, Z. X., MAMINISHKIS, A., GRUNWALD, G. B. & PHILP, N. J. 2012. Microphthalmia-associated transcription factor (MITF) promotes differentiation of human retinal pigment epithelium (RPE) by regulating microRNAs-204/211 expression. *The Journal of Biological Chemistry,* 287**,** 20491-20503.

ALLEN, B. G. & WEEKS, D. L. 2005. Transgenic Xenopus laevis embryos can be generated using φC31 integrase. *Nature Methods,* 2**,** 975-979.

AMAN, A. & PIOTROWSKI, T. 2010. Cell migration during morphogenesis. *Developmental Biology,* 341**,** 20-33.

ANDO, R., HAMA, H., YAMAMOTO-HINO, M., MIZUNO, H. & MIYAWAKI, A. 2002. An optical marker based on the UV-induced green-to-red photoconversion of a fluorescent protein. *Proceedings of the National Academy of Sciences of the United States of America,* 99**,** 12651-12656.

ANDREWS, S. 2014. *FastQC A Quality Control tool for High Throughput Sequence Data*. http://www.bioinformatics.babraham.ac.uk/projects/fastqc/.

ARAGONA, M., PANCIERA, T., MANFRIN, A., GIULITTI, S., MICHIELIN, F., ELVASSORE, N., DUPONT, S. & PICCOLO, S. 2013. A mechanical checkpoint controls multicellular growth through YAP/TAZ regulation by actin-processing factors. *Cell,* 154**,** 1047-1059.

ARCE, G. R. 2005. *Nonlinear Signal Processing: A Statistical Approach.* United States of America: John Wiley & Sons, Inc.

ASAKAWA, K. & KAWAKAMI, K. 2008. Targeted gene expression by the Gal4-UAS system in zebrafish. *Development, Growth & Differentiation,* 50**,** 391-399.

AVANESOV, A. & MALICKI, J. 2010. Analysis of the retina in the zebrafish model. *Methods in Cell Biology,* 100**,** 153-204.

BAIER, P. C., BRZOZKA, M. M., SHAHMORADI, A., REINECKE, L., KROOS, C., WICHERT, S. P., OSTER, H., WEHR, M. C., TANEJA, R., HIRRLINGER, J. & ROSSNER, M. J. 2014. Mice lacking the circadian modulators SHARP1 and SHARP2 display altered sleep and mixed state endophenotypes of psychiatric disorders. *PLoS One,* 9**,** e110310.

BELMONT, L. D. & MITCHISON, T. J. 1996. Identification of a Protein That Interacts with Tubulin Dimers and Increases the Catastrophe Rate of Microtubules. *Cell,* 84**,** 623-631.

BEN-MOSHE, Z., ALON, S., MRACEK, P., FAIGENBLOOM, L., TOVIN, A., VATINE, G. D., EISENBERG, E., FOULKES, N. S. & GOTHILF, Y. 2014. The light-induced transcriptome of the zebrafish pineal gland reveals complex regulation of the circadian clockwork by light. *Nucleic Acids Research,* 42**,** 3750-3767.

BESSA, J., TENA, J. J., DE LA CALLE-MUSTIENES, E., FERNÁNDEZ-MIÑÁN, A., NARANJO, S., FERNÁNDEZ, A., MONTOLIU, L., AKALIN, A., LENHARD, B., CASARES,

F. & GÓMEZ-SKARMETA, J. L. 2009. Zebrafish enhancer detection (ZED) vector: A new tool to facilitate transgenesis and the functional analysis of cis-regulatory regions in zebrafish. *Developmental Dynamics,* 238**,** 2409-2417.

BHARTI, K., LIU, W., CSERMELY, T., BERTUZZI, S. & ARNHEITER, H. 2008. Alternative promoter use in eye development: the complex role and regulation of the transcription factor MITF. *Development,* 135**,** 1169-1178.

BHARTI, K., NGUYEN, M. T., SKUNTZ, S., BERTUZZI, S. & ARNHEITER, H. 2006. The other pigment cell: specification and development of the pigmented epithelium of the vertebrate eye. *Pigment Cell Research,* 19**,** 380-394.

BHAWAL, U. K., SATO, F., ARAKAWA, Y., FUJIMOTO, K., KAWAMOTO, T., TANIMOTO, K., ITO, Y., SASAHIRA, T., SAKURAI, T., KOBAYASHI, M., KASHIMA, I., KIJIMA, H., KUNIYASU, H., ABIKO, Y., KATO, Y. & SATO, S. 2011. Basic helix-loop-helix transcription factor DEC1 negatively regulates cyclin D1. *The Journal of Pathology,* 224**,** 420-429.

BOGDANOVIĆ, O., DELFINO-MACHÍN, M., NICOLÁS-PÉREZ, M., GAVILÁN, MARÍA P., GAGO-RODRIGUES, I., FERNÁNDEZ-MIÑÁN, A., LILLO, C., RÍOS, ROSA M., WITTBRODT, J. & MARTÍNEZ-MORALES, JUAN R. 2012b. Numb/Numbl-Opo Antagonism Controls Retinal Epithelium Morphogenesis by Regulating Integrin Endocytosis. *Developmental Cell,* 23**,** 782-795.

BOGDANOVIC, O., FERNANDEZ-MINAN, A., TENA, J. J., DE LA CALLE-MUSTIENES, E., HIDALGO, C., VAN KRUYSBERGEN, I., VAN HEERINGEN, S. J., VEENSTRA, G. J. & GOMEZ-SKARMETA, J. L. 2012a. Dynamics of enhancer chromatin signatures mark the transition from pluripotency to cell specification during embryogenesis. *Genome Research,* 22**,** 2043-2053.

BOK, D. 1993. The retinal pigment epithelium: a versatile partner in vision. *Journal of Cell Science Supplement,* 17**,** 189-195.

BONILHA, V. L. 2014. Retinal pigment epithelium (RPE) cytoskeleton in vivo and in vitro. *Experimental Eye Research,* 126**,** 38-45.

BRANCHEK, T. & BREMILLER, R. 1984. The development of photoreceptors in the zebrafish, Brachydanio rerio. I. Structure. *The Journal of Comparative Neurology,* 224**,** 107-115.

BROWN, K. E., KELLER, P. J., RAMIALISON, M., REMBOLD, M., STELZER, E. H. K., LOOSLI, F. & WITTBRODT, J. 2010. Nlcam modulates midline convergence during anterior neural plate morphogenesis. *Developmental Biology,* 339**,** 14-25.

BRYAN, C. D., CHIEN, C.-B. & KWAN, K. M. 2016. Loss of laminin alpha 1 results in multiple structural defects and divergent effects on adhesion during vertebrate optic cup morphogenesis. *Developmental Biology,* 416**,** 324-337.

BRYAN, C. D., PFEIFFER, R. L., JONES, B. W. & KWAN, K. M. 2018. Neural crest cells regulate optic cup morphogenesis by promoting extracellular matrix assembly. *bioRxiv***,** 374470.

BUCKLEY, C. E., REN, X., WARD, L. C., GIRDLER, G. C., ARAYA, C., GREEN, M.

J., CLARK, B. S., LINK, B. A. & CLARKE, J. D. W. 2013. Mirror-symmetric microtubule assembly and cell interactions drive lumen formation in the zebrafish neural rod. *The EMBO journal,* 32**,** 30-44.

CARDINALE, C. J., HAKONARSON, H., PELLEGRINO, R., DINGES, D. F., GOEL, N., PACK, A. I., MAISLIN, G., KUNA, S. T., TUFIK, S., KAVAKLI, I. H., VAN DONGEN, H. P. A. & HOGENESCH, J. B. 2014. A Novel BHLHE41 Variant is Associated with Short Sleep and Resistance to Sleep Deprivation in Humans. *Sleep,* 37**,** 1327-1336.

CARPENTER, A. C., SMITH, A. N., WAGNER, H., COHEN-TAYAR, Y., RAO, S., WALLACE, V., ASHERY-PADAN, R. & LANG, R. A. 2015. Wnt ligands from the embryonic surface ectoderm regulate 'bimetallic strip' optic cup morphogenesis in mouse. *Development,* 142**,** 972-982.

CARRINGTON, B., VARSHNEY, G. K., BURGESS, S. M. & SOOD, R. 2015. CRISPR-STAT: an easy and reliable PCR-based method to evaluate target-specific sgRNA activity. *Nucleic acids research,* 43**,** e157.

CASTANON, I. & GONZÁLEZ-GAITÁN, M. 2011. Oriented cell division in vertebrate embryogenesis. *Current Opinion in Cell Biology,* 23**,** 697-704.

CAVODEASSI, F. 2014. Integration of anterior neural plate patterning and morphogenesis by the Wnt signaling pathway. *Developmental Neurobiology,* 74**,** 759-771.

CAVODEASSI, F. 2018. Dynamic Tissue Rearrangements during Vertebrate Eye Morphogenesis: Insights from Fish Models. *Journal of Developmental Biology,* 6.

CAVODEASSI, F., IVANOVITCH, K. & WILSON, S. W. 2013. Eph/Ephrin signalling maintains eye field segregation from adjacent neural plate territories during forebrain morphogenesis. *Development,* 140**,** 4193-4202.

CECHMANEK, P. B. & MCFARLANE, S. 2017. Retinal pigment epithelium expansion around the neural retina occurs in two separate phases with distinct mechanisms. *Developmental Dynamics,* 246**,** 598-609.

CHAUHAN, B. K., DISANZA, A., CHOI, S. Y., FABER, S. C., LOU, M., BEGGS, H. E., SCITA, G., ZHENG, Y. & LANG, R. A. 2009. Cdc42- and IRSp53-dependent contractile filopodia tether presumptive lens and retina to coordinate epithelial invagination. *Development,* 136**,** 3657-3667.

CHEN, L., ZHOU, J., XU, H., XU, G. & XUE, J. 2010. Identification and developmental expression of Dec2 in zebrafish. *Fish Physiology and Biochemistry,* 36**,** 667-675.

CHUANG, J.-H., YARMISHYN, A. A., HWANG, D.-K., HSU, C.-C., WANG, M.-L., YANG, Y.-P., CHIEN, K.-H., CHIOU, S.-H., PENG, C.-H. & CHEN, S.-J. 2018. Expression profiling of cell-intrinsic regulators in the process of differentiation of human iPSCs into retinal lineages. *Stem Cell Research & Therapy,* 9**,** 140.

CHUNG, J. H., WHITELEY, M. & FELSENFELD, G. 1993. A 5′ element of the chicken β-globin domain serves as an insulator in human erythroid cells and protects against position effect in Drosophila. *Cell,* 74**,** 505-514.

COHEN-TAYAR, Y., COHEN, H., MITIAGIN, Y., ABRAVANEL, Z., LEVY, C., IDELSON, M., REUBINOFF, B., ITZKOVITZ, S., RAVIV, S., KAESTNER, K. H., BLINDER, P., ELKON, R. & ASHERY-PADAN, R. 2018. Pax6 regulation of Sox9 in the mouse retinal pigmented epithelium controls its timely differentiation and choroid vasculature development. *Development,* 145**,** dev163691.

COLE, L. K. & ROSS, L. S. 2001. Apoptosis in the Developing Zebrafish Embryo. *Developmental Biology,* 240**,** 123-142.

CVEKL, A. & ASHERY-PADAN, R. 2014. The cellular and molecular mechanisms of vertebrate lens development. *Development,* 141**,** 4432-4447.

DAVIS, R. L. & TURNER, D. L. 2001. Vertebrate hairy and Enhancer of split related proteins: transcriptional repressors regulating cellular differentiation and embryonic patterning. *Oncogene,* 20**,** 8342-8357.

DEL RIO-TSONIS, K. D. & TSONIS, P. A. 2003. Eye regeneration at the molecular age. *Developmental Dynamics,* 226**,** 211-224.

DISTEL, M., HOCKING, J. C., VOLKMANN, K. & KÖSTER, R. W. 2010. The centrosome neither persistently leads migration nor determines the site of axonogenesis in migrating neurons in vivo. *The Journal of Cell Biology,* 191**,** 875-890.

DOCTOR, R. B. 2006. The Actin Cytoskeleton in the Apical Domain of Epithelial Cells. *Advances in Molecular and Cell Biology.* Elsevier.

EDEN, E., NAVON, R., STEINFELD, I., LIPSON, D. & YAKHINI, Z. 2009. GOrilla: a tool for discovery and visualization of enriched GO terms in ranked gene lists. *BMC Bioinformatics,* 10**,** 48.

EIRAKU, M., TAKATA, N., ISHIBASHI, H., KAWADA, M., SAKAKURA, E., OKUDA, S., SEKIGUCHI, K., ADACHI, T. & SASAI, Y. 2011. Self-organizing optic-cup morphogenesis in three-dimensional culture. *Nature,* 472**,** 51-56.

EL-BROLOSY, M. A., KONTARAKIS, Z., ROSSI, A., KUENNE, C., GÜNTHER, S., FUKUDA, N., KIKHI, K., BOEZIO, G. L. M., TAKACS, C. M., LAI, S.-L., FUKUDA, R., GERRI, C., GIRALDEZ, A. J. & STAINIER, D. Y. R. 2019. Genetic compensation triggered by mutant mRNA degradation. *Nature,* 568**,** 193–197.

EL-BROLOSY, M. A. & STAINIER, D. Y. R. 2017. Genetic compensation: A phenomenon in search of mechanisms. *PLOS Genetics,* 13**,** e1006780.

ENGLAND, S. J., BLANCHARD, G. B., MAHADEVAN, L. & ADAMS, R. J. 2006. A dynamic fate map of the forebrain shows how vertebrate eyes form and explains two causes of cyclopia. *Development,* 133**,** 4613.

FEIGE, E., YOKOYAMA, S., LEVY, C., KHALED, M., IGRAS, V., LIN, R. J., LEE, S., WIDLUND, H. R., GRANTER, S. R., KUNG, A. L. & FISHER, D. E. 2011. Hypoxia-induced transcriptional repression of the melanoma-associated oncogene MITF. *Proceedings of the National Academy of Sciences of the United States of America,* 108**,** E924-E933.

FUHRMANN, S. 2010. Eye morphogenesis and patterning of the optic vesicle. *Current*

Topics in Developmental Biology, 93**,** 61-84.

FUJIMURA, N., KLIMOVA, L., ANTOSOVA, B., SMOLIKOVA, J., MACHON, O. & KOZMIK, Z. 2015. Genetic interaction between Pax6 and β-catenin in the developing retinal pigment epithelium. *Development Genes and Evolution,* 225**,** 121-128.

FUJIMURA, N., TAKETO, M. M., MORI, M., KORINEK, V. & KOZMIK, Z. 2009. Spatial and temporal regulation of Wnt/β-catenin signaling is essential for development of the retinal pigment epithelium. *Developmental Biology,* 334**,** 31-45.

GAGO-RODRIGUES, I., FERNÁNDEZ-MIÑÁN, A., LETELIER, J., NARANJO, S., TENA, J. J., GÓMEZ-SKARMETA, J. L. & MARTINEZ-MORALES, J. R. 2015. Analysis of opo cis-regulatory landscape uncovers Vsx2 requirement in early eye morphogenesis. *Nature Communications,* 6**,** 7054.

GALY, A., NERON, B., PLANQUE, N., SAULE, S. & EYCHENE, A. 2002. Activated MAPK/ERK kinase (MEK-1) induces transdifferentiation of pigmented epithelium into neural retina. *Developmental Biology,* 248**,** 251-264.

GARCÍA, D. M. & KOKE, J. R. 1996. The cytoskeleton of the retinal pigment epithelium. *In:* MALHOTRA, S. K. (ed.) *Advances in Structural Biology.* JAI.

GEHRING, W. J. & IKEO, K. 1999. Pax 6: mastering eye morphogenesis and eye evolution. *Trends in Genetics,* 15**,** 371-377.

GESTRI, G., BAZIN-LOPEZ, N., SCHOLES, C. & WILSON, S. W. 2018. Cell Behaviors during Closure of the Choroid Fissure in the Developing Eye. *Frontiers in Cellular Neuroscience,* 12**,** 42-42.

GILMOUR, D., REMBOLD, M. & LEPTIN, M. 2017. From morphogen to morphogenesis and back. *Nature,* 541**,** 311-320.

GREGORY-EVANS, K. & BHATTACHARYA, S. S. 1998. Genetic blindness: current concepts in the pathogenesis of human outer retinal dystrophies. *Trends in Genetics,* 14**,** 103-108.

GUGLIELMI, G., FALK, H. J. & DE RENZIS, S. 2016. Optogenetic Control of Protein Function: From Intracellular Processes to Tissue Morphogenesis. *Trends in Cell Biology,* 26**,** 864-874.

HAMILTON, K. A., WANG, Y., RAEFSKY, S. M., BERKOWITZ, S., SPANGLER, R., SUIRE, C. N., CAMANDOLA, S., LIPSKY, R. H. & MATTSON, M. P. 2018. Mice lacking the transcriptional regulator Bhlhe40 have enhanced neuronal excitability and impaired synaptic plasticity in the hippocampus. *PLoS One,* 13**,** e0196223.

HANOVICE, N. J., LEACH, L. L., SLATER, K., GABRIEL, A. E., ROMANOVICZ, D., SHAO, E., COLLERY, R., BURTON, E. A., LATHROP, K. L., LINK, B. A. & GROSS, J. M. 2019. Regeneration of the zebrafish retinal pigment epithelium after widespread genetic ablation. *PLoS Genet,* 15**,** e1007939.

HASSANPOUR, H., SAMADIANI, N. & MAHDI SALEHI, S. M. 2015. Using morphological transforms to enhance the contrast of medical images. *The Egyptian Journal of Radiology and Nuclear Medicine,* 46**,** 481-489.

HE, Y., JONES, C. R., FUJIKI, N., XU, Y., GUO, B., HOLDER, J. L., ROSSNER, M. J., NISHINO, S. & FU, Y.-H. 2009. The Transcriptional Repressor DEC2 Regulates Sleep Length in Mammals. *Science,* 325**,** 866-870.

HEERMANN, S., SCHUTZ, L., LEMKE, S., KRIEGLSTEIN, K. & WITTBRODT, J. 2015. Eye morphogenesis driven by epithelial flow into the optic cup facilitated by modulation of bone morphogenetic protein. *Elife,* 4**,** e05216.

HERNANDEZ-BEJARANO, M., GESTRI, G., SPAWLS, L., NIETO-LOPEZ, F., PICKER, A., TADA, M., BRAND, M., BOVOLENTA, P., WILSON, S. W. & CAVODEASSI, F. 2015. Opposing Shh and Fgf signals initiate nasotemporal patterning of the zebrafish retina. *Development,* 142**,** 3933-3942.

HILFER, S. R. 1983. Development of the eye of the chick embryo. *Scanning Electron Microscopy***,** 1353-1369.

HONMA, S., KAWAMOTO, T., TAKAGI, Y., FUJIMOTO, K., SATO, F., NOSHIRO, M., KATO, Y. & HONMA, K. 2002. Dec1 and Dec2 are regulators of the mammalian molecular clock. *Nature,* 419**,** 841-844.

HORSFORD, D. J., NGUYEN, M. T., SELLAR, G. C., KOTHARY, R., ARNHEITER, H. & MCINNES, R. R. 2005. Chx10 repression of Mitf is required for the maintenance of mammalian neuroretinal identity. *Development,* 132**,** 177-187.

HOWE, D. G., BRADFORD, Y. M., CONLIN, T., EAGLE, A. E., FASHENA, D., FRAZER, K., KNIGHT, J., MANI, P., MARTIN, R., MOXON, S. A., PADDOCK, H., PICH, C., RAMACHANDRAN, S., RUEF, B. J., RUZICKA, L., SCHAPER, K., SHAO, X., SINGER, A., SPRUNGER, B., VAN SLYKE, C. E. & WESTERFIELD, M. 2013. ZFIN, the Zebrafish Model Organism Database: increased support for mutants and transgenics. *Nucleic Acids Research,* 41**,** D854-D860.

HSU, P. D., SCOTT, D. A., WEINSTEIN, J. A., RAN, F. A., KONERMANN, S., AGARWALA, V., LI, Y., FINE, E. J., WU, X., SHALEM, O., CRADICK, T. J., MARRAFFINI, L. A., BAO, G. & ZHANG, F. 2013. DNA targeting specificity of RNA-guided Cas9 nucleases. *Nature Biotechnology,* 31**,** 827-832.

HWANG, W. Y., FU, Y., REYON, D., MAEDER, M. L., TSAI, S. Q., SANDER, J. D., PETERSON, R. T., YEH, J. R. J. & JOUNG, J. K. 2013. Efficient genome editing in zebrafish using a CRISPR-Cas system. *Nature Biotechnology,* 31**,** 227-229.

HYER, J., MIMA, T. & MIKAWA, T. 1998. FGF1 patterns the optic vesicle by directing the placement of the neural retina domain. *Development,* 125**,** 869-877.

INOUE, T., NAKAMURA, S. & OSUMI, N. 2000. Fate Mapping of the Mouse Prosencephalic Neural Plate. *Developmental Biology,* 219**,** 373-383.

IVANOVITCH, K., CAVODEASSI, F. & WILSON, S. W. 2013. Precocious acquisition of neuroepithelial character in the eye field underlies the onset of eye morphogenesis. *Developmental Cell,* 27**,** 293-305.

JAMES, A., LEE, C., WILLIAMS, A. M., ANGILERI, K., LATHROP, K. L. & GROSS,

J. M. 2016. The hyaloid vasculature facilitates basement membrane breakdown during choroid fissure closure in the zebrafish eye. *Developmental Biology,* 419**,** 262-272.

JARJOUR, N. N., BRADSTREET, T. R., SCHWARZKOPF, E. A., LIN, C.-C., COOK, M. E., HUANG, S. C.-C., TANEJA, R., RANDOLPH, G. J., URBAN, J. F. & EDELSON, B. T. 2018. The transcription factor Bhlhe40 is a novel regulator of large peritoneal macrophages and type 2 immunity. *The Journal of Immunology,* 200**,** 52.38.

JAYARAM, M. A. & FLEYEH, H. 2016. Convex Hulls in Image Processing: A Scoping Review. *American Journal of Intelligent Systems,* 6**,** 48-58.

KAJITA, M., SUGIMURA, K., OHOKA, A., BURDEN, J., SUGANUMA, H., IKEGAWA, M., SHIMADA, T., KITAMURA, T., SHINDOH, M., ISHIKAWA, S., YAMAMOTO, S., SAITOH, S., YAKO, Y., TAKAHASHI, R., OKAJIMA, T., KIKUTA, J., MAIJIMA, Y., ISHII, M., TADA, M. & FUJITA, Y. 2014. Filamin acts as a key regulator in epithelial defence against transformed cells. *Nature Communications,* 5**,** 4428.

KAWAKAMI, K., ASAKAWA, K., HIBI, M., ITOH, M., MUTO, A. & WADA, H. 2016. Chapter Three - Gal4 Driver Transgenic Zebrafish: Powerful Tools to Study Developmental Biology, Organogenesis, and Neuroscience. *In:* FOULKES, N. S. (ed.) *Advances in Genetics.* Academic Press.

KELLER, R. 2006. Mechanisms of elongation in embryogenesis. *Development,* 133**,** 2291.

KEPIRO, M., VARKUTI, B. H., BODOR, A., HEGYI, G., DRAHOS, L., KOVACS, M. & MALNASI-CSIZMADIA, A. 2012. Azidoblebbistatin, a photoreactive myosin inhibitor. *Proceedings of the National Academy of Sciences of the United States of America,* 109**,** 9402-9407.

KEPIRO, M., VARKUTI, B. H., RAUSCHER, A. A., KELLERMAYER, M. S. Z., VARGA, M. & MALNASI-CSIZMADIA, A. 2015. Molecular tattoo: subcellular confinement of drug effects. *Chemistry & Biology,* 22**,** 548-558.

KIM, J. Y., PARK, R., LEE, J. H. J., SHIN, J., NICKAS, J., KIM, S. & CHO, S.-H. 2016. Yap is essential for retinal progenitor cell cycle progression and RPE cell fate acquisition in the developing mouse eye. *Developmental Biology,* 419**,** 336-347.

KIMMEL, C. B., BALLARD, W. W., KIMMEL, S. R., ULLMANN, B. & SCHILLING, T. F. 1995. Stages of embryonic development of the zebrafish. *Developmental Dynamics,* 203**,** 253-310.

KIMURA, Y., HISANO, Y., KAWAHARA, A. & HIGASHIJIMA, S. 2014. Efficient generation of knock-in transgenic zebrafish carrying reporter/driver genes by CRISPR/Cas9-mediated genome engineering. *Scientific Reports,* 4**,** 6545.

KWAN, K. M., FUJIMOTO, E., GRABHER, C., MANGUM, B. D., HARDY, M. E., CAMPBELL, D. S., PARANT, J. M., YOST, H. J., KANKI, J. P. & CHIEN, C. B. 2007. The Tol2kit: a multisite gateway-based construction kit for Tol2 transposon transgenesis constructs. *Developmental Dynamics,* 236**,** 3088-3099.

KWAN, K. M., OTSUNA, H., KIDOKORO, H., CARNEY, K. R., SAIJOH, Y. & CHIEN,

C. B. 2012. A complex choreography of cell movements shapes the vertebrate eye. *Development,* 139**,** 359-372.

LAND, M. F. 2012. *Animal eyes,* 2nd edition. Oxford New York: New York Oxford University Press.

LANE, B. M. & LISTER, J. A. 2012. Otx but not Mitf transcription factors are required for zebrafish retinal pigment epithelium development. *PLoS One,* 7**,** e49357.

LEASK, A., BYRNE, C. & FUCHS, E. 1991. Transcription factor AP2 and its role in epidermal-specific gene expression. *Proceedings of the National Academy of Sciences of the United States of America,* 88**,** 7948-52.

LETELIER, J., BOVOLENTA, P. & MARTÍNEZ-MORALES, J. R. 2017. The pigmented epithelium, a bright partner against photoreceptor degeneration. *Journal of Neurogenetics,* 31**,** 203-215.

LI, M., ZHU, F., HONG, N., ZHANG, L. & HONG, Y. 2014. Alternative transcription generates multiple Mitf isoforms with different expression patterns and activities in medaka. *Pigment Cell & Melanoma Research,* 27**,** 48-58.

LI, Y., SHEN, Q., KIM, H.-T., BISSONNETTE, R. P., LAMPH, W. W., YAN, B. & BROWN, P. H. 2011. The rexinoid bexarotene represses cyclin D1 transcription by inducing the DEC2 transcriptional repressor. *Breast Cancer Research and Treatment,* 128**,** 667-677.

LI, Z., HU, M., OCHOCINSKA, M. J., JOSEPH, N. M. & EASTER JR., S. S. 2000b. Modulation of cell proliferation in the embryonic retina of zebrafish (Danio rerio). *Developmental Dynamics,* 219**,** 391-401.

LI, Z., JOSEPH, N. M. & EASTER JR., S. S. 2000a. The morphogenesis of the zebrafish eye, including a fate map of the optic vesicle. *Developmental Dynamics,* 218**,** 175-188.

LISTER, J. A., CLOSE, J. & RAIBLE, D. W. 2001. Duplicate mitf Genes in Zebrafish: Complementary Expression and Conservation of Melanogenic Potential. *Developmental Biology,* 237**,** 333-344.

LIU, Y., WANG, L., LIN, X.-Y., WANG, J., YU, J.-H., MIAO, Y. & WANG, E.-H. 2013. The transcription factor DEC1 (BHLHE40/STRA13/SHARP-2) is negatively associated with TNM stage in non-small-cell lung cancer and inhibits the proliferation through cyclin D1 in A549 and BE1 cells. *Tumor Biology,* 34**,** 1641-1650.

LOCASCIO, A. & NIETO, M. A. 2001. Cell movements during vertebrate development: integrated tissue behaviour versus individual cell migration. *Current Opinion in Genetics & Development,* 11**,** 464-469.

MACDONALD, R., BARTH, K. A., XU, Q., HOLDER, N., MIKKOLA, I. & WILSON, S. W. 1995. Midline signalling is required for Pax gene regulation and patterning of the eyes. *Development,* 121**,** 3267-3278.

MAÎTRE, J.-L., BERTHOUMIEUX, H., KRENS, S. F. G., SALBREUX, G., JÜLICHER, F., PALUCH, E. & HEISENBERG, C.-P. 2012. Adhesion Functions in Cell Sorting by Mechanically Coupling the Cortices of Adhering Cells. *Science,* 338**,** 253-256.

MARTINEZ-MORALES, J.-R., DEL BENE, F., NICA, G., HAMMERSCHMIDT, M., BOVOLENTA, P. & WITTBRODT, J. 2005. Differentiation of the Vertebrate Retina Is Coordinated by an FGF Signaling Center. *Developmental Cell,* 8**,** 565-574.

MARTINEZ-MORALES, J. R. 2016. Vertebrate Eye Gene Regulatory Networks. *In:* J., C.-G. H. & P., B. (eds.) *Organogenetic Gene Networks.* : Springer, Cham.

MARTINEZ-MORALES, J. R., CAVODEASSI, F. & BOVOLENTA, P. 2017. Coordinated Morphogenetic Mechanisms Shape the Vertebrate Eye. *Frontiers in Neuroscience,* 11**,** 721.

MARTINEZ-MORALES, J. R., DOLEZ, V., RODRIGO, I., ZACCARINI, R., LECONTE, L., BOVOLENTA, P. & SAULE, S. 2003. OTX2 activates the molecular network underlying retina pigment epithelium differentiation. *Journal of Biolical Chemistry,* 278**,** 21721-21731.

MARTINEZ-MORALES, J. R. & LOCASCIO, A. 2016. Vertebrate Eye Evolution. *In:* J., C.-G. H. & P., B. (eds.) *Organogenetic Gene Networks.* Springer, Cham.

MARTINEZ-MORALES, J. R., REMBOLD, M., GREGER, K., SIMPSON, J. C., BROWN, K. E., QUIRING, R., PEPPERKOK, R., MARTIN-BERMUDO, M. D., HIMMELBAUER, H. & WITTBRODT, J. 2009. ojoplano-mediated basal constriction is essential for optic cup morphogenesis. *Development,* 136**,** 2165-2175.

MARTINEZ-MORALES, J. R., RODRIGO, I. & BOVOLENTA, P. 2004. Eye development: a view from the retina pigmented epithelium. *Bioessays,* 26**,** 766-777.

MARTINEZ-MORALES, J. R., SIGNORE, M., ACAMPORA, D., SIMEONE, A. & BOVOLENTA, P. 2001. Otx genes are required for tissue specification in the developing eye. *Development,* 128**,** 2019-2030.

MAY-SIMERA, H. L., WAN, Q., JHA, B. S., HARTFORD, J., KHRISTOV, V., DEJENE, R., CHANG, J., PATNAIK, S., LU, Q., BANERJEE, P., SILVER, J., INSINNA-KETTENHOFEN, C., PATEL, D., LOTFI, M., MALICDAN, M., HOTALING, N., MAMINISHKIS, A., SRIDHARAN, R., BROOKS, B., MIYAGISHIMA, K., GUNAY-AYGUN, M., PAL, R., WESTLAKE, C., MILLER, S., SHARMA, R. & BHARTI, K. 2018. Primary Cilium-Mediated Retinal Pigment Epithelium Maturation Is Disrupted in Ciliopathy Patient Cells. *Cell Reports,* 22**,** 189-205.

MENGER, G. J., KOKE, J. R. & CAHILL, G. M. 2005. Diurnal and circadian retinomotor movements in zebrafish. *Visual Neuroscience,* 22**,** 203-209.

MI, H., MURUGANUJAN, A., CASAGRANDE, J. T. & THOMAS, P. D. 2013. Large-scale gene function analysis with the PANTHER classification system. *Nature Protocols,* 8**,** 1551-1566.

MIESFELD, J. B., GESTRI, G., CLARK, B. S., FLINN, M. A., POOLE, R. J., BADER, J. R., BESHARSE, J. C., WILSON, S. W. & LINK, B. A. 2015. Yap and Taz regulate retinal pigment epithelial cell fate. *Development,* 142**,** 3021-3032.

MIESFELD, J. B. & LINK, B. A. 2014. Establishment of transgenic lines to monitor and manipulate Yap/Taz-Tead activity in zebrafish reveals both evolutionarily conserved and divergent functions of the Hippo pathway. *Mechanisms of Development,* 133**,** 177-188.

MONIER, B. & SUZANNE, M. 2015. Chapter Twelve - The Morphogenetic Role of

Apoptosis. *In:* STELLER, H. (ed.) *Current Topics in Developmental Biology.* Academic Press.

MORENO-MARMOL, T., CAVODEASSI, F. and BOVOLENTA, P. 2018. Setting Eyes on the Retinal Pigment Epithelium. *Frontiers in Cell and Developmental Biology*, 6, 145.

MORENO-MATEOS, M. A., VEJNAR, C. E., BEAUDOIN, J.-D., FERNANDEZ, J. P., MIS, E. K., KHOKHA, M. K. & GIRALDEZ, A. J. 2015. CRISPRscan: designing highly efficient sgRNAs for CRISPR-Cas9 targeting in vivo. *Nature Methods,* 12**,** 982-988.

MÜLLER, F., ROHRER, H. & VOGEL-HÖPKER, A. 2007. Bone morphogenetic proteins specify the retinal pigment epithelium in the chick embryo. *Development,* 134**,** 3483-3493.

NAKANO, T., ANDO, S., TAKATA, N., KAWADA, M., MUGURUMA, K., SEKIGUCHI, K., SAITO, K., YONEMURA, S., EIRAKU, M. & SASAI, Y. 2012. Self-Formation of Optic Cups and Storable Stratified Neural Retina from Human ESCs. *Cell Stem Cell,* 10**,** 771-785.

NASEVICIUS, A. & EKKER, S. C. 2000. Effective targeted gene 'knockdown' in zebrafish. *Nature Genetics,* 26**,** 216-220.

NAWROCKI, L., BREMILLER, R., STREISINGER, G. & KAPLAN, M. 1985. Larval and adult visual pigments of the zebrafish, Brachydanio rerio. *Vision Research,* 25**,** 1569-1576.

NGUYEN, M. & ARNHEITER, H. 2000. Signaling and transcriptional regulation in early mammalian eye development: a link between FGF and MITF. *Development,* 127**,** 3581-3591.

NICOLAS-PEREZ, M., KUCHLING, F., LETELIER, J., POLVILLO, R., WITTBRODT, J. & MARTINEZ-MORALES, J. R. 2016. Analysis of cellular behavior and cytoskeletal dynamics reveal a constriction mechanism driving optic cup morphogenesis. *Elife,* 5**,** e15797.

NISHIHARA, D., YAJIMA, I., TABATA, H., NAKAI, M., TSUKIJI, N., KATAHIRA, T., TAKEDA, K., SHIBAHARA, S., NAKAMURA, H. & YAMAMOTO, H. 2012. Otx2 is involved in the regional specification of the developing retinal pigment epithelium by preventing the expression of sox2 and fgf8, factors that induce neural retina differentiation. *PLoS One,* 7**,** e48879.

OKUDA, S., TAKATA, N., HASEGAWA, Y., KAWADA, M., INOUE, Y., ADACHI, T., SASAI, Y. & EIRAKU, M. 2018. Strain-triggered mechanical feedback in self-organizing optic-cup morphogenesis. *Science Advances,* 4**,** eaau1354.

OLTEAN, A., HUANG, J., BEEBE, D. C. & TABER, L. A. 2016. Tissue growth constrained by extracellular matrix drives invagination during optic cup morphogenesis. *Biomechanics and Modeling in Mechanobiology,* 15**,** 1405-1421.

OTTESON, D. C. & HITCHCOCK, P. F. 2003. Stem cells in the teleost retina: persistent neurogenesis and injury-induced regeneration. *Vision Research,* 43**,** 927-936.

PALUCH, E. & HEISENBERG, C.-P. 2009. Biology and Physics of Cell Shape Changes in Development. *Current Biology,* 19**,** R790-R799.

PHILIPS, G. T., STAIR, C. N., YOUNG LEE, H., WROBLEWSKI, E., BERBEROGLU, M. A., BROWN, N. L. & MASTICK, G. S. 2005. Precocious retinal neurons: Pax6 controls timing of differentiation and determination of cell type. *Developmental Biology,* 279**,** 308-321.

PICKER, A., CAVODEASSI, F., MACHATE, A., BERNAUER, S., HANS, S., ABE,

G., KAWAKAMI, K., WILSON, S. W. & BRAND, M. 2009. Dynamic Coupling of Pattern Formation and Morphogenesis in the Developing Vertebrate Retina. *PLoS Biology,* 7**,** e1000214.

PITTACK, C., GRUNWALD, G. B. & REH, T. A. 1997. Fibroblast growth factors are necessary for neural retina but not pigmented epithelium differentiation in chick embryos. *Development,* 124**,** 805-16.

POPE, K. L. & HARRIS, T. J. 2008. Control of cell flattening and junctional remodeling during squamous epithelial morphogenesis in Drosophila. *Development,* 135**,** 2227-38.

PORAZINSKI, S., WANG, H., ASAOKA, Y., BEHRNDT, M., MIYAMOTO, T., MORITA, H., HATA, S., SASAKI, T., KRENS, S. F. G., OSADA, Y., ASAKA, S., MOMOI, A., LINTON, S., MIESFELD, J. B., LINK, B. A., SENGA, T., SHIMIZU, N., NAGASE, H., MATSUURA, S., BAGBY, S., KONDOH, H., NISHINA, H., HEISENBERG, C. P. & FURUTANI-SEIKI, M. 2015. YAP is essential for tissue tension to ensure vertebrate 3D body shape. *Nature,* 521**,** 217-221.

QIAN, Y. & CHEN, X. 2008. ID1, inhibitor of differentiation/DNA binding, is an effector of the p53-dependent DNA damage response pathway. *The Journal of Biological Chemistry,* 283**,** 22410-22416.

RAUSCHER, A. A., GYIMESI, M., KOVACS, M. & MALNASI-CSIZMADIA, A. 2018. Targeting Myosin by Blebbistatin Derivatives: Optimization and Pharmacological Potential. *Trends in Biochemal Sciences,* 43**,** 700-713.

RAUZI, M. & LENNE, P.-F. 2011. Chapter four - Cortical Forces in Cell Shape Changes and Tissue Morphogenesis. *In:* LABOUESSE, M. (ed.) *Current Topics in Developmental Biology.* Academic Press.

REBAGLIATI, M. R., TOYAMA, R., HAFFTER, P. & DAWID, I. B. 1998. cyclops encodes a nodal-related factor involved in midline signaling. *Proceedings of the National Academy of Sciences of the United States of America,* 95**,** 9932-9937.

REMBOLD, M., LOOSLI, F., ADAMS, R. J. & WITTBRODT, J. 2006. Individual Cell Migration Serves as the Driving Force for Optic Vesicle Evagination. *Science,* 313**,** 1130-1134.

ROSCHGER, C. & CABRELE, C. 2017. The Id-protein family in developmental and cancer-associated pathways. *Cell Communication and Signaling,* 15**,** 7.

SCHINDELIN, J., ARGANDA-CARRERAS, I., FRISE, E., KAYNIG, V., LONGAIR, M., PIETZSCH, T., PREIBISCH, S., RUEDEN, C., SAALFELD, S., SCHMID, B., TINEVEZ, J.-Y., WHITE, D. J., HARTENSTEIN, V., ELICEIRI, K., TOMANCAK, P. & CARDONA, A. 2012. Fiji: an open-source platform for biological-image analysis. *Nature Methods,* 9**,** 676-682.

SCHLÜßLER, R., MÖLLMERT, S., ABUHATTUM, S., COJOC, G., MÜLLER, P., KIM, K., MÖCKEL, C., ZIMMERMANN, C., CZARSKE, J. & GUCK, J. 2018. Mechanical Mapping of Spinal Cord Growth and Repair in Living Zebrafish Larvae by Brillouin Imaging. *Biophysical Journal,* 115**,** 911-923.

SCHWARZ, M., CECCONI, F., BERNIER, G., ANDREJEWSKI, N., KAMMANDEL, B., WAGNER, M. & GRUSS, P. 2000. Spatial specification of mammalian eye territories by

reciprocal transcriptional repression of Pax2 and Pax6. *Development,* 127**,** 4325-4334.

SELTMANN, K., FRITSCH, A. W., KAS, J. A. & MAGIN, T. M. 2013. Keratins significantly contribute to cell stiffness and impact invasive behavior. *Proceedings of the National Academy of Sciences of the United States of America,* 110**,** 18507-18512.

SERRA, J. & VINCENT, L. 1992. An overview of morphological filtering. *Circuits, Systems and Signal Processing,* 11**,** 47-108.

SIDHAYE, J. & NORDEN, C. 2017. Concerted action of neuroepithelial basal shrinkage and active epithelial migration ensures efficient optic cup morphogenesis. *Elife,* 6.

SINN, R. & WITTBRODT, J. 2013. An eye on eye development. *Mechanisms of Development,* 130**,** 347-358.

SPARROW, J. R., HICKS, D. & HAMEL, C. P. 2010. The retinal pigment epithelium in health and disease. *Current molecular medicine,* 10**,** 802-823.

SRDANOVIĆ, S., ÞORSTEINSSON, H., FRIÐRIKSSON, Þ., PÉTURSSON, S. Ó., MAIER, V. H. & KARLSSON, K. Æ. 2017. Transient knock-down of kcna2 reduces sleep in larval zebrafish. *Behavioural Brain Research,* 326**,** 13-21.

STEINFELD, J., STEINFELD, I., BAUSCH, A., CORONATO, N., HAMPEL, M.-L., DEPNER, H., LAYER, P. G. & VOGEL-HÖPKER, A. 2017. BMP-induced reprogramming of the neural retina into retinal pigment epithelium requires Wnt signalling. *Biology Open,* 6**,** 979-992.

STEINFELD, J., STEINFELD, I., CORONATO, N., HAMPEL, M. L., LAYER, P. G., ARAKI, M. & VOGEL-HOPKER, A. 2013. RPE specification in the chick is mediated by surface ectoderm-derived BMP and Wnt signalling. *Development,* 140**,** 4959-4969.

STEMMER, M., THUMBERGER, T., DEL SOL KEYER, M., WITTBRODT, J. & MATEO, J. L. 2015. CCTop: An Intuitive, Flexible and Reliable CRISPR/Cas9 Target Prediction Tool. *PLoS One,* 10**,** e0124633.

STEPANOVA, T., SLEMMER, J., HOOGENRAAD, C. C., LANSBERGEN, G., DORTLAND, B., DE ZEEUW, C. I., GROSVELD, F., VAN CAPPELLEN, G., AKHMANOVA, A. & GALJART, N. 2003. Visualization of Microtubule Growth in Cultured Neurons via the Use of EB3-GFP (End-Binding Protein 3-Green Fluorescent Protein). *The Journal of Neuroscience,* 23**,** 2655-2664.

STRAUSS, O. 2005. The Retinal Pigment Epithelium in Visual Function. *Physiological Reviews,* 85**,** 845-881.

STUART, G. W., VIELKIND, J. R., MCMURRAY, J. V. & WESTERFIELD, M. 1990. Stable lines of transgenic zebrafish exhibit reproducible patterns of transgene expression. *Development,* 109**,** 577-584.

SUN, H., GHAFFARI, S. & TANEJA, R. 2007. bHLH-Orange Transcription Factors in Development and Cancer. *Translational Oncogenomics,* 2**,** 107-120.

SUN, H. & TANEJA, R. 2000. Stra13 expression is associated with growth arrest and represses transcription through histone deacetylase (HDAC)-dependent and HDAC-indepen-

dent mechanisms. *Proceedings of the National Academy of Sciences of the United States of America,* 97**,** 4058-4063.

SUZANNE, M. & STELLER, H. 2013. Shaping organisms with apoptosis. *Cell death and differentiation,* 20**,** 669-675.

TAKE-UCHI, M., CLARKE, J. D. W. & WILSON, S. W. 2003. Hedgehog signalling maintains the optic stalk-retinal interface through the regulation of Vax gene activity. *Development,* 130**,** 955-968.

TEE, S.-Y., FU, J., CHEN, C. S. & JANMEY, P. A. 2011. Cell shape and substrate rigidity both regulate cell stiffness. *Biophysical journal,* 100**,** L25-L27.

TOTARO, A., PANCIERA, T. & PICCOLO, S. 2018. YAP/TAZ upstream signals and downstream responses. *Nature Cell Biology,* 20**,** 888-899.

TRAPNELL, C., ROBERTS, A., GOFF, L., PERTEA, G., KIM, D., KELLEY, D. R., PIMENTEL, H., SALZBERG, S. L., RINN, J. L. & PACHTER, L. 2012. Differential gene and transcript expression analysis of RNA-seq experiments with TopHat and Cufflinks. *Nature Protocols,* 7**,** 562-578.

TROUSSE, F., ESTEVE, P. & BOVOLENTA, P. 2001. BMP4 Mediates Apoptotic Cell Death in the Developing Chick Eye. *The Journal of Neuroscience,* 21**,** 1292-1301.

TURKSEN, K., OPAS, M. & KALNINS, V. I. 1989. Cytoskeleton, adhesion, and extracellular matrix of fetal human retinal pigmented epithelial cells in culture. *Ophthalmic Research,* 21**,** 56-66.

VARSHNEY, G. K., PEI, W., LAFAVE, M. C., IDOL, J., XU, L., GALLARDO, V., CARRINGTON, B., BISHOP, K., JONES, M., LI, M., HARPER, U., HUANG, S. C., PRAKASH, A., CHEN, W., SOOD, R., LEDIN, J. & BURGESS, S. M. 2015. High-throughput gene targeting and phenotyping in zebrafish using CRISPR/Cas9. *Genome Res,* 25**,** 1030-1042.

VISHAVKARMA, R., RAGHAVAN, S., KUYYAMUDI, C., MAJUMDER, A., DHAWAN, J. & PULLARKAT, P. A. 2014. Role of Actin Filaments in Correlating Nuclear Shape and Cell Spreading. *PLoS One,* 9**,** e107895.

WEISS, O., KAUFMAN, R., MICHAELI, N. & INBAL, A. 2012. Abnormal vasculature interferes with optic fissure closure in lmo2 mutant zebrafish embryos. *Developmental Biology,* 369**,** 191-198.

WESTERFIELD, M. 1993. *The zebrafish: a guide for the laboratory use of zebrafish (Brachydanio reriro)*, 4th edition. Eugene. Oregon: Inst. of Neuroscience, University of Oregon.

WRIGHT, A. F., CHAKAROVA, C. F., ABD EL-AZIZ, M. M. & BHATTACHARYA, S. S. 2010. Photoreceptor degeneration: genetic and mechanistic dissection of a complex trait. *Nature Reviews Genetics,* 11**,** 273-284.

WU, R. S., LAM, I. I., CLAY, H., DUONG, D. N., DEO, R. C. & COUGHLIN, S. R. 2018. A Rapid Method for Directed Gene Knockout for Screening in G0 Zebrafish. *Developmental Cell,* 46**,** 112-125.

XU, Q., HOLDER, N., PATIENT, R. & WILSON, S. W. 1994. Spatially regulated expression

of three receptor tyrosine kinase genes during gastrulation in the zebrafish. *Development,* 120**,** 287-299.

YAMADA, K. & MIYAMOTO, K. 2005. Basic helix-loop-helix transcription factors, BHLHB2 and BHLHB3; their gene expressions are regulated by multiple extracellular stimuli. *Frontiers in Bioscience,* 10**,** 3151-3171.

YAO, J., WANG, L., CHEN, L., ZHANG, S., ZHAO, Q., JIA, W. & XUE, J. 2006. Cloning and developmental expression of the DEC1 ortholog gene in zebrafish. *Gene Expression Patterns,* 6**,** 919-927.

APPENDIX I

Enriched GO terms of genes up-regulated in the 18 hpf RPE when compared with 16 hpf retinal progenitors obtained with the GOrilla tool.

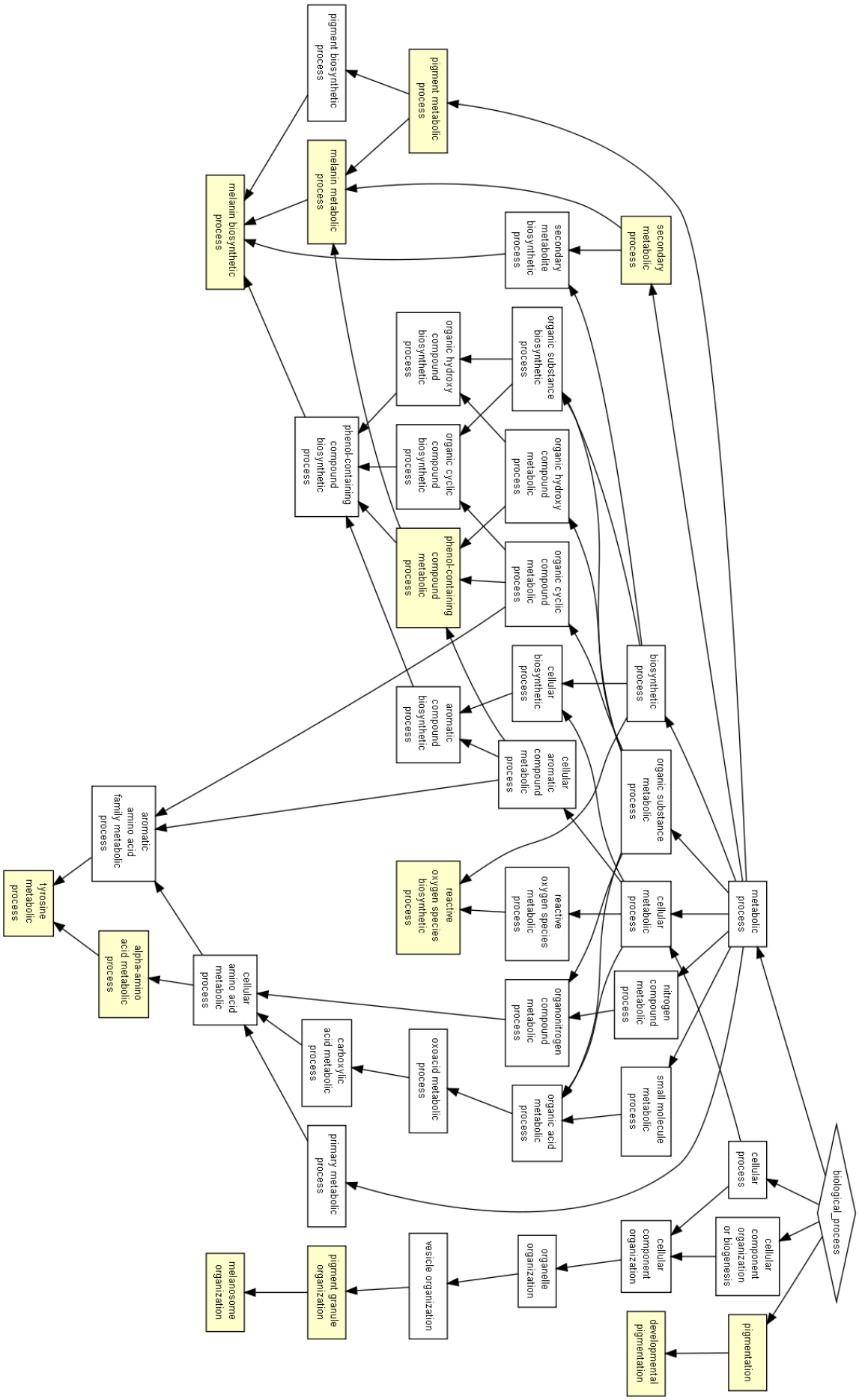
biological_process
metabolic process
cellular process
pigmentation
developmental pigmentation
cellular component organization or biogenesis
cellular component organization
organelle organization
vesicle organization
pigment granule organization
melanosome organization
primary metabolic process
small molecule metabolic process
organic acid metabolic process
oxoacid metabolic process
carboxylic acid metabolic process
organic substance metabolic process
nitrogen compound metabolic process
organonitrogen compound metabolic process
cellular metabolic process
reactive oxygen species metabolic process
reactive oxygen species biosynthetic process
cellular amino acid metabolic process
alpha-amino acid metabolic process
tyrosine metabolic process
aromatic amino acid family metabolic process
biosynthetic process
cellular aromatic compound metabolic process
aromatic compound biosynthetic process
cellular biosynthetic process
organic cyclic compound metabolic process
phenol-containing compound metabolic process
organic hydroxy compound metabolic process
organic substance biosynthetic process
organic cyclic compound biosynthetic process
organic hydroxy compound biosynthetic process
phenol-containing compound biosynthetic process
secondary metabolic process
secondary metabolite biosynthetic process
melanin biosynthetic process
melanin metabolic process
pigment metabolic process
pigment biosynthetic process

Enriched GO terms of genes up-regulated in the 23 hpf RPE when compared with 16 hpf retinal progenitors obtained with the GOrilla tool.

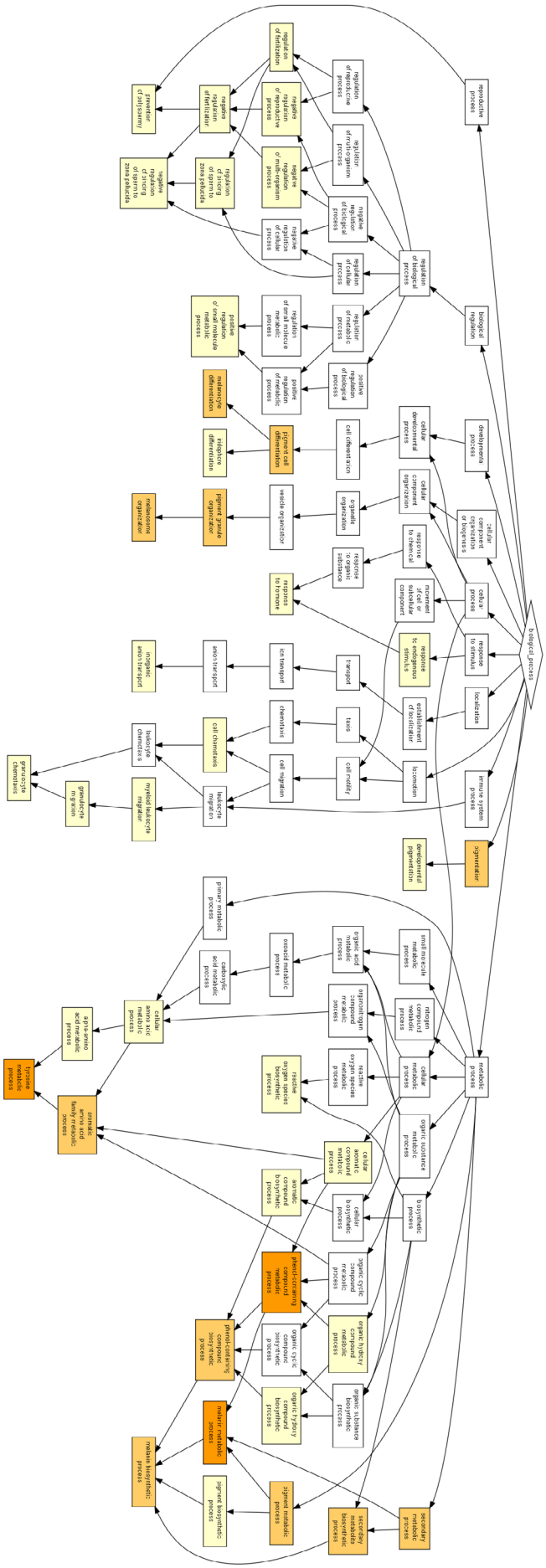
biological_process
reproduction
reproductive process
regulation of fertilization
regulation of reproductive process
negative regulation of fertilization
negative regulation of reproductive process
prevention of polyspermy
regulation of multi-organism process
negative regulation of multi-organism process
regulation of entry of sperm to zona pellucida
negative regulation of entry of sperm to zona pellucida
regulation of biological process
negative regulation of cellular process
regulation of cellular process
biological regulation
regulation of biological process
regulation of small molecule metabolic process
positive regulation of small molecule metabolic process
regulation of metabolic process
positive regulation of metabolic process
melanosome differentiation
pigment cell differentiation
developmental process
cellular developmental process
cell differentiation
cellular component organization
cellular component organization or biogenesis
organelle organization
vesicle organization
melanosome organization
pigment granule organization
response to chemical
response to organic substance
response to nitrosative stress
movement of cell or subcellular component
cellular process
response to stimulus
response to endogenous stimulus
localization
establishment of localization
transport
ion transport
anion transport
inorganic anion transport
taxis
cell motility
locomotion
cell chemotaxis
chemotaxis
leukocyte chemotaxis
granulocyte chemotaxis
cell migration
leukocyte migration
myeloid leukocyte migration
granulocyte migration
immune system process
pigmentation
developmental pigmentation
pigmentation
primary metabolic process
carboxylic acid metabolic process
oxoacid metabolic process
organic acid metabolic process
small molecule metabolic process
cellular amino acid metabolic process
alpha-amino acid metabolic process
tyrosine metabolic process
organonitrogen compound metabolic process
nitrogen compound metabolic process
cellular metabolic process
reactive oxygen species metabolic process
reactive oxygen species biosynthetic process
metabolic process
organic substance metabolic process
cellular aromatic compound metabolic process
aromatic compound biosynthetic process
cellular biosynthetic process
biosynthetic process
aromatic amino acid family metabolic process
phenol-containing compound metabolic process
organic cyclic compound metabolic process
organic cyclic compound biosynthetic process
phenol-containing compound biosynthetic process
organic substance biosynthetic process
organic hydroxy compound metabolic process
organic hydroxy compound biosynthetic process
tyrosine biosynthetic process
melanin biosynthetic process
pigment biosynthetic process
pigment metabolic process
secondary metabolite biosynthetic process
secondary metabolic process

Enriched GO terms of genes down-regulated in the 18 hpf RPE when compared with 16 hpf retinal progenitors obtained with the GOrilla tool.

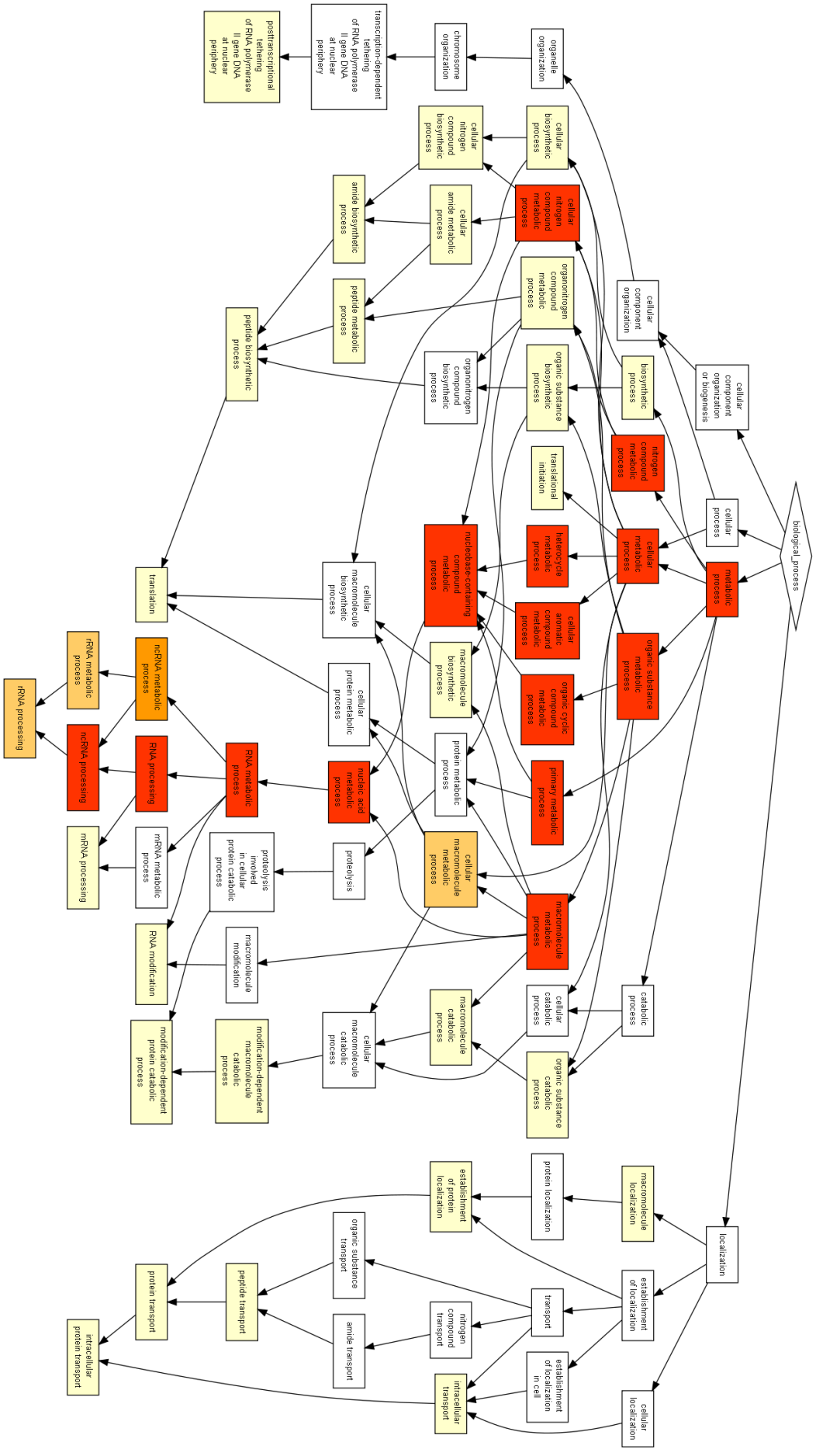
biological_process
cellular process
metabolic process
cellular component organization or biogenesis
cellular component organization
localization
establishment of localization
transport
cellular localization
establishment of localization in cell
intracellular transport
macromolecule localization
establishment of protein localization
protein localization
organic substance transport
peptide transport
protein transport
amide transport
nitrogen compound transport
intracellular protein transport
cellular metabolic process
nitrogen compound metabolic process
organic substance metabolic process
biosynthetic process
cellular biosynthetic process
organic substance biosynthetic process
translational initiation
heterocycle metabolic process
cellular aromatic compound metabolic process
organic cyclic compound metabolic process
primary metabolic process
macromolecule metabolic process
cellular macromolecule metabolic process
protein metabolic process
cellular protein metabolic process
nucleic acid metabolic process
RNA metabolic process
RNA processing
ncRNA processing
rRNA processing
ncRNA metabolic process
rRNA metabolic process
mRNA processing
mRNA metabolic process
RNA modification
macromolecule modification
proteolysis
proteolysis involved in cellular protein catabolic process
modification-dependent protein catabolic process
modification-dependent macromolecule catabolic process
translation
cellular macromolecule biosynthetic process
macromolecule biosynthetic process
nucleobase-containing compound metabolic process
organonitrogen compound biosynthetic process
peptide biosynthetic process
peptide metabolic process
amide biosynthetic process
amide metabolic process
cellular nitrogen compound biosynthetic process
cellular nitrogen compound metabolic process
organonitrogen compound metabolic process
catabolic process
cellular catabolic process
macromolecule catabolic process
cellular macromolecule catabolic process
organic substance catabolic process
chromosome organization
organelle organization
transcription-dependent tethering of RNA polymerase II gene DNA at nuclear periphery
posttranscriptional tethering of RNA polymerase II gene DNA at nuclear periphery

Enriched GO terms of genes down-regulated in the 23 hpf RPE when compared with 16 hpf retinal progenitors obtained with the GOrilla tool.

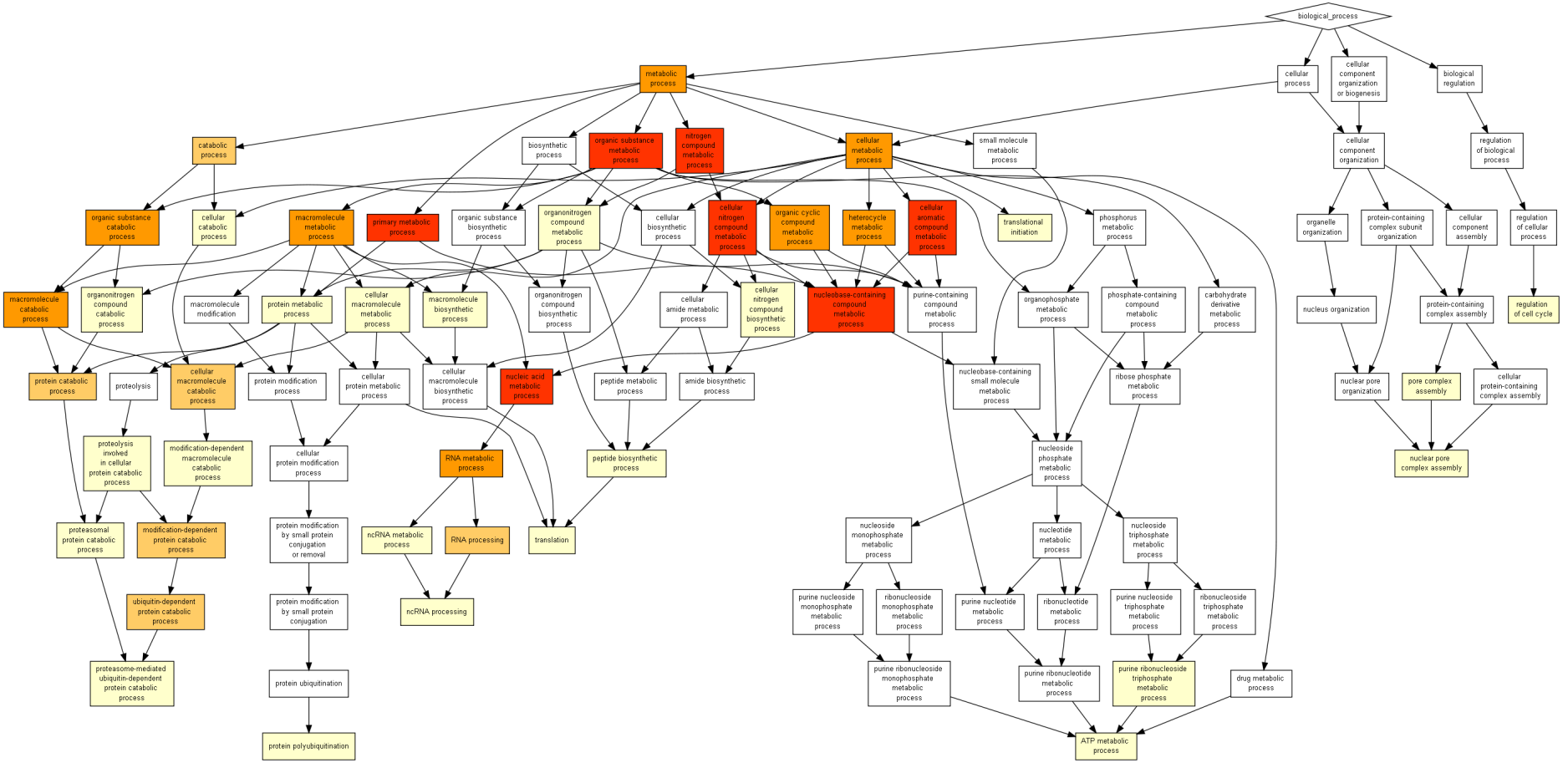
biological_process
metabolic process
cellular process
cellular component organization or biogenesis
biological regulation
catabolic process
biosynthetic process
organic substance metabolic process
nitrogen compound metabolic process
cellular metabolic process
small molecule metabolic process
cellular component organization
regulation of biological process
organic substance catabolic process
cellular catabolic process
macromolecule metabolic process
primary metabolic process
organic substance biosynthetic process
organonitrogen compound metabolic process
cellular biosynthetic process
cellular nitrogen compound metabolic process
organic cyclic compound metabolic process
heterocycle metabolic process
cellular aromatic compound metabolic process
translational initiation
phosphorus metabolic process
organelle organization
protein-containing complex subunit organization
cellular component assembly
regulation of cellular process
macromolecule catabolic process
organonitrogen compound catabolic process
macromolecule modification
protein metabolic process
cellular macromolecule metabolic process
macromolecule biosynthetic process
organonitrogen compound biosynthetic process
cellular amide metabolic process
cellular nitrogen compound biosynthetic process
nucleobase-containing compound metabolic process
purine-containing compound metabolic process
organophosphate metabolic process
phosphate-containing compound metabolic process
carbohydrate derivative metabolic process
nucleus organization
protein-containing complex assembly
regulation of cell cycle
protein catabolic process
proteolysis
cellular macromolecule catabolic process
protein modification process
cellular protein metabolic process
cellular macromolecule biosynthetic process
nucleic acid metabolic process
peptide metabolic process
amide biosynthetic process
nucleobase-containing small molecule metabolic process
ribose phosphate metabolic process
nuclear pore organization
pore complex assembly
cellular protein-containing complex assembly
proteolysis involved in cellular protein catabolic process
modification-dependent macromolecule catabolic process
cellular protein modification process
RNA metabolic process
peptide biosynthetic process
nucleoside phosphate metabolic process
nuclear pore complex assembly
proteasomal protein catabolic process
modification-dependent protein catabolic process
protein modification by small protein conjugation or removal
ncRNA metabolic process
RNA processing
translation
nucleoside monophosphate metabolic process
nucleotide metabolic process
nucleoside triphosphate metabolic process
ubiquitin-dependent protein catabolic process
protein modification by small protein conjugation
ncRNA processing
purine nucleoside monophosphate metabolic process
ribonucleoside monophosphate metabolic process
purine nucleotide metabolic process
ribonucleotide metabolic process
purine nucleoside triphosphate metabolic process
ribonucleoside triphosphate metabolic process
proteasome-mediated ubiquitin-dependent protein catabolic process
protein ubiquitination
purine ribonucleoside monophosphate metabolic process
purine ribonucleotide metabolic process
purine ribonucleoside triphosphate metabolic process
drug metabolic process
protein polyubiquitination
ATP metabolic process